The Dissertation Committee for Florencia Chavarria Certifies that this is the approved version of the following dissertation:

EFFECTS OF POLYMER-ORGANOCLAY INTERACTIONS AND PROCESSING METHODS ON NANOCOMPOSITE STRUCTURE AND PROPERTIES

Committee:

Donald R. Paul, Supervisor

Benny D. Freeman

Desiderio Kovar

Isaac C. Sanchez

Thomas M. Truskett

EFFECTS OF POLYMER-ORGANOCLAY INTERACTIONS AND PROCESSING METHODS ON NANOCOMPOSITE STRUCTURE AND PROPERTIES

by

Florencia Chavarria, B.S.; M.S.E.

Dissertation

Presented to the Faculty of the Graduate School of

The University of Texas at Austin

in Partial Fulfillment

of the Requirements

for the Degree of

Doctor of Philosophy

The University of Texas at Austin

December 2006

Dedication

To my husband, parents and sister.

Acknowledgements

I would like to acknowledge Dr. Benny Freeman, Dr. Desiderio Kovar, Dr. Isaac Sanchez, and Dr. Thomas Truskett for having served on my committee. I am especially grateful to Dr. Don Paul, whose wisdom, guidance and support have helped me gain invaluable experience that will be very useful for my future career and professional development.

I would also like to thank the people at Southern Clay Products for providing technical support and donation of the clay materials used in this work. I am particularly grateful to Dr. Doug Hunter, Ben Knesek, Tony Gonzalez, Randy Chapman, Joe Ortiz, and Ryan Dennis for their collaboration in research, technical advice, and friendship. My sincere appreciation goes to Dr. John Mendenhall and Dr. Ji-Ping Zhou for their help, and support in TEM sample preparation and imaging, as well as a much cherished friendship. I would also like to thank the people in Dr. Paul's group and the department staff, past and present, for their training and assistance over the years.

Lastly, I am forever grateful to my family and friends for their endless support and encouragement. I especially thank my parents, Claudia and Jaime, and my sister, Deborah, for believing in me and teaching me (by example) to always do my best regardless of the circumstances. I am indebted to my loving husband Ian for his support and encouragement, and more over, for the many sacrifices he has made for the pursuit of my career ambitions.

This work was funded by the Air Force Office of Scientific Research and the Consejo Nacional de Ciencia y Tecnología (CONACYT) of Mexico.

EFFECTS OF POLYMER-ORGANOCLAY INTERACTIONS AND PROCESSING METHODS ON NANOCOMPOSITE STRUCTURE AND PROPERTIES

Publication No._____

Florencia Chavarria, Ph.D.

The University of Texas at Austin, 2006

Supervisor: Donald R. Paul

Polymer-layered silicate nanocomposites based on polyamide, thermoplastic polyurethane, and polyolefin matrices and several organoclays were prepared by melt processing. The effects of types of matrices, organoclay structures, silicate layer charge, and processing conditions on the morphology and mechanical properties of nanocomposites were analyzed to obtain a greater understanding of the exfoliation process. Polyamide structure strongly influences the degree of platelet dispersion and mechanical property enhancement; nylon 6 nanocomposites show superior clay dispersion and matrix reinforcement than nylon 66 nanocomposites. The affinity of nylon 6 for the organoclay appears to be greater than that of nylon 66, which must be related to some aspect of their differences in chemical structure.

Mixing conditions created by twin screw extruders also have significant effects on morphology and properties of nylon 6 nanocomposites. Mixing the molten polymer with the organoclay under low shear, and applying a medium level of shear throughout the

extruder for a longer residence time leads to high platelet dispersion and matrix reinforcement. Mixing the solid polymer with the organoclay under high shear leads to short particle lengths and lower matrix reinforcement; this is believed to be due to attrition of clay platelets under these conditions. Nanocomposites formed in a DSM micro-compounder yield similar morphologies and modulus trends than conventional twin screw extruders.

The affinity between polymer and organoclay is also critical to produce high platelet dispersion and mechanical property enhancement. It is determined, to some extent, by the polarity of the polymer and the degree of silicate surface coverage given by the clay layer charge and the organoclay structure. Organoclays with reduced layer charge lead to lower exfoliation and modulus enhancement of nylon 6 and polypropylene-based nanocomposites than organoclays with no layer charge reduction; this was attributed to heterogeneities in layer charge and charge distribution produced during the charge reduction process. Thermoplastic polyurethane nanocomposites show similar trends than nylon 6 nanocomposites regarding organoclay structure, i.e., a higher exfoliation and matrix reinforcement was observed for organoclays with one alkyl tail that provide less coverage of the silicate surface. In the case of polyurethanes, the high affinity of the matrix for hydroxy ethyl functional groups appears to aid clay dispersion.

Table of Contents

List of Tables

List of Figures

CHAPTER 1

INTRODUCTION

Inorganic fillers have been used for many decades to improve properties of polymers such as stiffness, toughness, barrier properties, resistance to fire and ignition, or simply to reduce cost. The dimensions of most filler particles range from several microns to a few millimeters; the use of such large particles often compromises matrix properties like increasing brittleness, opacity, or surface finish.

Polymer-layered silicate nanocomposites are a new class of materials consisting of nanometer-sized filler dispersed in a polymer matrix. The nanometer length scales of the filler dominate the morphology and properties of these materials, producing higher property enhancements than those obtained from conventional fillers [1]. Typically, such nanocomposites contain clay-based layered silicates as the reinforcing filler. These silicates may be naturally occurring, like montmorillonite (MMT) or other smectites, or synthetic, like flourohectorite or flouromica [2]. They have thicknesses in the nanometer range and high aspect ratios (30-10,000) that have proven to be ideal for polymer reinforcement. Numerous studies have shown that a very low percentage of layered silicates, i.e., 3 to 6 wt%, can lead to significant enhancements of many properties, such as stiffness and strength [3, 4], flame retardancy [2, 5], gas barrier properties [6, 7], ionic conductivity [8, 9], thermal stability [10] and tunable biodegradability [2]. Such small amounts of filler produce almost no sacrifice in matrix properties, making them easy to process to near-final shape and simplifying their manufacture [1].

All these properties make these materials interesting prospects for a wide variety of applications, such as automotive, electronics, food packaging, biotechnology and many

others. Since high levels of stiffness and strength are obtained with significantly less amounts of high-density filler, they are much lighter than conventional composites. Weight advantages could offer great environmental benefits, like fuel efficiency and simpler packaging materials; the increased heat distortion temperature of these materials has also extended the use of nanocomposites to higher temperature environments, like under-the-hood applications in automobiles [1].

Polymer nanocomposites are materials with properties that offer significant commercial potential. Even though their commercial status is at an early stage, the current amount of research and development activities and patent publications in both industry and academia indicate that the widespread use of nanocomposites is imminent [11].

Although significant improvements have been made in developing nanocomposites with varying polymer matrices, a general understanding has yet to emerge. Critical questions are yet to be fully addressed, such as what allows nanocomposites to be both stiffer and tougher than conventional composites without sacrificing other properties, how can we utilize specific molecular interactions to control nanocomposite structure and morphology, and how can material properties be predicted from theoretical modeling [1]. Until now, substantial property enhancement has been demonstrated in only a fraction of the polymer nanocomposites fabricated to date; a high level of clay dispersion has only been obtained in clay nanocomposites made from nylon 6 and epoxy, and this phenomenon is not yet fully understood. In spite of this, nanocomposites based on low cost polyolefins, such as polypropylene, are being made

due to their great commercial importance, and some of these nanocomposites are now being used in automotive parts [12].

DISSERTATION SCOPE AND ORGANIZATION

This research addresses a number of fundamental issues involved in the melt processing of polymer nanocomposites with the purpose of obtaining a greater understanding of the clay exfoliation process. More specifically, it is desired to understand the effects of different polymer matrices, organoclay structures, and processing conditions on the morphology and mechanical properties of polymer-layered silicate nanocomposites prepared by melt processing.

This dissertation is divided into eight chapters. Chapters 2 and 3 were written to familiarize the reader with the basic knowledge and terminology that is used in this work and will aid in the understanding of the results and conclusions presented thereafter. Chapter 2 presents a background on the structure of layered silicates, more specifically montmorillonite, and the properties which make them unique for use in polymer nanocomposites. It also describes the most common polymer nanocomposite formation methods and explains how huge property enhancements are achieved, and the characteristics necessary to achieve them. Chapter 3 explains how polymer layered silicate nanocomposites are characterized, as well as the materials and equipment used to perform the analysis. The subsequent chapters methodically analyze different polymer-layered silicate nanocomposite systems and types of processing to assess their effects on morphology and mechanical properties.

Chapter 4 addresses the effect of polyamide type and processing temperature on the morphology and mechanical properties of nanocomposites made from nylon 6 (PA-6) and nylon 6,6 (PA-66). Chapter 5 further establishes the effect of processing on the

exfoliation of PA-6 nanocomposites. Chapters 6 and 7 analyze the effect of different types of organoclays on the morphology and properties of nanocomposites. Specifically, Chapter 6 explores the effect of the total clay layer charge on the degree of exfoliation in various polymer matrices, while Chapter 7 evaluates the effect of organoclay structure on the morphology and properties of thermoplastic polyurethane nanocomposites. Finally, Chapter 8 presents a summary and the general conclusions obtained from the current work, including recommendations for future work on this subject.

REFERENCES

[1] Vaia RA, Krishnamoorti R, *Polymer Nanocomposites: Synthesis, Characterization, and Modeling*. Krishnamoorti R,Vaia RA, Eds., ACS Symposium Series. Oxford University Press, Washington, D.C., 2001.

[2] Schmidt D, Shah D, Giannelis EP. Curr Opin Solid State Mater Sci 2002;6(3):205-212.

[3] Liu L, Qi Z, Zhu X. J Appl Polym Sci 1999;71(7):1133-1138.

[4] Wang Z, Pinnavaia TJ. Chem Mater 1998;10(12):3769-3771.

[5] Hu Y, Wang S, Ling Z, Zhuang Y, Chen Z, Fan W. Macromol Mater Engng 2003;288:272-276.

[6] Yano K, Usuki A, Okada A, Kurauchi T, Kamigaito O. J Polym Sci, Part A: Polym Chem 1993;31(10):2493-2498.

[7] Messersmith PB, Giannelis EP. J Polym Sci, Part A: Polym Chem 1995;33(7):1047-1057.

[8] Chen W, Xu Q, Yuan RZ. Materials Science & Engineering, B: Solid-State Materials for Advanced Technology 2000;B77(1):15-18.

[9] Chen W, Xu Q, Yuan RZ. Compos Sci Technol 2001;61(7):935-939.

[10] Yoon PJ, Fornes TD, Paul DR. Polymer 2002;43(25):6727-6741.

[11] Collister J, Commercialization of Polymer Nanocomposites. in *Polymer Nanocomposites: Synthesis, Characterization, and Modeling* Krishnamoorti R,Vaia RA, Eds. Oxford University Press, Washington, D.C., 2001, vol. 804, pp. 7-14.

[12] Garces JM, Moll DJ, Bicerano J, Fibiger R, McLeod DG. Adv Mater 2000;12(23):1835-1839.

CHAPTER 2

BACKGROUND

CLAY STRUCTURE AND MODIFICATION

Montmorillonite is the most commonly used clay for nanocomposite formation. It belongs to the smectite group of phyllosilicate clays containing a 2:1 layer consisting of two-dimensional layers where two tetrahedral sheets are fused to a central octahedral sheet. In the case of MMT, the tetrahedral sheets are composed of Si oxide, while the octahedral sheet is comprised of Al, Mg, and Fe oxides and hydroxides.

In the tetrahedral sheets (of composition Si_2O_5 in the case of MMT), the individual tetrahedra are linked together by sharing three oxygens each (called basal oxygens) to form a hexagonal structure. The fourth tetrahedral oxygen (called apical oxygen) lays in a direction normal to the sheet forming part of the adjacent octahedral sheet. In the octahedral sheet, the individual octahedra are linked together by sharing octahedral edges. The common plane between the tetrahedral and octahedral sheets consists of the shared apical oxygens and the unshared OH groups that lie at the center of each tetrahedra same z-level as the apical oxygens [1].

These layers organize themselves one on top of another to form stacks with a regular van der Waals gap in between them called the interlayer or gallery [2]. Most clays present some degree of isomorphic substitution, where the tetrahedral or octahedral cations are substituted by cations of lower oxidation number creating a charge deficiency that is balanced by metal cations located in the surface and interlayer spacing. The amount of isomorphic substitution and its location, i.e., in the tetrahedral or octahedral

sheets, determines the total layer charge and, hence the number of cations needed to neutralize the charge imbalance.

Montmorillonite clays present an isomorphic substitution of Al^{3+} cations in the octahedral sheets by cations such as Mg^{2+} or Fe^{2+}, this charge deficiency is balanced by hydrated cations situated in the interlayer. Figure 2.1 shows the structure of two MMT layers balanced by hydrated Na^{+} cations. Since the isomorphic substitution in MMT takes place in the inner octahedral sheet, the charge and the overall attraction of ions at the surface is small; this allows the layers to expand when hydrated. The ability to swell is one of the most important characteristics of these types of clays because they can expand as much as to lose interaction with one another which allows small molecules to intercalate readily between the layers [2, 3]. The extent of swelling depends on the size of the intercalated molecule and the total charge of the clay layers.

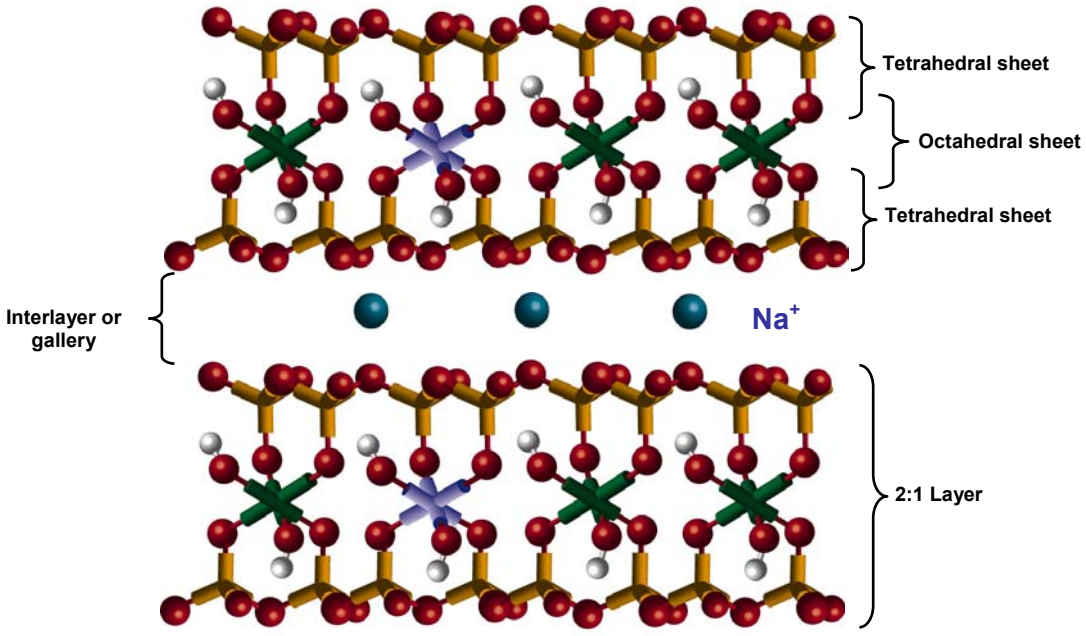

Figure 2.1 Structure of sodium montmorillonite

Because inorganic silicate layers tend to be hydrophilic and the polymers tend to be organophilic, organic treatment is required in most cases to improve compatibility with the polymer matrix for nanocomposite formation [2, 4]. For this reason, swelling smectite clays are unique because they can be rendered organophilic by exchanging the surface cations with organic cations. The cations most commonly used for nanocomposite formation are alkyl ammonium surfactants and the clays organically modified with these surfactants are termed *organoclays*. Alkyl ammonium surfactants are comprised of a polar head group (a quaternary ammonium ion) and one or many non-polar alkyl tails; the remaining substituents can be non-polar or polar functional groups, such as methyl or hydroxy ethyl substituents, respectively. Figure 2.2 illustrates the structure of an alkyl ammonium surfactant.

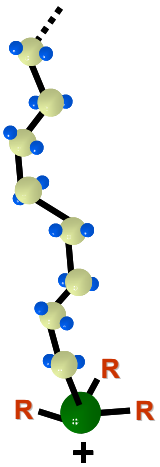

Figure 2.2 Structure of an alkyl ammonium surfactant.

The intercalation of alkyl ammonium surfactants between the clay layers not only increases the organophilic character of the clay, but it also expands the interlayer distance; thereby promoting the separation of the individual layers and the diffusion of the matrix polymer chains inside the clay galleries. The increase in gallery height

depends on the molecular weight and volume occupied by the surfactant and on the total layer charge or cation exchange capacity (CEC), which is the sum of the total number of exchangeable cations that can be adsorbed (expressed in milliequivalents per 100 g of clay). Figure 2.3 illustrates the cation exchange reaction that takes place during organoclay formation. As the negative charge originates in the silicate layer, the cationic head-group of the alkyl ammonium surfactant preferentially resides at the layer surface, while the surfactant molecules pack efficiently in the space available inside the gallery.

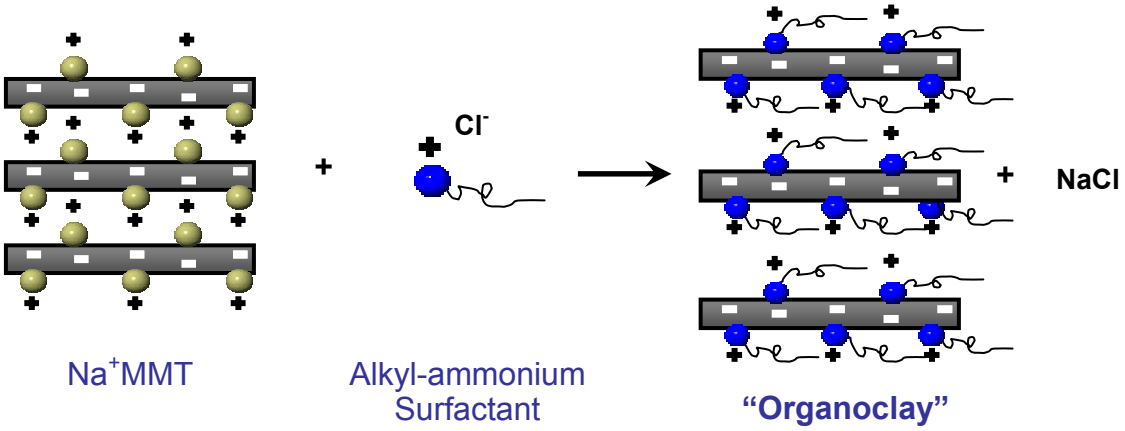

Figure 2.3 Cation exchange reaction in organoclay formation.

METHODS OF PREPARATION

The three most widely used methods for nanocomposite preparation are *in-situ* polymerization, solvent blending, and melt processing. *In-situ* polymerization consists in cationically exchanging the montmorillonite clay with a polymerization initiator or catalyst prior to swelling within a liquid monomer or monomer solution [2]; polymerization is then initiated in the clay surface and the silicate platelets are dispersed within the polymer matrix. The Toyota research laboratories sparked a large interest in

nanocomposites prepared by this technique due to the superior strength, modulus, heat distortion temperature, and water and gas barrier properties of PA-6 nanocomposites with respect to pure PA-6 [5-9]. Solvent blending involves dispersing the montmorillonite clay in a polymer solution; the polymer then adsorbs onto the silicate layers and the solvent is extracted [2]. This method generally leads only to low levels of platelet separation due to the rearrangement of the silicate layers when the solvent is removed [10]. Lastly, melt processing involves melt blending the polymer and the organoclay using conventional extrusion processes, where the shear created by the extruder promotes interactions between the polymer and the organoclay and the diffusion of the polymer chains inside the organoclay galleries.

For most technologically important polymers, approaches such as *in-situ* polymerization and solvent blending are limited, since neither a suitable monomer nor a compatible polymer-host solvent system is always available [11]. On the other hand, melt processing provides a good alternative for most commercial polymers. It has proven to be an efficient and environmentally safe method of producing materials with comparable properties to those prepared by the other techniques, thereby offering flexibility of formulation for the end user and cost reduction [12, 13]. The nanocomposite materials presented in this dissertation were fabricated via melt processing.

EXFOLIATION IS THE KEY TO HIGH PERFORMANCE

Each clay particle is originally about eight microns in size, and there are more than three thousand individual layers or platelets in each particle. The preparation of a true nanocomposite requires complete dispersion, or exfoliation of the distinct clay layers

within the polymer matrix, without any aggregation into larger units [3]. This is shown in Figure 2.4. Once complete exfoliation of the clay platelets is achieved, enhanced improvements in polymer performance are observed. A complete dispersion optimizes the number of reinforcing elements (individual platelets) for carrying applied load, while the high aspect ratios decrease gas permeability and solvent uptake as well as increase thermal stability and fire retardancy. All of these benefits are unattainable with larger-scaled fillers [3]. Complete exfoliation can lead to an exceptionally large interfacial area between the constituents even at very low filler levels.

Since many properties of nanocomposites improve with the degree of dispersion of the individual clay particles, clay exfoliation is the subject of a great deal of research in the field of nanocomposites [4].

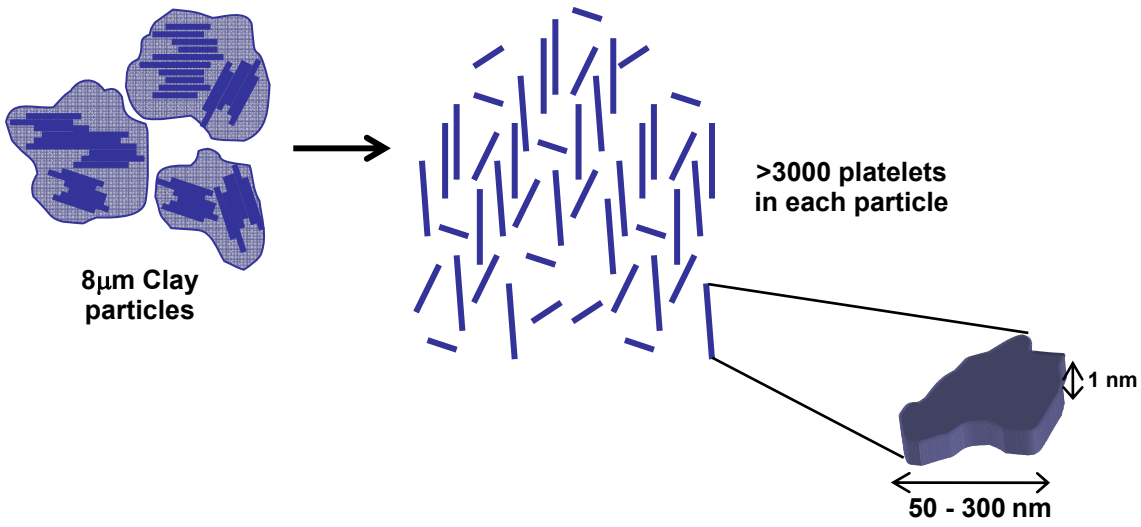

Figure 2.4 Clay particles and clay platelets.

High levels of exfoliation require favorable polymer-organoclay interactions and optimal processing conditions. The affinity of the polymer with the surface of the clay

and/or with the organic surfactant of the organoclay is essential to promote favorable interactions between these species and hence obtain a good exfoliation. In the case of nanocomposite formation by melt processing, processing conditions such as temperature, shear stresses, and residence time, affect the melt viscosity of the polymer matrix and the organoclay degradation, which ultimately influence clay dispersion and exfoliation.

REFERENCES

[1] Bailey SW, *Crystal Structures of Clay Minerals and their X-ray Identification*. Brindley GW,Brown G, Eds., Mineralogical Society. Spottiswoode Ballantyne Ltd., London, 1980, pp. 945.

[2] Alexandre M, Dubois P. Materials Science & Engineering, R: Reports 2000;R28(1-2):1-63.

[3] Carrado KA, Polymer-Clay Nanocomposites. in *Advanced Polymeric Materials: Structure Property Relationships* Shonaike GO,Advani SG, Eds. CRC Press LLC, Boca Raton, FL, 2003 pp. 349-396.

[4] Collister J, Commercialization of Polymer Nanocomposites. in *Polymer Nanocomposites: Synthesis, Characterization, and Modeling* Krishnamoorti R,Vaia RA, Eds. Oxford University Press, Washington, D.C., 2001, vol. 804, pp. 7-14.

[5] Kojima Y, Usuki A, Kawasumi M, Okada A, Fukushima Y, Kurauchi T, Kamigaito O. J Mater Res 1993;8(5):1185-1189.

[6] Usuki A, Koiwai A, Kojima Y, Kawasumi M, Okada A, Kurauchi T, Kamigaito O. J Appl Polym Sci 1995;55(1):119-123.

[7] Kojima Y, Usuki A, Kawasumi M, Okada A, Kurauchi T, Kamigaito O. J Polym Sci, Part A: Polym Chem 1993;31(4):983-986.

[8] Kojima Y, Usuki A, Kawasumi M, Okada A, Kurauchi T, Kamigaito O. J Appl Polym Sci 1993;49(7):1259-1264.

[9] Kojima Y, Fukimori K, Usuki A, Okada A, Kurauchi T. J Mater Sci Lett 1993;12:889-890.

[10] Fornes TD. Ph.D. Thesis, The University of Texas at Austin, 2003.

[11] Vaia RA, Giannelis EP. Macromolecules 1997;30(25):7990-7999.

[12] Cho JW, Paul DR. Polymer 2000;42(3):1083-1094.

[13] Fornes TD, Hunter DL, Paul DR. Macromolecules 2004;37(5):1793-1798.

CHAPTER 3

EXPERIMENTAL TECHNIQUES

This chapter describes the materials and equipment and the characterization techniques used in this work. The first section gives information on the techniques applied to evaluate the morphology and mechanical properties of polymer nanocomposites, while the materials, equipment, and processing conditions employed in this dissertation are discussed afterwards. Each subsequent chapter contains a brief description of the materials, equipment and techniques used in that chapter, as well as any additional information specific to that study.

CHARACTERIZATION TECHNIQUES

As mentioned before, the properties of polymer-clay silicate nanocomposites are highly dependent upon the degree of clay dispersion, or delamination, of clay particles that is determined by the nature of the components used, e.g., the type of polymer matrix and organoclay, and by the method of preparation. Based on this, nanocomposites are generally grouped into three main categories: phase separated or immiscible, intercalated, and exfoliated nanocomposites [1]. An immiscible nanocomposite is formed when the polymer is unable to penetrate between the silicate layers giving place to a morphology composed of large stacks of platelets surrounded by the polymer matrix; these large stacks of platelets are often referred to as tactoids or agglomerates [2]. An intercalated composite is obtained when a small amount of polymer enters the gallery spacing between the clay platelets; in this case, the individual platelets are separated from one another but their ordered structure still remains. Lastly, an exfoliated or delaminated

composite is referred to the case when the silicate layers are fully dispersed in the polymer matrix. Figure 3.1 illustrates each type of composite.

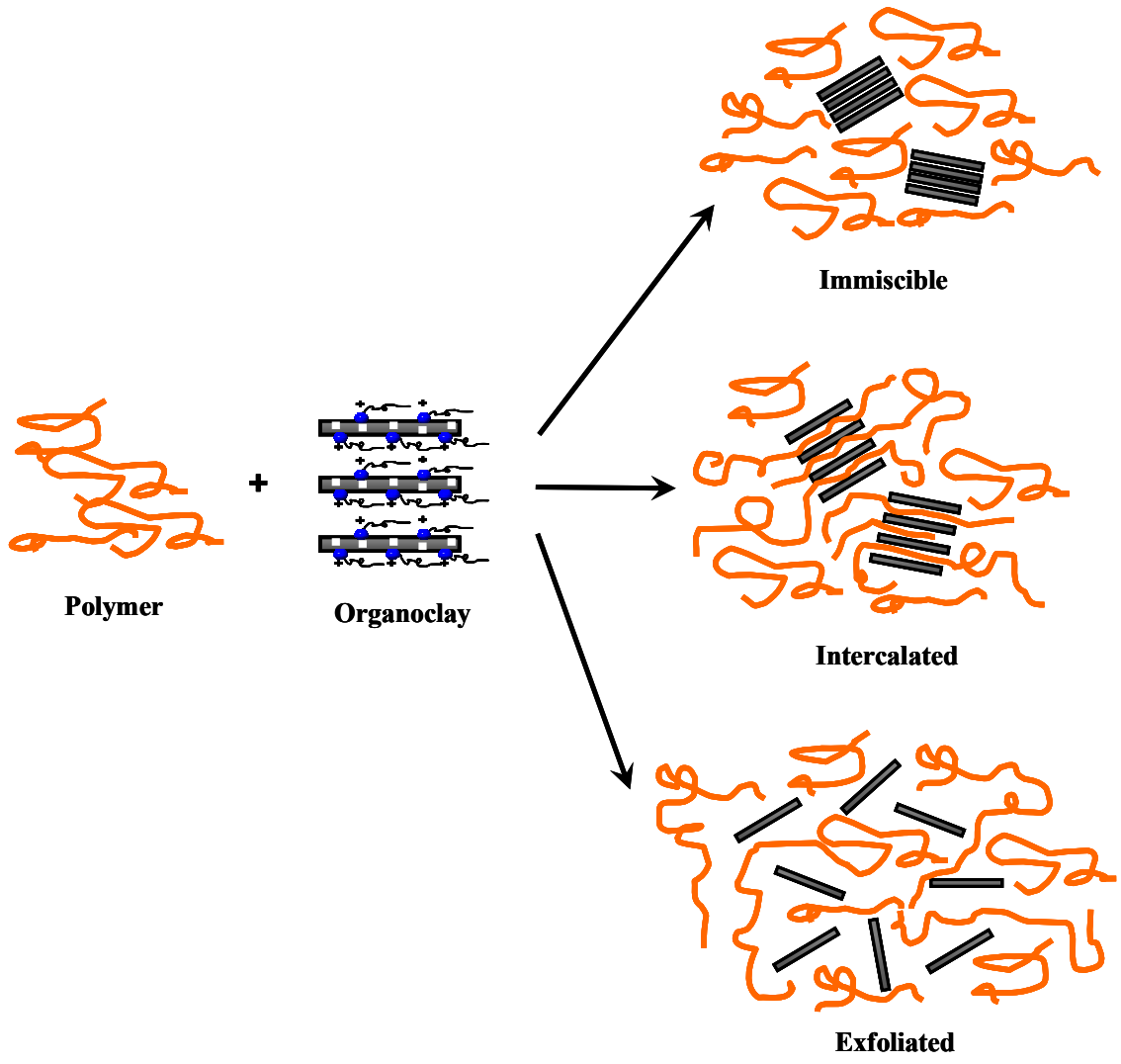

Figure 3.1 Illustration of the different types of nanocomposites that may be produced from the combination of a polymer matrix and an organoclay.

Wide Angle X-ray Scattering and TEM Imaging

Wide angle X-ray scattering (WAXS) and transmission electron microscopy (TEM) imaging are generally combined to characterize the morphology of these nanocomposites. WAXS characterizes the repetitive multilayer structures that change as the polymer intercalates into the clay galleries by determining the interlayer spacing between the silicate layers. The angle corresponding to the first order diffraction peak is related to the interlayer spacing through Bragg's relation:

$$\lambda = 2d\sin\theta \tag{3.1}$$

where λ corresponds to the wavelength of the X-ray radiation used, d is the spacing between the diffractional lattice planes, and θ is the measured diffraction angle [1]. Immiscible composites show WAXS patterns with basal spacings similar to those of the pure organoclays. In intercalated composites, the peak position generally shifts to lower angles or higher d-spacings of the order of 20 to 30 Å [2]. As the intercalation increases, the peak decreases in height and broadens until no peak is observed; which is the typical WAXS pattern for exfoliated composites. In completely exfoliated structures, no diffraction peaks are visible because the large spacing between the silicate layers exceeds the sensitivity of the X-ray diffraction machine. Figure 3.2 shows examples of the typical composite structures and their corresponding WAXS patterns and TEM images.

Besides the well-defined structures described above, mixed structures and high levels of clay platelet disorder can be present, which are not characterized accurately by WAXS. These mixed structures broaden the X-ray peak and increase the interference of the X-ray signal. For this reason, TEM imaging is a very illustrative and a much needed complimentary tool to monitor clay dispersion. Since TEM imaging techniques sample a very small area due to the high magnifications required to distinguish the nanometer-

sized clay platelets, a large number of particles have to be analyzed to draw representative conclusions.

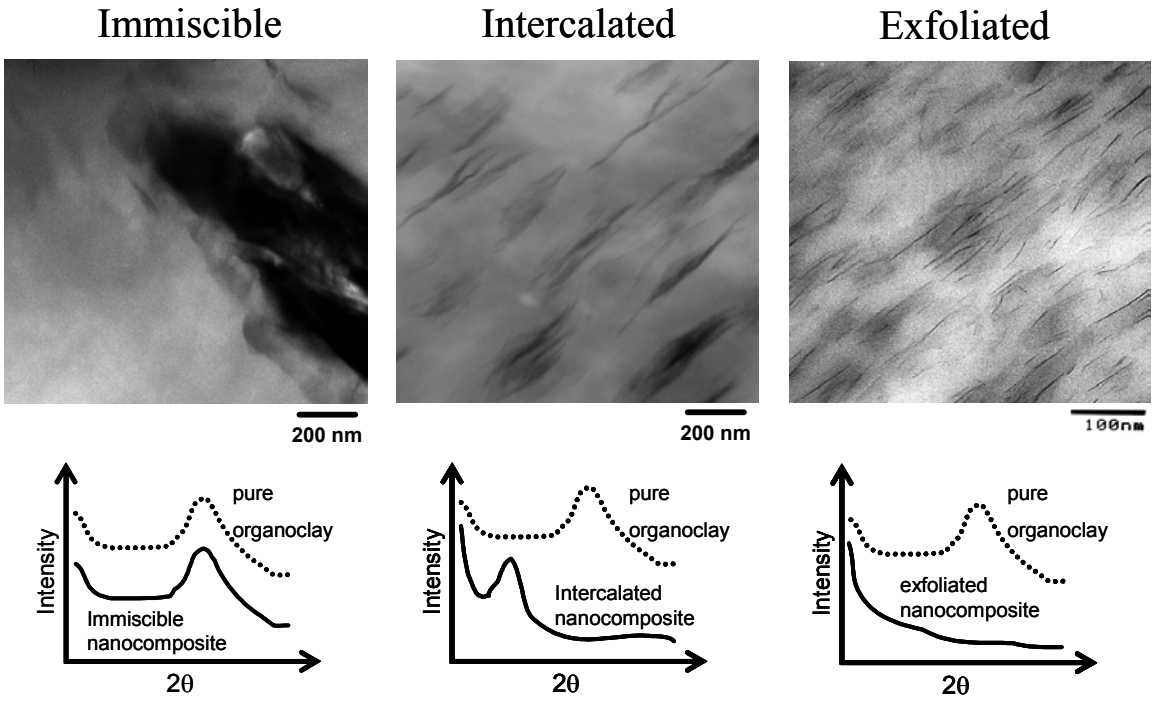

Figure 3.2 TEM and WAXS illustration of the three different classifications of nanocomposite morphology

Dark-field scanning transmission electron microscopy (dark-field STEM) is sometimes used to corroborate the morphology analyzed by WAXS and TEM. When using the dark-field STEM technique, the MMT platelets appear white while the polymer matrix, holes in the specimen, or any other low-atomic-density constituent are seen as a black background.

Mechanical Properties

Mechanical properties of materials are among the most important properties for material selection and end-use applications. Since practically all applications involve

some kind of loading, mechanical property research is most logical because it predicts the response of materials under mechanical loading. The assessment of mechanical properties involves measuring tensile and flexural properties and impact strength. In this dissertation, only tensile properties were measured since they provide the essential information for most applications such as Young's modulus, yield strength, elongation at yield, elongation at break, tensile strength, and ultimate tensile strength. The sample shape for this technique is a characteristic dumbbell or dogbone that localizes sample displacement in the central region for higher accuracy [3]. Figure 3.3 shows a typical stress-strain curve for nylon 6 (PA-6) and points out the tensile properties outlined above.

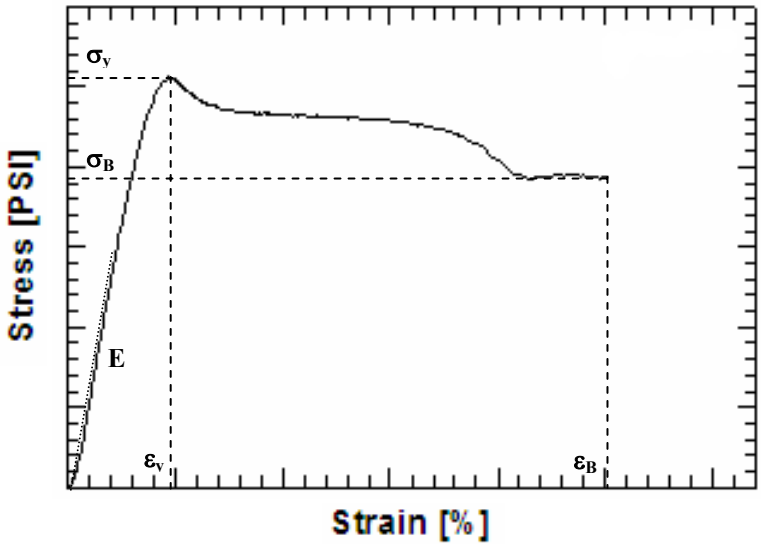

Figure 3.3 Typical stress-strain curve for PA-6.

The slope of the initial linear portion of the stress-strain curve is the Young's modulus,

$$E = d\sigma/d\varepsilon \tag{3.2}$$

where σ is the stress or the measured force of displacement divided by the cross sectional area of the sample in the central region and ε is the strain or the change in length divided

by the original length of the specimen. The modulus is a parameter unique to a specific material and it is a measure of its stiffness, i.e., the resistance to deformation when an external force is applied. The point where the curve deviates from linear or elastic behavior commencing permanent deformation is the yield point, characterized by the stress at yield σ_y and the elongation at yield ε_y. The yield strength of the material is obtained by dividing the stress at yield by the cross sectional area of the sample and it is a measure of the strength of the material before permanent deformation. The end of the curve indicates the failure of the material, which is characterized by the stress at break σ_B and the elongation at break ε_B. The ultimate tensile strength (UTS) is the strength at the breaking point and the tensile strength (TS) is the strength at the point of maximum stress; this may or may not be equal to the yield strength or ultimate tensile strength [3, 4].

In composite materials, the mechanical properties depend on the properties of the individual constituents, on the shape of the reinforcing component, and on the nature of the interface between the phases. The addition of a rigid filler or reinforcing component generally increases the modulus more or less independent of the extent of adhesion between the matrix and the filler. In polymer-layered silicate nanocomposites, the addition of clay substantially increases the Young's modulus with respect to the pure polymer even at loadings as small as 1.5 wt% MMT. The yield strength increases with the addition of clay, as clay loading is increased, and as clay dispersion is improved. It is a measure of the interfacial strength between the matrix and the filler and it increases as the particle size decreases and the interfacial area increases. The rate of increase in yield strength depends greatly on the adhesion between the matrix and the filler and on the degree of exfoliation of the clay in the polymer matrix, since large aggregates produce small interfacial areas and may break as the load is applied. Generally, fillers cause a

decrease in elongation at yield and elongation at break; the ductility of polymer-layered silicate nanocomposites is reduced with the addition of clay, with increased clay concentration, and with low clay dispersion.

Particle Analysis and Composite Theory Modeling

The properties of polymer-clay silicate nanocomposites are highly dependent upon the ultimate aspect ratio of the filler, which is related to the degree of exfoliation and the inherent geometry of the pristine clay platelets. In most cases in the literature, a qualitative assessment is made between the degree of exfoliation, as determined by WAXS and TEM, and the corresponding mechanical properties of nanocomposites. But this is only sufficient for the *distinction* between a well- and a poorly-exfoliated system. Taking into account the fact that sometimes a qualitative judgment is not enough, we have conducted detailed particle analysis of TEM photomicrographs in an effort to provide quantitative assessments of clay structure-nanocomposite property relationships.

Particle analysis of polymer nanocomposites is not a trivial task due to the low contrast of TEM micrographs. Particle-analyzing software requires an image with high contrast between the background and the particles to perform an accurate analysis. In nanocomposite TEM micrographs, the background has many shades of gray corresponding to slight variations in thickness. These thick areas sometimes have the same shade of gray as some organoclay particles, which make it difficult for the program to distinguish between a thick area and a particle. Because of this, TEM micrographs have to be transformed into high contrast images that can be accurately analyzed by software. A semi-automated method to obtain these high contrast images was developed in this lab by Fornes et al. [5, 6]. This technique, which was originally developed for characterizing the morphology of polymer-polymer blends, involves manually tracing the

particles from an original TEM image and analyzing the result with particle-analyzing software. Even though these manual methods are subjective, since the results may vary to some extent from user to user, they seem to quantify the morphology of PA-6 nanocomposites in a way that produces acceptable results for theoretical modeling [5, 7].

As used here, the term particle refers to either a single platelet or multiple platelets in a stack or agglomerate. In agglomerates many platelets are stacked together while the single platelets are separate from any other organoclay material. The average particle density is the average number of particles per μm^2, while the specific particle density is the average particle density normalized to a specific clay concentration, i.e., 1 and 5.5 wt% MMT. At the same clay concentration, the particle density is an indicator of the extent of exfoliation of clay platelets in the polymer matrix. Samples with a low particle density have large particles with high platelet agglomeration and, as the particle density increases, the particle size decreases as a result of the breakup of large particles, producing better dispersion. The average number of platelets per particle is determined, on the micrograph with the best contrast, by manually counting the number of platelets in each of the identified particles. The average particle thickness is obtained considering that the thickness of each particle is defined as

$$t_{particle} = d_{001}(n-1) + t_{platelet} \tag{3.3}$$

where $t_{particle}$ is the thickness of each particle, d_{001} is the repeat spacing for the intercalated clay or organoclay, n is the number of platelets per particle, and $t_{platelet}$ is the thickness of each individual MMT platelet. Fornes and Paul suggest that the appropriate values for this equation are $d_{001} \cong 1.8$ nm, and $t_{platelet} = 0.94$ nm, based on a variety of information explained in their paper [5]. The same values were used in this work. The average aspect ratio is taken as the ratio of the number average particle length to the number average thickness.

Theoretical modeling is an appealing approach for the design of polymer nanocomposite systems; however, one must keep in mind the assumptions that are typically made. In all cases, it is assumed that the polymer matrix is not affected by the presence of the filler, and in many cases, it is also assumed that the filler is perfectly aligned, that there is good bonding between the matrix and the filler, that the matrix and the filler are isotropic, and that there are no filler particle-particle interactions or agglomeration [5]. The theories do not account for the effect of crystallinity level (or type) of the matrix that may be changed by the filler. In spite of this, Fornes et al. showed that the Halpin-Tsai and Mori-Tanaka composite theories capture the modulus behavior of nylon 6 nanocomposites to an acceptable extent [5]. The same modeling approach was applied to some results reported here.

It is useful to note that the Halpin-Tsai theory considers the particles as rectangular platelets while the Mori-Tanaka theory regards them as ellipsoidal particles and takes the Poisson's ratio into account. A more complete discussion of these and other issues was given by Fornes et al. [5]. Hine et al. showed that, for fiber composites, with a distribution of fiber lengths, the use of the number average fiber length in the Halpin-Tsai equations gives the best match to more rigorous modeling that fully accounts of the length distribution [8]. Based on this reasoning, the aspect ratio was calculated as the ratio of the number average particle length to the number average particle thickness, i.e., $(\bar{\ell})_n / (\bar{t})_n$, obtained from the particle analysis mentioned earlier. It is important to note that this ratio is not the same as the number average aspect ratio, i.e., $(\ell / t)_n$.

Other Characterization Techniques

Other characterization techniques involve determining the actual MMT content in each nanocomposite blend, loss on ignition (LOI) tests, Brabender torque rheometry,

isothermal thermo-gravimetric analysis (TGA), differential scanning calorimetry (DSC) analysis, and cation exchange capacity (CEC) determination. The actual MMT in the nanocomposite samples is determined from the ash content of dried pellets heated at 900ºC for 45 min. The residual ash is weighted and corrected for the loss of structural OH groups in the form of water from heating the clay at high temperatures (dehydroxilation) by the following equation [6, 9].

$$\% \text{ MMT} = \%\text{MMT}_{ash} / 0.935 \quad (3.4)$$

where % MMT_{ash} is the mass after incineration, relative to the original nanocomposite mass. All data in this work are reported in terms of weight percent montmorillonite (wt% MMT) in the composite rather than the amount of organoclay, since the silicate is the reinforcing component.

The percentage loss on ignition (LOI) is obtained by applying the same heating procedure to dry organoclay in powder form; which is the amount of organic modifier contained within the galleries of the pristine organoclay.

Since the melt viscosity of the polymer matrix has a significant influence on the degree of exfoliation of clay in polymer-layered silicate nanocomposites [6], Brabender torque rheometry is used to compare the relative melt viscosity of different materials at different processing temperatures to asses differences in clay dispersion. In this technique, the torque is measured every minute until it reaches an equilibrium value at approximately 10 min. The equilibrium torque is recorded and compared to the equilibrium torque of other materials.

The high temperatures encountered in the extrusion process cause degradation of the organic modifier in organoclays [10]. Isothermal TGA measurements are performed on the dry organoclay to determine the effect of processing temperature on the stability of the organic modifier. In this procedure, the weight of the sample is measured as the

temperature is increased. Generally, as the sample degrades, the decomposition products volatilize, resulting in a change of weight [3]. Montmorillonite is known to withstand temperatures as high as 1000ºC, while organic modifiers begin to degrade above about 190ºC or higher [10]. Through isothermal TGA performed at the processing temperature, the percentage loss of organic modifier can be calculated for the average residence time of the extruder.

The addition of clay particles has an effect on the rate of crystallization and percent crystallinity of the matrix for polymer-layered silicate nanocomposites [11]. Differential scanning calorimetry (DSC) is performed on nanocomposite samples in order to determine the percent crystallinity of the polymer matrix. In this procedure, the energy required to heat a sample to a specified temperature, with respect to a reference, is measured. When a sample goes through a transition such as from an amorphous to a crystalline state, or vice versa, heat is either absorbed or emitted without a corresponding change in the temperature of the sample; these heat flows are shown as endothermic peaks or exothermic valleys in a DCS scan [3]. In this work, the sample was heated at a specific rate, from room temperature to above its melting point. The change from a solid (crystalline) to a molten (amorphous) state produces an endothermic peak that can be used to calculate the heat of fusion for a specific sample by integrating the heat flow over the temperature range involved in this transition. The percent crystallinity was calculated as the ratio of the heat of fusion of the sample (ΔH_f) to the heat of fusion of the purely crystalline form of the polymer matrix (ΔH^o_f).

CEC determination was performed on dry montmorillonite clays by saturating the exchange sites with ammonium ions followed by the extraction and titration of the exchanged ammonium. This is done by two cation exchange reactions: in the first one, the surface and inter-gallery cations of the clay are exchanged with ammonium ions by

reacting the clay with ammonium acetate, the remaining clay is then purified with ethanol, and pure ammonium-MMT is obtained. In the second cation exchange reaction, the ammonium-MMT is reacted with sodium hydroxide to extract the ammonium ions; the extracted solution is heated to produce ammonia, which is distilled, into an excess of boric acid. Hydrochloric acid is then used to titrate the ammonium borate and measure the amount of exchangeable cations in the clay, i.e., the cation exchange capacity of the clay.

MATERIALS AND EQUIPMENT USED IN THIS STUDY

Materials

All polymer materials and most of the organoclays employed in this work are commercially available and can be obtained in large quantities at relatively low cost. Six types of polymer matrices were used here: nylon 6, nylon 66 (PA-66), two thermoplastic polyurethanes (TPU's), with different chemical structures and hard segment concentrations, and polypropylene/polypropylene modified with maleic anhydride (PP/PP-g-MA) systems. These polymer materials are described in Table 3.1. The polyamide and polyurethane materials are extrusion or injection molding grades, chosen to have high melt viscosities in order to promote the exfoliation of the organoclay [6]. The polyolefin materials used were selected based on previous work from our laboratories, regarding the effect of the ratio of PP-*g*-MA to organoclay on the structure-property relationships for PP-based nanocomposites [12]. Polyamide- and polyurethane-containing materials were dried in a vacuum oven at 80ºC for a minimum of 16 h prior to each processing step, while the polyolefin-based materials were used as received.

Table 3.1 Polymer materials used in this work.

Material (designation used here)	Supplier designation	Specifications	Supplier
Nylon 6 (PA-6)	Capron B135WP	M_n = 29,300[a] MFI = 1.2 g/10 min	Honeywell
Nylon 66 (PA-66)	Zytel 42A	Not available	Dupont
Medium-Hardness TPU (M-H TPU)	Pellethane 2102-90AE	Polyester-based TPU: *Methylenediphenyl diisocyanate* *1,4 - butanediol* *ε - caprolactone* Shore D hardness = 58D	Dow Plastics
High-Hardness TPU (H-H TPU)	Elastollan 1174D50	Polyether-based TPU: *Methylenediphenyl diisocyanate* *Poly (tetrahydrofuran)* Shore D hardness = 73D	BASF
Polypropylene (PP)	Hi-Fax PH020	MFI = 37 g/10min (230ºC)	Basell
Maleated Polypropylene (PP-*g*-MA)	Polybond 3200	wt% MA = 1.0	Uniroyal Chemical Co.

[a] M_n determined via intrinsic viscosity using *m*-cresol at 25ºC

Two different types of organoclays were used in this work, commercial organoclays and organoclays containing reduced cation exchange capacities. The commercial organoclays were donated by Southern Clay Products and were used as received. They were formed by a cation exchange reaction between sodium montmorillonite and various alkyl ammonium surfactants derived from natural products such as tallow and coco oils. These alkyl ammonium compounds were supplied by Akzo Nobel to Southern Clay Products. The chemical structures of these surfactants are shown in Fig. 3.4 and a description of these organoclays is made in Table 3.2. The nomenclature used to describe the substituents on the ammonium compounds are as

follow: The letters M, and HE represent methyl and 2-hydroxy-ethyl substituents, respectively, while C*, T, and HT represent units that consist of a distribution of saturated and unsaturated long chain hydrocarbon units (C* denotes coconut oil -predominantly C_{12} alkyl chains-, T is for tallow -predominantly C_{18} alkyl chains-, and HT refers to a tallow-based product in which the majority of the double bonds have been hydrogenated).

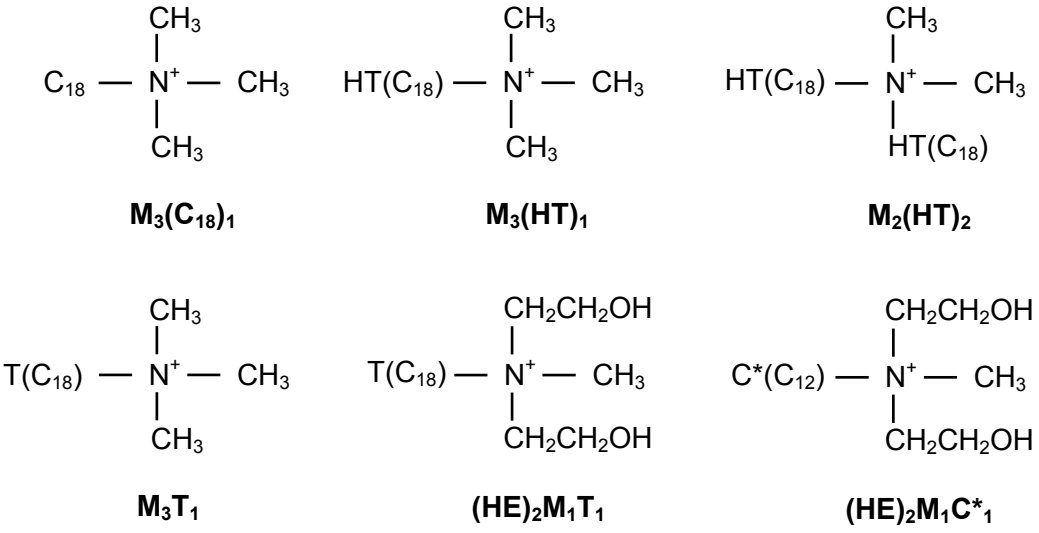

Figure 3.4 Molecular structure and nomenclature of the amines used to form the organoclays used in this work.

Organoclays containing reduced cation exchange capacities were formed by the cation exchange reaction of $M_3(HT)_1$ and $(HE)_2M_1T_1$ alkyl ammonium surfactants and several montmorillonite clays with reduced cation exchange capacities. These montmorillonite clays were supplied by the Commonwealth Scientific and Industrial Research Organization Laboratories (CSIRO) in Australia, and they were produced by exchanging specific percentages of Na^+ cations on pristine sodium montmorillonite with Li^+ cations. Subsequent heating at temperatures between 150 and 300ºC for more than 24

hours produces the fixation of Li^+ cations into the silicate layers, reducing the cation exchange capacity of the clay. More details on this procedure are given in Chapter 6.

Table 3.2 Commercial organoclays used in this work.

Organoclay	Supplier designation	Specifications	Supplier
$M_3(C_{18})_1$	**Experimental:** Octadecyltrimethyl ammonium chloride organoclay	95 MER[a] Organic content = 29.6 wt% d_{001} spacing = 18.1 Å	SCP[b]
$M_3(HT)_1$	**Experimental:** Trimethyl hydrogenated-tallow ammonium chloride organoclay	95 MER Organic content = 29.6 wt% d_{001} spacing = 18.0 Å	SCP
$M_2(HT)_2$	**Cloisite 20A:** Dimethyl bis(hydrogenated-tallow) ammonium chloride organoclay	95 MER Organic content = 39.6 wt% d_{001} spacing = 24.2 Å	SCP
M_3T_1	**Experimental:** Trimethyl tallow quaternary ammonium chloride organoclay	95 MER Organic content = 29.1 wt% d_{001} spacing = 17.8 Å	SCP
$(HE)_2M_1T_1$	**Cloisite 30B:** Bis(2-hydroxy-ethyl)methyl tallow ammonium chloride organoclay	90 MER Organic content = 31.5 wt% d_{001} spacing = 17.9 Å	SCP
$(HE)_2M_1C^*_1$	**Experimental:** Bis(2-hydroxy-ethyl)methyl coco ammonium chloride organoclay	95 MER Organic content = 26.4 wt% d_{001} spacing = 15.2 Å	SCP

[a] MER: Milliequivalent ratio of surfactant added for the reaction [mequiv/ 100 g of clay].
[b] Southern Clay Products (SCP), Gonzales, TX, USA.

Equipment and processing conditions

Melt processing

As mentioned earlier, all the nanocomposites analyzed in this dissertation were prepared by melt processing techniques. Polymer and organoclay were melt mixed using a twin screw extruder at a temperature slightly above the melt temperature of the

polymer. These composites were subsequently injection molded into tensile bars using an injection molding machine. After molding, the specimens were subjected to tensile tests for mechanical property evaluation and microtomed to form samples for TEM morphology analysis.

Three twin screw extruders were used in this dissertation. The first two extruders are co-rotating, intermeshing twin screw extruders (TSE's): a Werner and Pfleiderer ZSK 25 (diameter = 25 mm, L/D = 48), and a Haake (diameter = 30.5 mm, L/D = 10); while the third one is a 5 mL DSM micro-compounder that consists of a vertical barrel with two conical screws (screw diameter ranges from 0.43 to 1 cm, screw length = 10.75 cm). The DSM micro-compounder is a batch-type compounder where roughly 3 g of polymer are added at a time. Diagrams of these compounders are illustrated in Chapter 5, Figure 5.1.

The extrudates of the ZSK 25 and Haake TSE's were pelletized, and later injection molded into ASTM D638 tensile specimens using an Arburg Allrounder 305-210-700 injection molding machine. Each 3 g batch produced in the DSM micro-compounder was injection molded into custom (7.3 x 1 x 0.32 cm) bars using a DSM bench-top micro-injection molder. After molding, the specimens were sealed and placed in a vacuum desiccator for a minimum of 24 h prior to mechanical testing.

Characterization

Mechanical testing was performed according to ASTM D638 using an Instron 1137 testing machine. Values for modulus, using an extensometer, and yield strength were obtained at a crosshead speed of 0.51 cm/min, while elongation at break was determined at 0.51 cm/min and/or 5.1 cm/min and calculated from crosshead travel using an effective gauge length of 9.04 cm. The values reported here represent an average of five specimens for modulus and yield strength, and three to six specimens for elongation

at break for the samples injection molded in the Arburg Allrounder 305-210-700 injection molding machine, while the Young's modulus from the samples molded in the DSM micro-injection molder was obtained by testing a total of three specimens five times each, and averaging the responses; these five repetitions were performed under 1% strain where no hysteresis could be detected [13]. The Young's modulus is the only tensile property that can be measured for the samples prepared in the DSM micro-compounder since the bars formed by the DSM micro-injection molder do not have tabs needed to measure failure properties.

WAXS scans were made using a Scintag XDS 2000 diffractometer in reflection mode, with an incident wavelength of 1.542 angstroms at a scan rate of 1.0 deg/min. The analysis was performed using tensile bars for the polymer samples while the clay was analyzed in powder form. The TEM micrographs were obtained using a JEOL 2010F transmission electron microscope operating at an accelerating voltage of 120 kV and/or a Phillips EM208 transmission electron microscope with an accelerating voltage of 80 kV. TEM samples for particle characterization were cryogenically cut into ultra thin sections (30-70 nm thick) with a diamond knife at temperatures of -40 ºC and below using a Reichert-Jung Ultracut E microtome and/or a RMC PowerTome XL ultramicrotome with a CR-X universal cryosectioning system. These sections were taken from the central part of tensile bars in different orientations with respect to the mold filling direction during tensile bar formation. There are three major orientations for TEM specimen imaging that are used in this work: a) specimen microtomed normal to the flow direction (FD) and viewed in TEM parallel to the flow direction, b) microtomed normal to the transverse direction (TD) and viewed parallel to the transverse direction, and c) microtomed normal

to the normal direction (ND) and viewed parallel to the normal direction. Figure 3.5 shows the WAXS and TEM orientations used in this work.

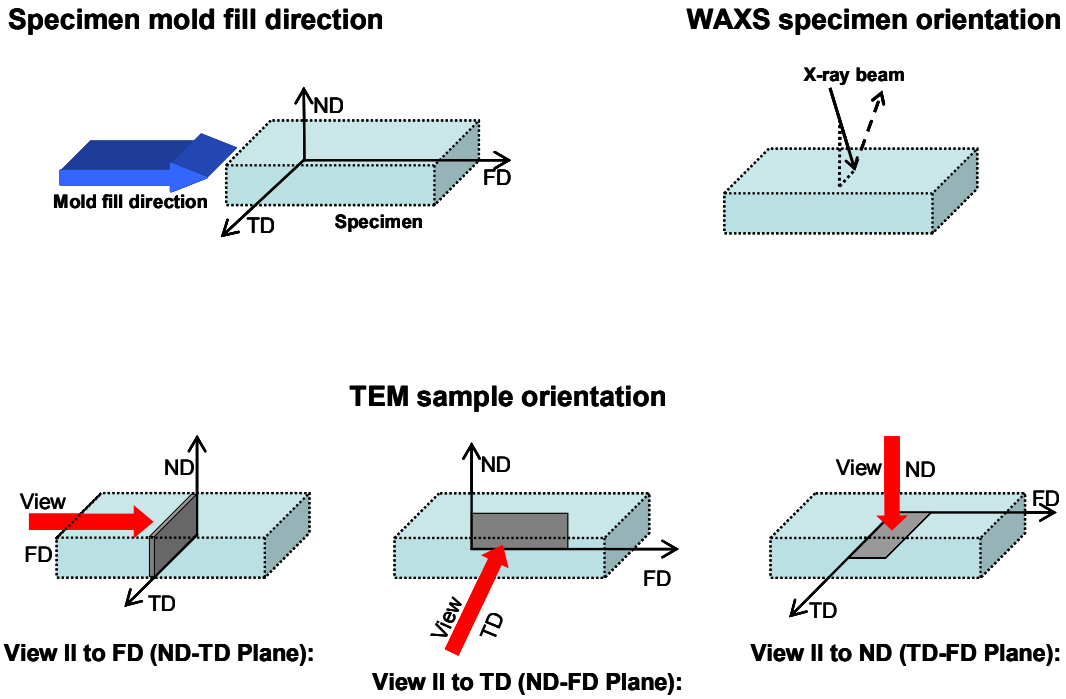

Figure 3.5 Specimen mold fill direction, WAXS specimen orientation, and TEM sample orientations used in this work.

The particle analysis was done with Adobe Photoshop, using three TEM micrographs, or a minimum of 400 particles, with a magnification that allows the observation of a relatively large number of particles. The average particle length was determined by tracing the organoclay particles electronically, within Adobe Photoshop, into a transparent layer [14] as outlined in a previous study [7]. The zoom tool on the program was used to identify and distinguish the particles more clearly. Figure 3.6 shows an example of a TEM micrograph and the resulting high contrast image. The high

contrast images were later analyzed by automated image analysis using Scion Image Software developed by National Institutes of Health and/or by using the Image Processing Toolkit (IPTK)^{TM} 5.0 software; a commercially available set of plug-ins, for use with Adobe Photoshop, developed by Reindeer Graphics Inc. [15].

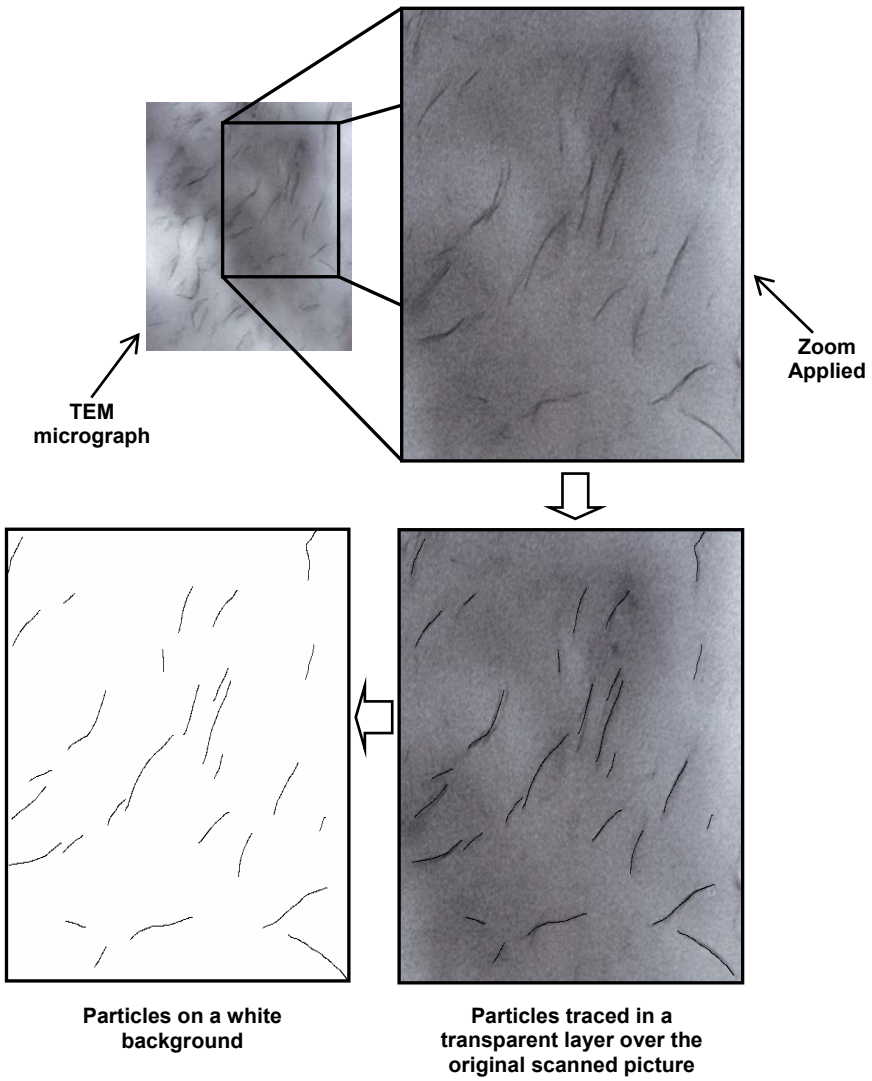

Figure 3.6 Illustration of particle analysis using Adobe Photoshop.

Brabender torque measurements for each polymer were made by adding 58 g of pure polymer to a preheated Brabender Plasticoder outfitted with a 60 mL mixing head and standard rotors operating at 60 rpm. The torque was recorded every minute for twenty minutes. The values reported in this study were taken after 10 min of mixing in the torque rheometer.

Isothermal TGA experiments were performed using a Perkin-Elmer TGA7 analyzer, at specific processing temperatures for 40 min. The initial weight of the samples was approximately 10 mg. Dry air and nitrogen atmospheres were used at a gas flow rate of 20 mL/min. The percentage of remaining organic modifier on the organoclay was calculated considering its percentage on the total organoclay weight, and that it is the only part of the organoclay that degrades at high temperatures. Differential scanning calorimetry was performed using a Perkin-Elmer DSC 7 calorimeter. Samples were taken from the central part of a dry tensile bar and heated at a rate of 20^{o}C/min.

REFERENCES

[1] Alexandre M, Dubois P. Materials Science & Engineering, R: Reports 2000;R28:1-63.

[2] Dennis HR, Hunter DL, Chang D, Kim S, White JL, Cho JW, Paul DR. Polymer 2001;42:9513-9522.

[3] Hylton DC, *Understanding Plastics Testing*. Hanser Gardener Publications Inc., Cincinnati, OH, First Ed., 2004, pp. 93.

[4] Nielsen LE, Landel RF, *Mechanical Properties of Polymers and Composites*. Marcel Dekker, Inc., New York, NY, Second Ed., 1994, pp. 557.

[5] Fornes TD, Paul DR. Polymer 2003;44:4993-5013.

[6] Fornes TD, Yoon PJ, Keskkula H, Paul DR. Polymer 2001;42:9929-9940.

[7] Chavarria F, Paul DR. Polymer 2004;45:8501-8515.

[8] Hine PJ, Rudolf Lusti H, Gusev AA. Compos Sci Technol 2002;62:1445-1453.

[9] Van Olphen H, Clay Mineralogy. in *An introduction to clay colloid chemistry: for clay technologists, geologists, and soil scientists*. Wiley, New York, 1977 pp. Chapter 5.

[10] Shah RK, Paul DR. Polymer 2006;47:4075-4084.

[11] Fornes TD, Paul DR. Polymer 2003;44:3945-3961.

[12] Kim DH, Fasulo PD, Rodgers WR, Paul DR. *Article in preparation*

[13] Stretz HA. Ph.D. Thesis, The University of Texas at Austin, 2005.

[14] Layers are similar to transparent sheets stacked on top of the original image. Layers allow you to draw or trace elements of the image without modifying the original. One can see through a layer to the ones below in the regions that are blank.

[15] The 'Image Processing Tool Kit' allows you to measure particle lengths and areas of particles contained in subsequent layers, within Adobe Photoshop.

CHAPTER 4

COMPARISON OF NANOCOMPOSITES BASED ON NYLON 6 AND NYLON 66

INTRODUCTION

Polyamides are widely used materials due to their tunable properties; nylon 6 (PA-6) and nylon 66 (PA-66) account for the majority of the commercial polyamide production and application. These polyamides physically differ in terms of melting point, glass-transition temperature, crystallinity, and tensile modulus, among other things. PA-66 has a melting point of 262^{o}C, which is higher than that of PA-6 at 219^{o}C; its glass-transition temperature is 65^{o}C, versus 52^{o}C for PA-6; the crystal structure of PA-66 is triclinic while PA-6 has a monoclinic structure; and its tensile modulus is around 2.9 GPa, while it is a little lower for PA-6. Some of these differences can be traced to the difference in symmetry of their repeat units and to the difference in configuration of functional units at the chains ends. PA-6 generally has one amine and one carboxylic acid group at the end of each chain; whereas, PA-66 contains a mixture of chains that have only amines, only acid groups, or combination of the two at their ends. Reports in the literature have shown that the differences in end group configuration can lead to significant differences in the morphology and properties of blends with functionalized polymers made from these two materials [1-3].

Work from the Toyota research laboratories on PA-6 nanocomposites made by in situ polymerization indicates that this process leads to a large number of polyamide molecules, referred to as nylon 6-clay hybrids (NCH), that are ion-bonded to the silicate

layers via the protonated amine chain ends, $-NH_3^+$, and that the enhancement in mechanical properties can be due to the large surface area and to the ionic bonds between the organic polymer and the inorganic silicate [4, 5].

Interestingly, PA-6 nanocomposites prepared by melt compounding using a twin screw extruder show comparable properties to those prepared by the in situ technique [6]. In melt compounding, one would not expect the amine to be protonated because it is only a physical blending process. Nevertheless, a comparable enhancement in properties is obtained. Prior studies show that the melt viscosity and the residence time in the extruder are very important to obtain a well-exfoliated structure. The degree of exfoliation of the organoclay in the polymer matrix has a direct effect on the modulus and the strength of the nanocomposite [6]. Matrices with higher molecular weight produce a higher degree of exfoliation which improves composite properties such as stiffness and strength with a marginal loss of ductility [7]. This phenomenon is attributed to the higher melt viscosity which translates to a higher shear stress imposed on clay particles inside the extruder.

There is some literature concerning PA-66 nanocomposites, starting with the work by Goettler et al. [8, 9], that analyzes the effect of compounding method, molecular weight, amine/carboxyl end group ratio, and cation exchange capacity of the organoclay on the mechanical properties of nanocomposites made with PA-6, PA-66, blends, and copolymers of PA-6 and PA-66. Some other studies report on the hydrogen bonding, crystallization behavior, thermal stability and flammability, mechanical properties, morphology, and molecular modeling of PA-66 nanocomposites [10-20].

To our knowledge, a direct comparison of the morphology and properties of nanocomposites made with PA-6 and PA-66 has not been made using the same melt

processing conditions. The purpose of this study is to analyze the effect of the polyamide type and processing temperature on the mechanical properties and the morphology of the nanocomposites formed from organically modified layered silicates by melt processing. Nanocomposites based on extrusion grade PA-6 and PA-66 were prepared using a twin screw extruder. Mechanical properties, transmission electron microscopy (TEM), wide-angle X-ray scattering (WAXS), percentage crystallinity, and isothermal thermo-gravimetric analysis (TGA) data are reported. A particle analysis was performed to quantitatatively characterize the morphology; these results are later employed in modeling the modulus of these materials using composite theory.

EXPERIMENTAL

To examine the effect of polyamide type and processing temperature, commercial extrusion grades of PA-6 and PA-66 were extruded with the organoclay based on $M_3(C_{18})_1$. The polyamides were chosen in order to have a high melt viscosity and promote the exfoliation of the organoclay, while the organoclay was selected based on a study, performed in our laboratories, on the effect of organoclay structure on the exfoliation and properties of nylon 6 nanocomposites by melt processing [21]. It showed very good performance, producing a high degree of exfoliation and a large enhancement in the mechanical properties of the materials. Specifications for these materials as well as explicit details on melt processing and characterization techniques are given in Chapter 3; conditions and specific information concerning this study follow.

PA-6 and PA-66 organoclay nanocomposites were prepared by melt compounding using the Haake twin screw extruder at a screw speed of 280 rpm with a feed rate of 1200 g/h at two different temperatures (240 and 270ºC). Test specimens were molded at two different conditions according to the extrusion temperature, as

outlined in Table 4.1. The injection pressure was 70 bar and the holding pressure was 35 bar under both conditions.

Table 4.1 Processing conditions used in this study.

Extrusion temperature	Injection molding temperature profile (from feed to nozzle)	Mold temperature
240ºC	240, 250, 255, 260ºC	80ºC
270ºC	270, 275, 290, 310ºC	85ºC

Isothermal TGA experiments were performed to obtain the percentage of remaining organic modifier on the organoclay. It was calculated considering that the organic modifier constitutes 29.6% of the total organoclay weight, while the remaining 70.4% is MMT.

DSC was performed to obtain the percent crystallinity of the polyamide. It was calculated as the ratio of the heat of fusion of the sample (ΔH_f), with units of Joules per gram of polymer (not the composite), to the heat of fusion of the purely crystalline forms of PA-6 and PA-66 (ΔH^o_f). The ΔH_f of each sample was determined by integrating the heat flow from 150^{o}C to 250^{o}C, for the samples processed at 240^{o}C, and from 170^{o}C to 270^{o}C for the samples processed at 270^{o}C. The ΔH^o_f values for each matrix were taken as 190.9 J/g for PA-6 and 195.9 J/g for PA-66 [22].

The TEM micrographs were obtained using a JEOL 2010F transmission electron microscope operating at an accelerating voltage of 120 kV. Samples for TEM were cryogenically cut into ultra thin sections (30 to 50 nm thick) with a diamond knife at a temperature of -40ºC using a Reichert-Jung Ultracut E microtome. These sections were

taken from the central part of a tensile bar normal to the flow direction (FD), and they were viewed parallel to the flow direction as shown in Figure 3.5.

RESULTS AND DISCUSSION

In order to make a valid comparison between the extent of exfoliation of the clay platelets in PA-6 and PA-66, it is necessary to do so at comparable process conditions. For example, two key issues are the melt viscosity of the polymer matrix, as outlined by Fornes et al. [7], and the degradation of the organic modifier on the clay. These have a direct effect on the degree of exfoliation of the clay, which in turn affects the mechanical properties of the nanocomposites. PA-6 and PA-66 have different melting temperatures and are generally extruded at 240 and 280^{o}C, respectively. Since a difference in processing temperature affects both the melt rheology and the organoclay chemical stability, it is important to ascertain the effects of processing temperature on the nanocomposites and to make comparisons under as nearly identical conditions as possible. To minimize the effect of melt viscosity differences, Brabender torque experiments were done at different temperatures to find where PA-6 and PA-66 may have similar melt viscosities. Table 4.2 shows the Brabender torque response after ten minutes for each polymer. As can be seen, the torque values for the two polymers are very similar at 270^{o}C, which suggests that comparisons of nanocomposites formed from PA-6 and PA-66 at this temperature would be relatively free of any differences due to melt viscosity effects.

The effect of the temperature on the degradation of the organic modifier on the clay in both air and nitrogen atmosphere is shown in Figure 4.1. As expected, the degradation is faster at higher temperature and in the more oxidative environment. The atmosphere in the extruder should lie somewhere between that of a nitrogen and pure air

atmosphere. The mean residence time in the extruder was found to be 3.4 minutes [23]; however, a portion of the residence time is spent heating to the final melt temperature, so this is only an approximate indicator of time for degradation. Nevertheless, at times of this order, there is significant loss of surfactant mass, as indicated in these TGA experiments. The difference between an extrusion temperature of 270°C versus 240°C is somewhere between 11 and 18% as seen in Figure 4.1. As judged by the mechanical properties of the nylon 6 nanocomposites shown later, there is no discernable practical difference between the two processing temperatures.

Table 4.2 Brabender torque of PA-6 and PA-66.

Nylon Type	Temperature [°C]	Torque (@10min) [N-m]
PA-6	240	10.4
	270	6.0
	280	4.5
PA-66	265	8.5
	270	5.9
	280	5.8

Mechanical properties

Nanocomposites from PA-6 were formed at both 240°C and 270°C to determine the effect of the melt processing temperature on the mechanical properties versus MMT content. Nanocomposites based on PA-66 could only be formed at 270°C because of its melting point of 262°C. Table 4.3 summarizes the tensile properties of the pure materials and selected nanocomposites; Figure 4.2 shows the shape of the stress-strain curves for pure PA-6 and PA-66 and nanocomposites containing 2.9 wt% MMT.

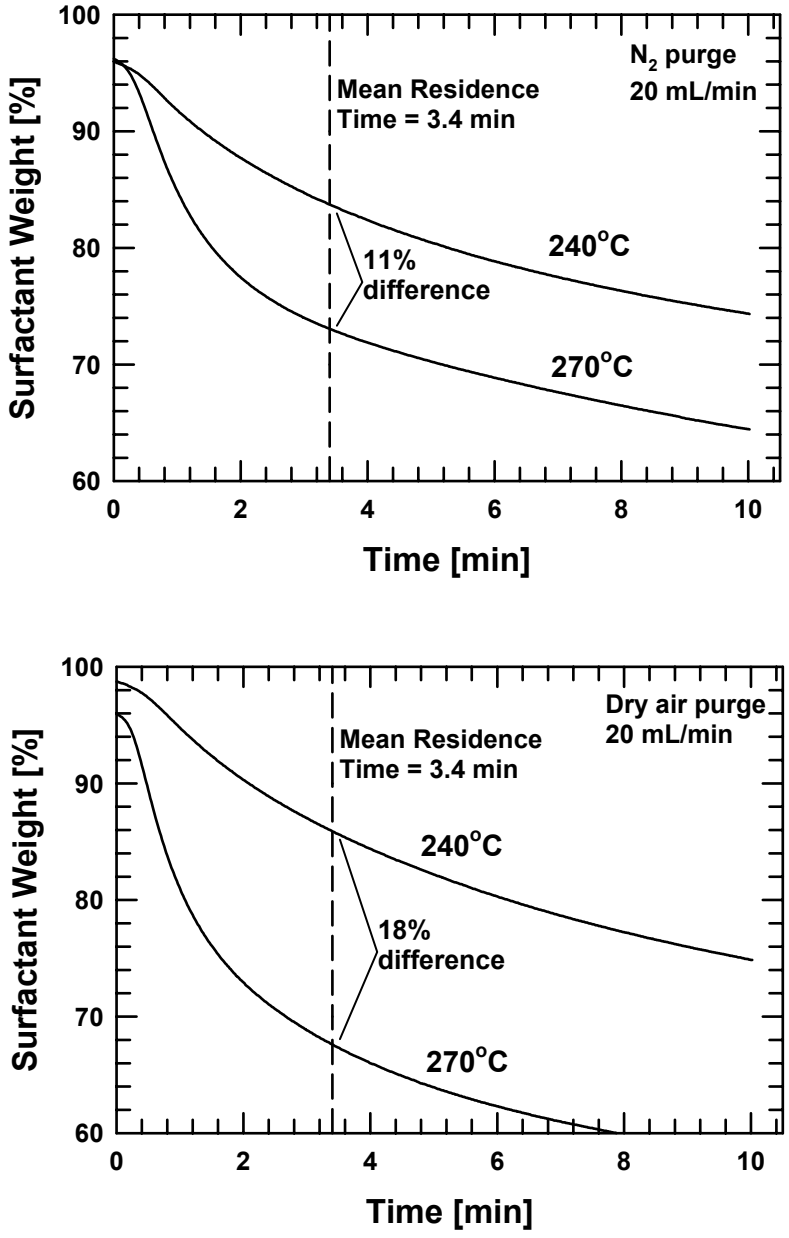

Figure 4.1 Kinetics of surfactant loss from organoclay at 240 and 270°C with nitrogen and dry air purge.

Table 4.3 Select tensile properties for PA-6 and PA-66 organoclay nanocomposites.

Organoclay nanocomposites	Modulus [GPa]	Yield strength [MPa]	Strain at yield [%]	Elongation at break [%] Crosshead speed 0.51 cm/min
PA-6 @ 240°C				
0.0 wt% MMT*	2.89	68.9	3.8	275
2.9 wt% MMT	4.09	85.3	3.2	191
4.3 wt% MMT	4.50	86.2	3.0	49
PA-6 @ 270°C				
0.0 wt% MMT*	2.80	66.6	3.7	272
2.7 wt% MMT	4.06	84.5	3.0	143
4.9 wt% MMT	4.67	87.4	2.7	7.5
PA-66 @ 270°C				
0.0 wt% MMT*	2.91	72.6	3.9	211
2.9 wt% MMT	3.92	80.4	4.0	10
4.4 wt% MMT**	4.24	---	---	4

* Injection-molded pure nylon
** PA-66 @ 270°C specimens broke before the yield point with MMT concentrations above 3%

Figure 4.3 shows the effect of montmorillonite content on the modulus for the three different samples. The addition of organoclay to the polymer matrix produces a substantial increase in the modulus in all cases even at low loadings. These results show that the modulus of the PA-6 nanocomposites is essentially independent of the processing temperature. PA-6 nanocomposites have a slightly higher modulus than PA-66 nanocomposites, and this difference becomes larger with increasing clay loading. The non-linear trend observed in the PA-66 samples may be due to a lesser capacity of PA-66 to exfoliate the clay versus PA-6. This may stem from the fact that for PA-66, the ability to exfoliate seems to decrease as the loading increases. This is confirmed by the particle analysis results shown below.

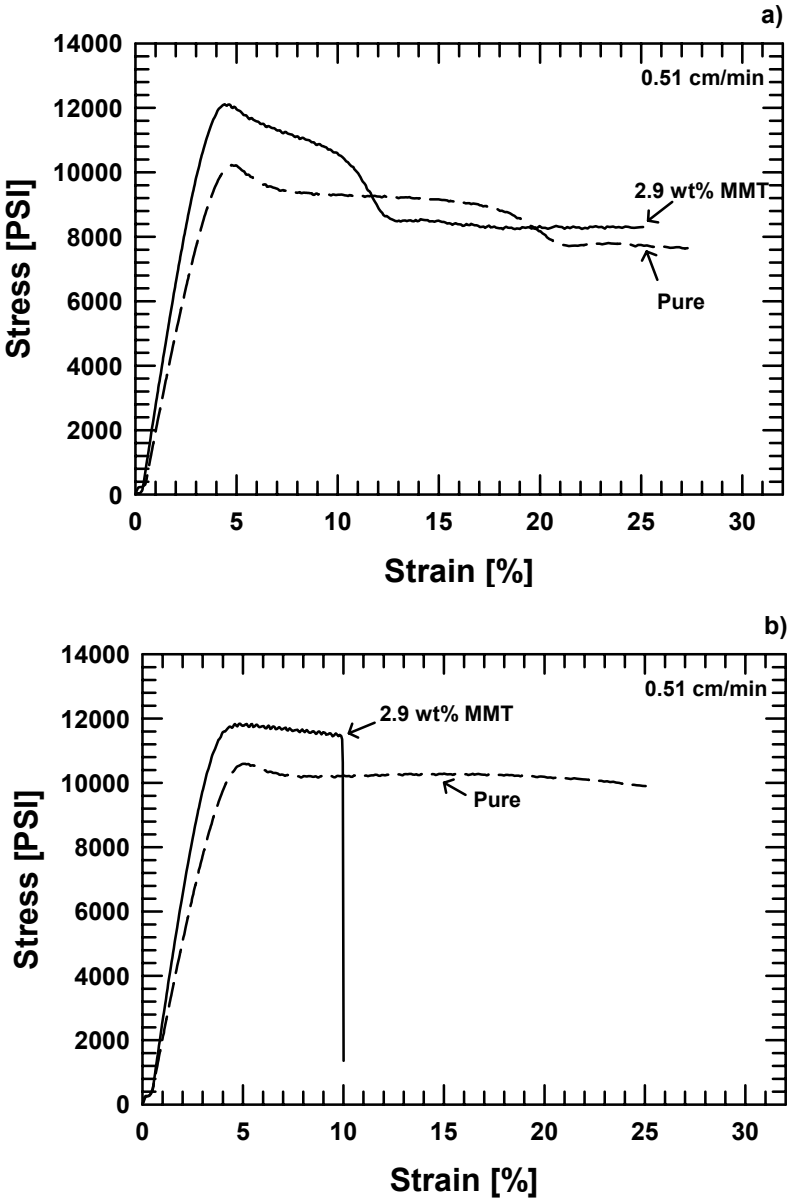

Figure 4.2 Stress-strain curves of a) PA-6 @ 240^{o}C and b) PA-66 samples.

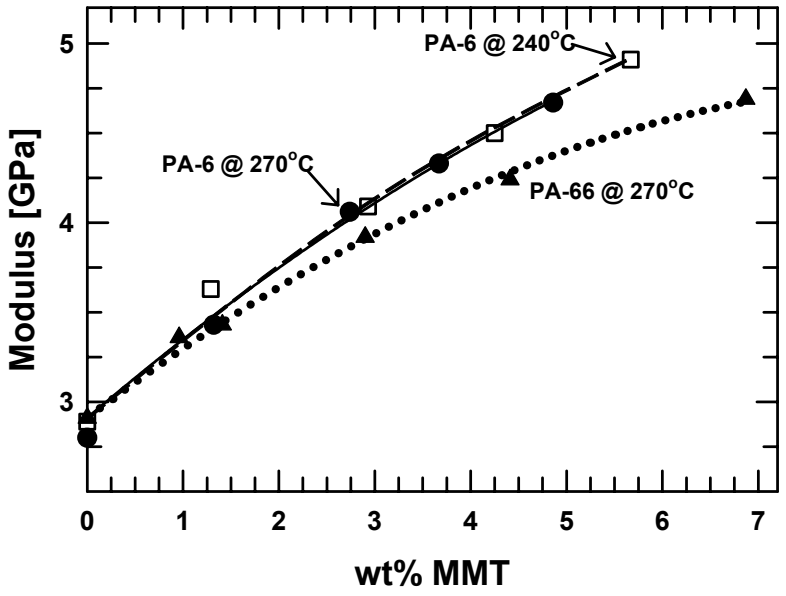

Figure 4.3 Modulus of PA-6 and PA-66 nanocomposites at different organoclay loadings.

A similar behavior is observed for the yield strength in Figure 4.4. The yield strength of the PA-6 nanocomposites increases rather rapidly with increasing MMT content and the effect of processing temperature is only slight. The neat PA-66 has higher yield strength than PA-6; however, its nanocomposites show a lower rate of increase than those of PA-6. PA-66 tensile bars with organoclay concentrations higher than 3 wt% MMT failed before reaching the yield point. As shown in Figure 4.5, the elongation at yield decreases with organoclay content for the PA-6 samples while it remains almost constant (within the experimental error) for the PA-66 nanocomposites.

The effect of MMT content on the elongation at break is shown in Figure 4.6 for a rate of extension of 0.51 cm/min. It shows that PA-6 samples processed at 240°C are very ductile at organoclay contents below 4.5 wt% MMT, while PA-6 samples processed

at 270°C are ductile below 4 wt% MMT. For PA-6 nanocomposites, the elongations at break are higher for the samples extruded at 240°C than those extruded at 270°C.

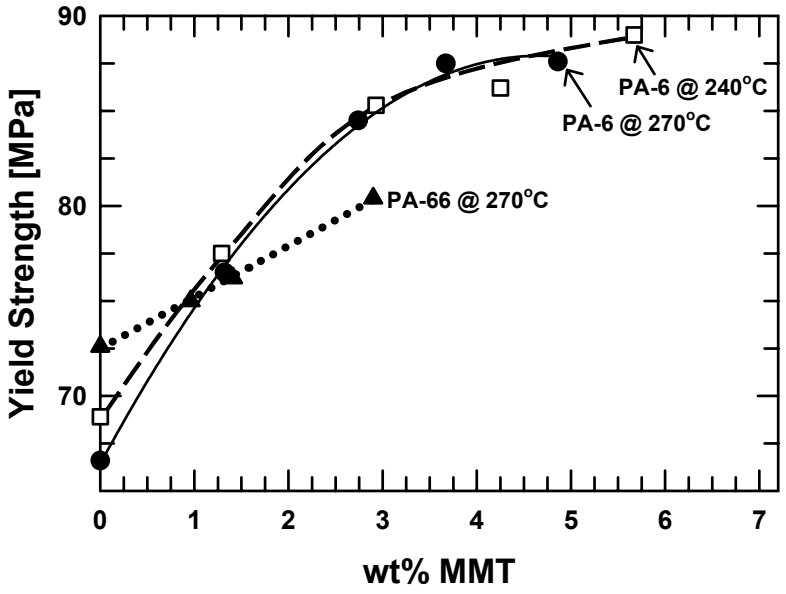

Figure 4.4 Yield strength of PA-6 and PA-66 nanocomposites at different organoclay loadings.

One might attribute these differences to the extent of exfoliation due to the lower matrix melt viscosity and/or the greater surfactant degradation at 270°C. Neither the modulus data in Figure 4.3 nor the TEM data shown later, suggest measurable differences in the extent of exfoliation at the two temperatures. Greater molecular weight degradation of the PA-6 matrix at 270°C [23] could be a possible cause for reduced elongation at break; however, the differences shown are not very great and could be considered within the experimental error. On the other hand, the PA-66 samples become

brittle at organoclay contents above 1.5 wt% MMT. The elongation at break decreases much faster in the PA-66 samples than in those based on PA-6.

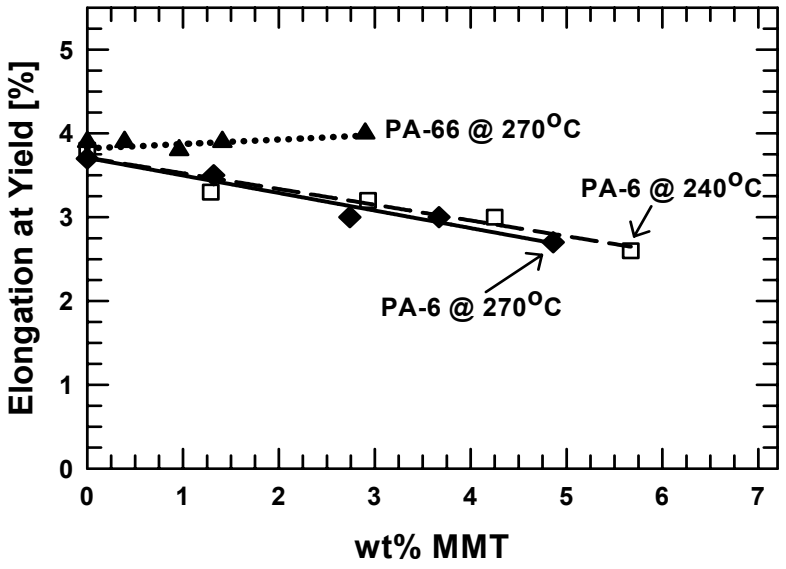

Figure 4.5 Elongation at yield of PA-6 and PA-66 nanocomposites at different organoclay loadings.

This transition between ductile and brittle behavior can be seen clearly by observation of the test specimens after testing, as seen in Figure 4.7. This figure shows that the PA-6 specimens have ductile behavior up to 4 to 4.5 wt% MMT; while PA-66 specimens show brittle behavior beyond 1.5 wt% MMT.

Crystallinity of the polyamide matrix

Clay particles, at low concentrations, serve as nucleating agents that increase the rate of crystallization of the polyamide matrix; however, at high concentrations of clay,

the rate of crystallization is retarded which may reduce the crystallinity observed in nanocomposites [24]. The retardation of crystallization rate, at high organoclay contents, is more pronounced as the level of exfoliation and organoclay concentration increase. This may be the reason why the percent crystallinity decreases as the clay loading increases, as seen in Figure 4.8. The crystallinity of PA-66 is intrinsically higher than that of PA-6, yet a similar decline is noted when organoclay is added. This suggests that there is a higher degree of exfoliation in the PA-6 samples which corroborates the mechanical properties and will also be seen in the morphology results shown next.

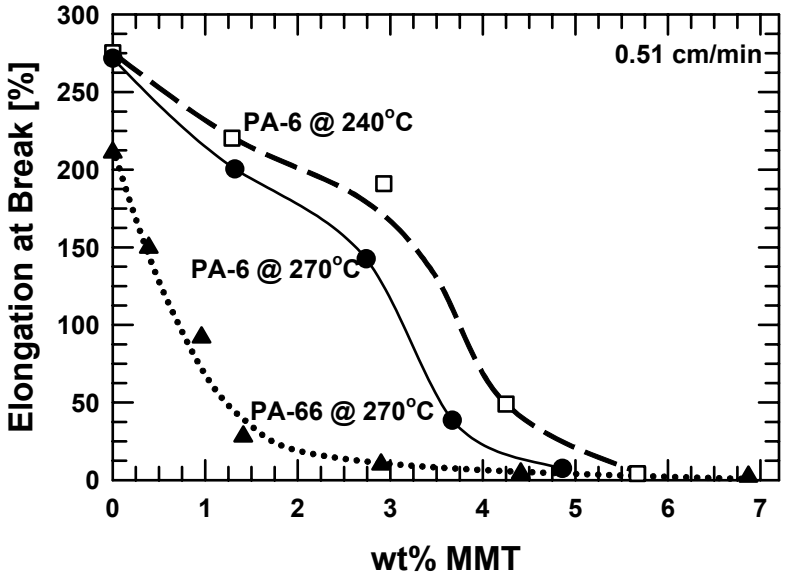

Figure 4.6 Elongation at break of PA-6 and PA-66 nanocomposites at different organoclay loadings and a test rate of 0.51 cm/min.

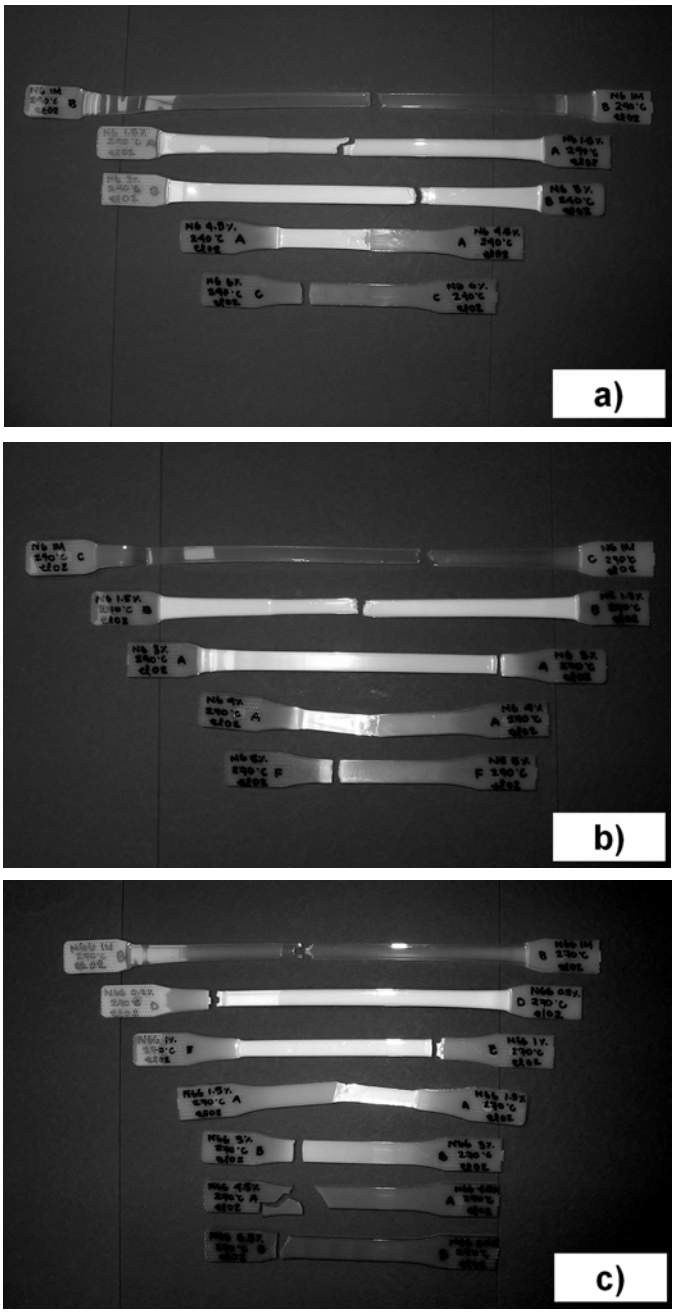

Figure 4.7 Visual illustration of injection molded tensile bars after testing at 0.51 cm/min. a) PA-6 (240^{o}C) and b) PA-6 (270^{o}C) with ~ 0, 1.5, 3, 4.5 and 6 wt% MMT from top to bottom and c) PA-66 (270^{o}C) with ~ 0, 0.5, 1, 1.5, 3, 4.5 and 6.5 wt% MMT from top to bottom.

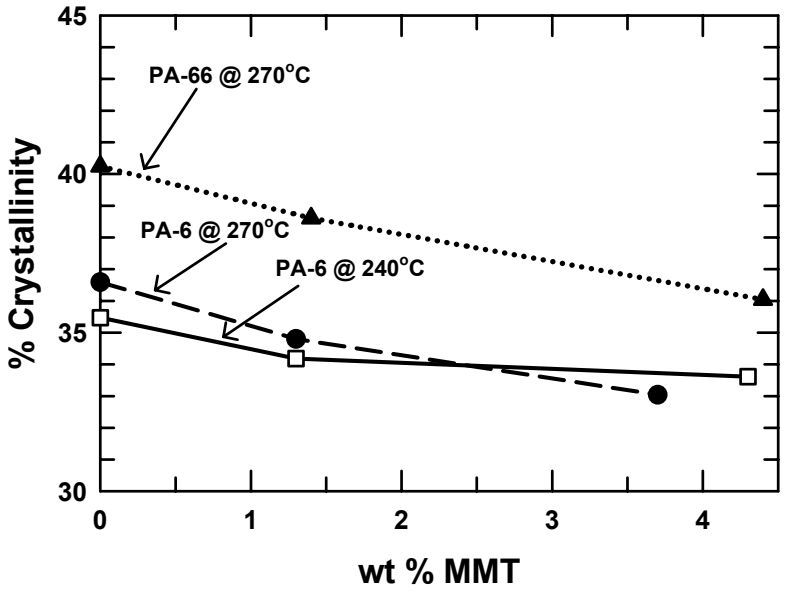

Figure 4.8 Percent crystallinity of PA-6 and PA-66 nanocomposites at different organoclay loadings.

Morphology

Figure 4.9 compares X-ray scattering patterns for the pure organoclay and nanocomposites containing ~3 wt% MMT. The pattern for the pure organoclay reveals a broad intense peak around $2\theta = 5^{o}$, which is characteristic of the basal spacings of the modified layered silicate. The PA-6 samples, processed at both 240 and 270°C are absent of any reflections, which suggests an exfoliated structure. The pattern for PA-66, on the other hand, reveals a low broad peak around the same value as that of the organoclay. This suggests that a measurable fraction of un-exfoliated organoclay exists.

TEM micrographs of PA-6 and PA-66 nanocomposites, like those shown in Figure 4.10, give a more complete understanding of the degree of exfoliation. PA-6 nanocomposites have well-exfoliated structures in agreement with the WAXS results.

PA-66 nanocomposites reveal a mixture of intercalated and exfoliated structures. A more complete analysis on the exfoliation of the organoclay in these polymer matrices follows.

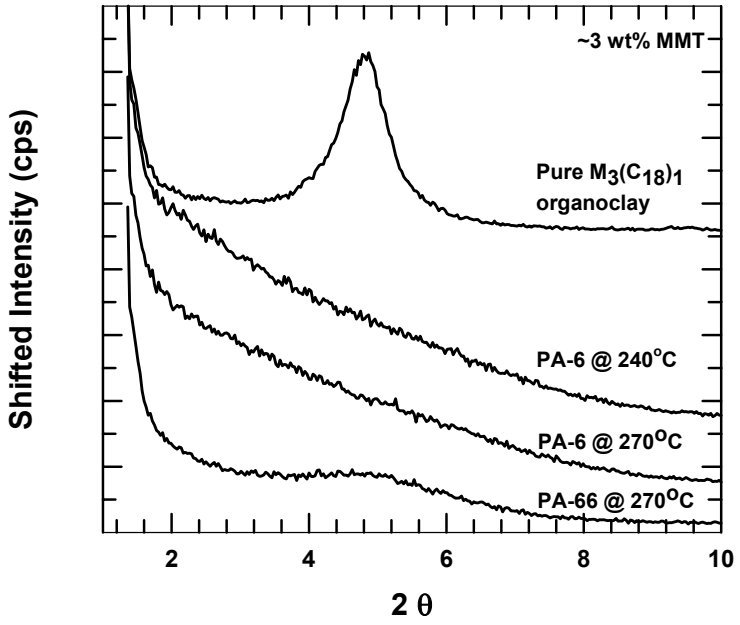

Figure 4.9 X-ray scans for pure $M_3(C_{18})_1$ organoclay plus PA-6 and PA-66 nanocomposites containing ~3 wt% MMT at 240 and 270°C. The curves are vertically offset for clarity.

Particle Analysis

Particle analysis was performed for the PA-6 and PA-66 samples used in this study, at low and high MMT concentrations. A summary of the results is shown in Table 4.4. Histograms of the particle analysis are shown in Figures 4.11 to 4.13 for PA-6 and PA-66 samples with high MMT concentrations. The average particle length in the low concentration samples is very similar for both PA-6 and PA-66; however, at the high concentration, the particle length is greater for the PA-66 samples.

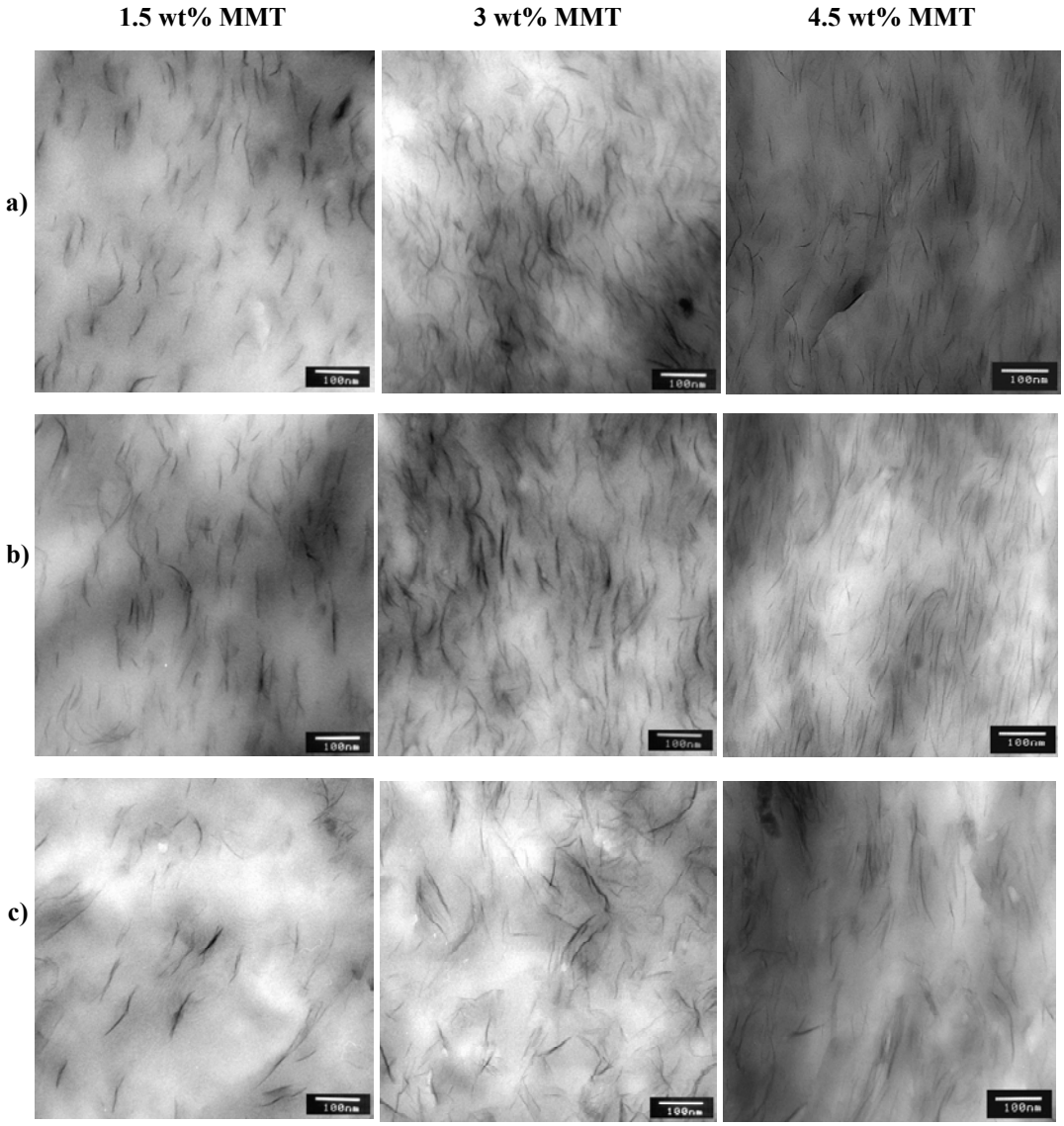

Figure 4.10 TEM micrographs of PA-6 and PA-66 nanocomposites with approximately 1.5, 3, and 4.5 wt% MMT. a) PA-6 nanocomposites processed at 240ºC, b) PA-6 nanocomposites processed at 270ºC, and c) PA-66 nanocomposites processed at 270ºC.

Table 4.4 Particle analysis results

Organoclay nanocomposites	Number average particle length $(\bar{\ell})_n$ [nm]	Weight average particle length $(\bar{\ell})_w$ [nm]	Number average platelets / particle	Weight average platelets / particle	Number average particle thickness $(\bar{t})_n$ [nm]	Weight average particle thickness $(\bar{t})_w$ [nm]
PA-6 @ 240°C	62	80	1.7	2.2	2.3	3.4
1.29 wt% MMT	55	80	1.3	1.6	1.5	2.2
4.3 wt% MMT						
PA-6 @ 270°C						
1.32 wt% MMT	65	87	1.8	2.4	2.3	3.9
3.67 wt% MMT	53	70	1.4	1.6	1.6	2.2
PA-66 @ 270°C						
1.41 wt% MMT	66	91	1.9	2.4	2.5	3.9
4.4 wt% MMT	61	81	1.7	2.2	2.2	3.5

Organoclay nanocomposites	Aspect ratio [a] $(\bar{\ell})_n / (\bar{t})_n$	Aspect ratio [b] $(\bar{\ell})_w / (\bar{t})_w$	Particle density [particles / μm^2]	Specific particle density (particle density @ 1 and 5.5 wt% MMT) [particles / μm^2]
PA-6 @ 240°C	27	23	156	201
1.29 wt% MMT	36	37	559	437
4.3 wt% MMT				
PA-6 @ 270°C				
1.32 wt% MMT	28	23	156	206
3.67 wt% MMT	33	32	555	373
PA-66 @ 270°C				
1.41 wt% MMT	26	24	93	131
4.4 wt% MMT	27	23	340	272

[a] These values of the aspect ratio were computed from the number average platelet lengths and thicknesses
[b] These values of the aspect ratio were computed from the weight average platelet lengths and thicknesses

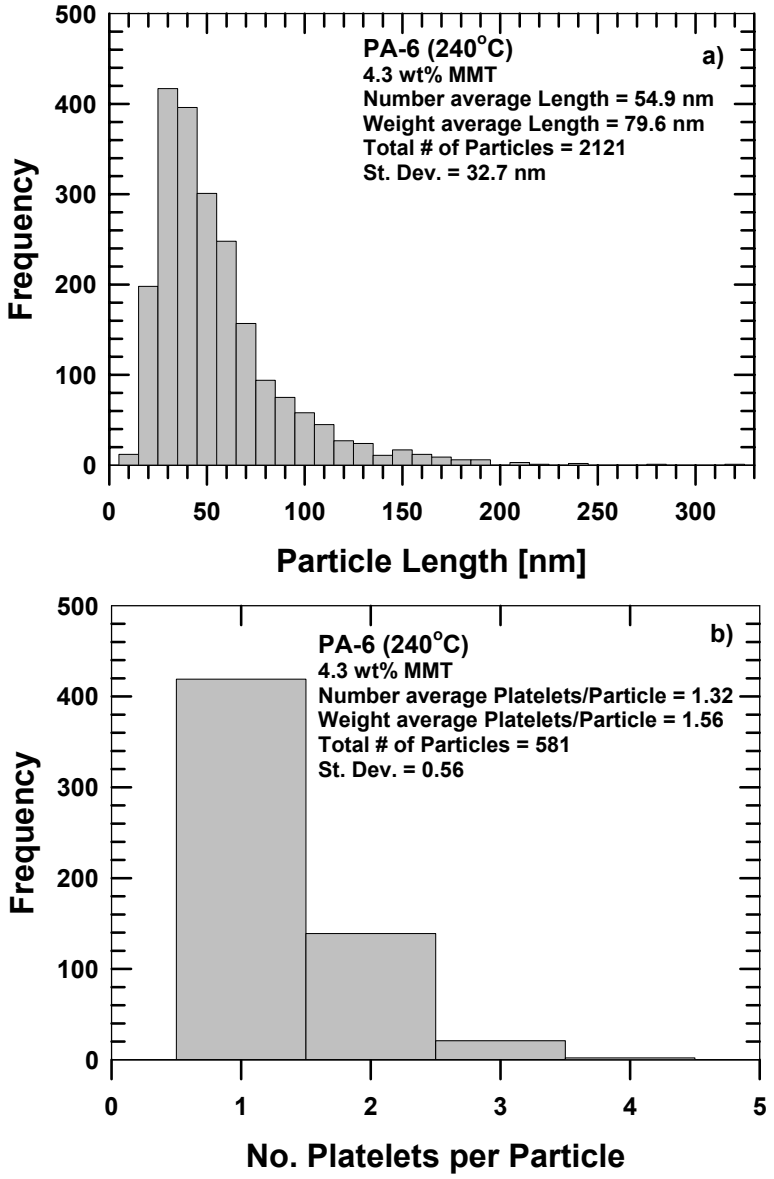

Figure 4.11 Histograms of a) particle length and b) number of platelets per particle for PA-6 nanocomposites with 4.3 wt% MMT processed at 240°C.

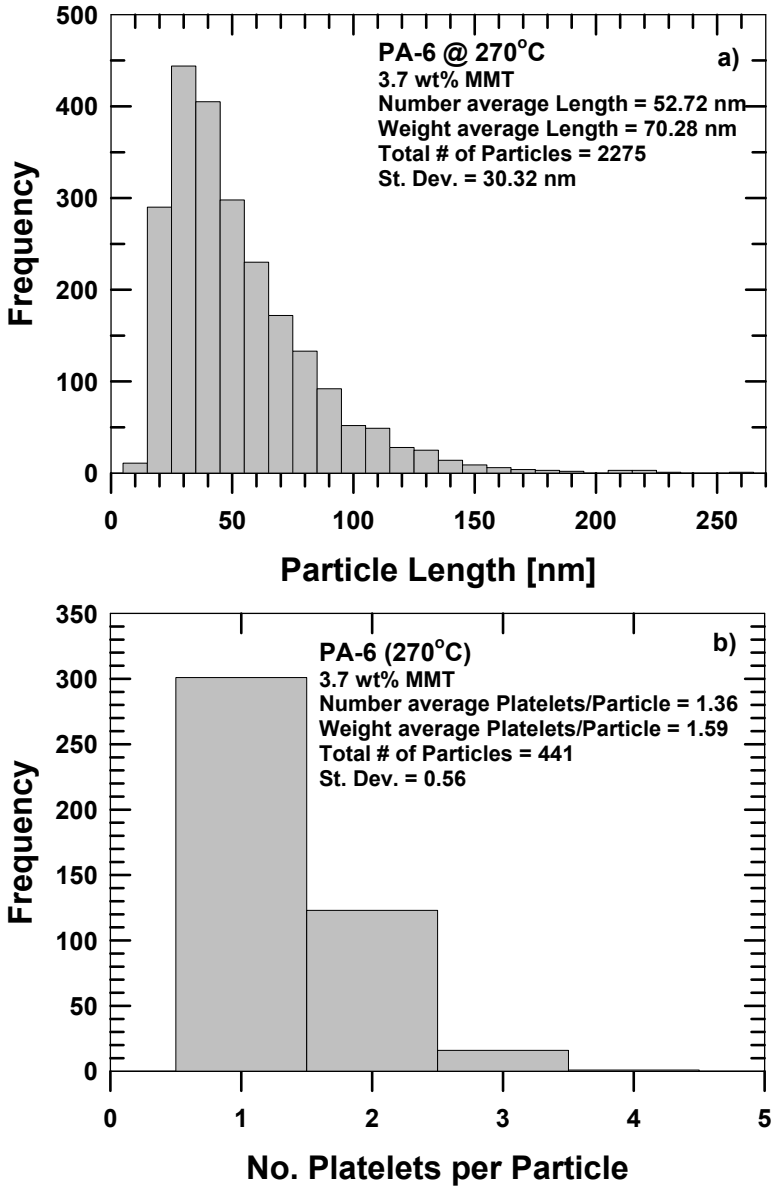

Figure 4.12 Histograms of a) particle length and b) number of platelets per particle for PA-6 nanocomposites with 3.7 wt% MMT processed at 270°C.

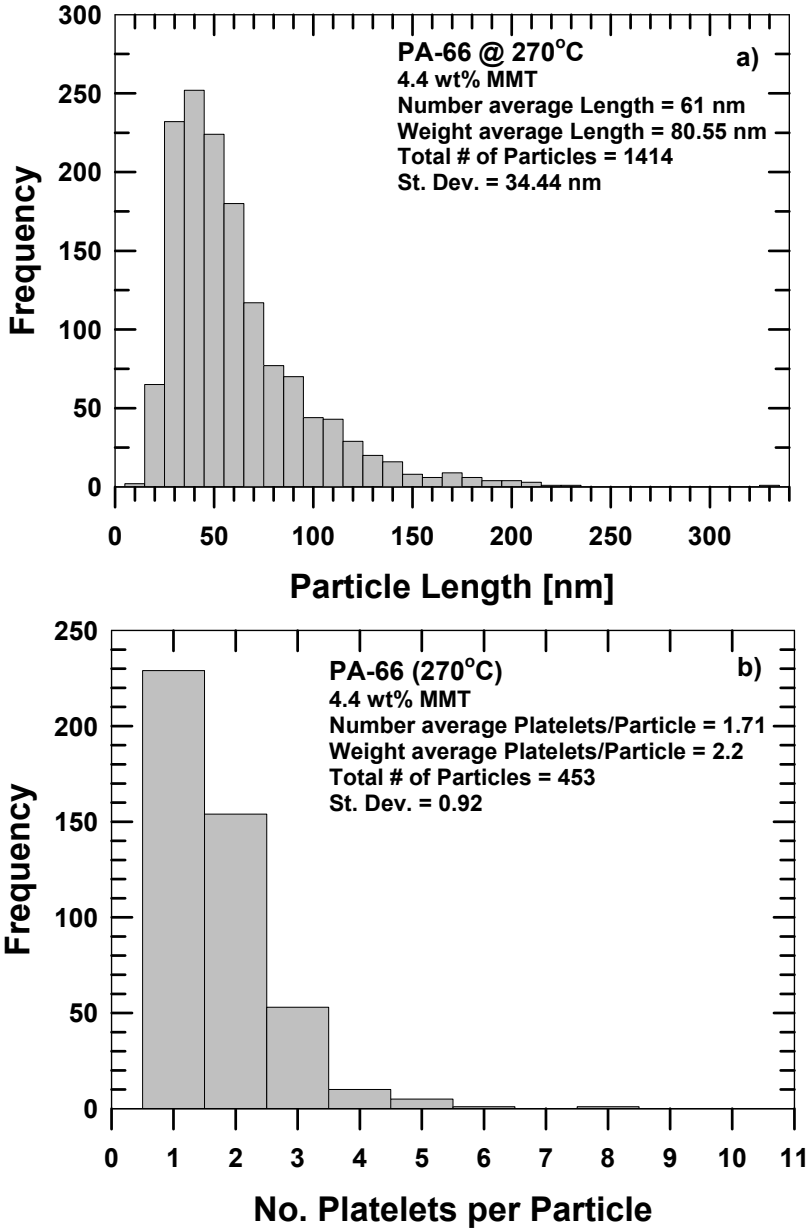

Figure 4.13 Histograms of a) particle length and b) number of platelets per particle for PA-66 nanocomposites with 4.4 wt% MMT processed at 270°C.

This can be explained considering that PA-6 samples have more single platelets while PA-66 samples have a larger number of agglomerates, which tend to have longer lengths than single platelets. A reason for this is illustrated in Figure 4.14; similar results were also observed by Fornes et al. [7]. The particle analysis results show no significant difference between the PA-6 samples processed at 240 and at 270°C, which agrees with the mechanical properties and morphology results shown previously. Regarding the differences between the nylon matrices, the particle density of PA-66 samples is considerably lower than that of PA-6. This confirms that PA-6 samples are more exfoliated than those made with PA-66. PA-66 also shows a larger average number of platelets per particle and a larger average thickness, also indicative of a lower degree of exfoliation of the clay. The aspect ratio increases with MMT concentration due to the separation of some agglomerates into single particles. These values are higher for the PA-6 samples with respect to PA-66.

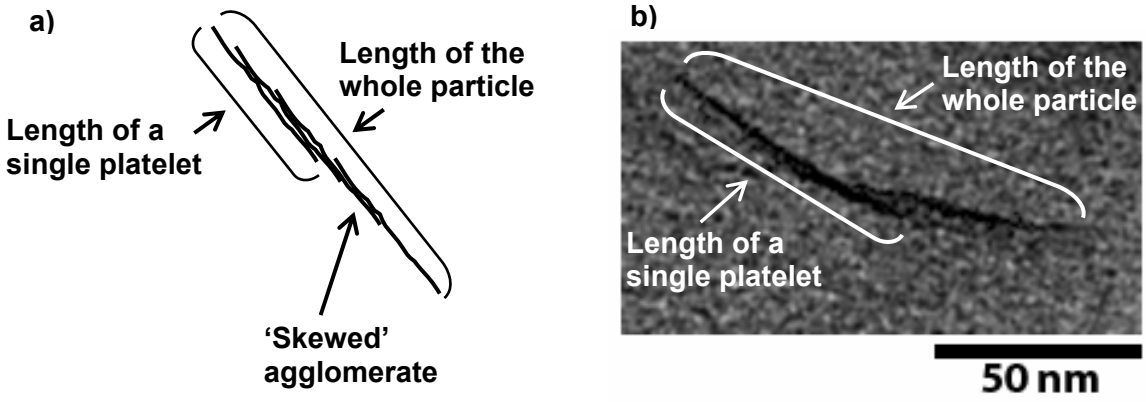

Figure 4.14 Illustration of larger average length for 'skewed' agglomerates. a) illustrative sketch and b) an example TEM micrograph.

Composite Theory Modeling

Figure 4.15 shows the experimental and theoretical stiffness results for PA-6 samples, with 4.3 wt% of MMT, processed at 240^{o}C, PA-6 samples with 3.7 wt% of MMT processed at 270^{o}C, and PA-66 samples with 4.4 wt% of MMT processed at 270^{o}C. These theoretical predictions are based on unidirectional reinforcement. In this figure, the lines are the theoretical results and the points are the experimental data. In the theoretical results, the dashed lines are the modeling results using the experimental aspect ratio obtained from the particle analysis and the solid lines are the modeling results using an aspect ratio that considers complete exfoliation. This 100% exfoliation aspect ratio was obtained by dividing the number average particle length, of that sample, by the thickness of one platelet (i.e. 0.94 nm).

These results show that the Mori-Tanaka model under predicts the experimental results in PA-6 samples processed at 240^{o}C and 270^{o}C. The Halpin-Tsai model predicts the results of the PA-6 samples processed at 240^{o}C to an acceptable extent, while the experimental points for PA-6 samples processed at 270^{o}C lay within the range of this model's predictions. The experimental results for PA-66 samples lie within the range of the Mori-Tanaka model, while the Halpin-Tsai model predicts the behavior acceptably up to a certain volume fraction where the non-linear behavior takes effect. In summary, the models give acceptable correlations with the experimentally observed behavior for these two polymer matrices.

CONCLUSION

PA-6 and PA-66 nanocomposites were prepared using a co-rotating twin screw extruder. PA-6 nanocomposites had superior mechanical properties than those made from PA-66. The tensile strength of PA-66 nanocomposites deviated from linearity at

high levels of MMT. WAXS and TEM results show that the PA-6 nanocomposites are better exfoliated than the PA-66 nanocomposites, which exhibit a mixture of intercalated and exfoliated structures. The mechanical properties are consistent with the morphology; exfoliated structures lead to better mechanical properties than mixed structures. DSC reveals a higher percentage of crystallinity in the PA-66 samples. Mechanical properties, WAXD, TEM, and crystallinity results indicate a minor difference between the PA-6 samples processed at 240ºC versus the ones processed at 270ºC.

Particle analysis reveals a higher average particle length and thickness, and a lower average particle density and aspect ratio for PA-66 nanocomposites; indicative of a lower degree of exfoliation. Again, there seems to be no significant difference between PA-6 nanocomposites at 240 and 270^{o}C. The Halpin-Tsai and Mori-Tanaka composite theories predict satisfactorily the behavior of PA-6 nanocomposites. For PA-66 nanocomposites, the modulus is acceptably predicted up to a certain volume fraction where a non-linear response becomes significant.

All results indicate a lower degree of exfoliation in the nanocomposites formed from PA-66. Since this comparison was made under very similar process and rheological conditions for the same organoclay, it appears that the affinity of PA-66 for the organoclay is less than that of PA-6. This must relate to some aspect of the difference in the chemical structure of the two polyamides; however, at this point, it is not possible to be more definitive about the underlying causes for this difference.

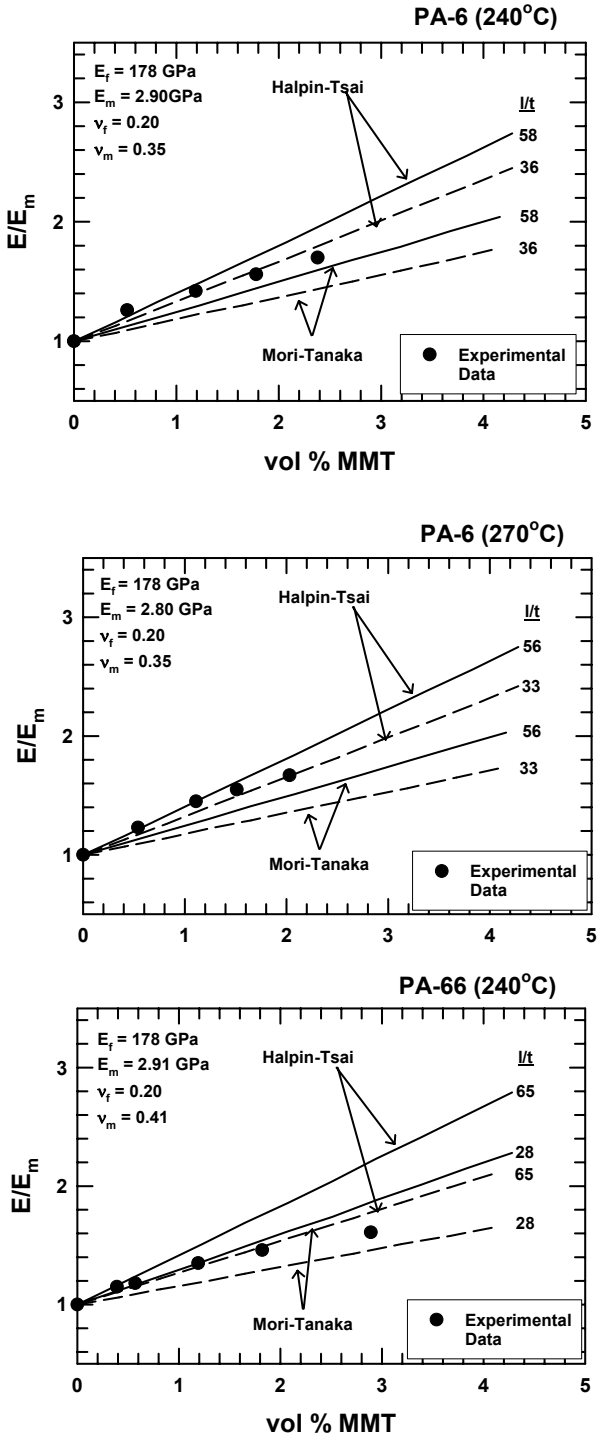

Figure 4.15 Experimental and theoretical relative modulus results for PA-6 (240°C), PA-6 (270°C), and PA-66 (270°C).

REFERENCES

[1] Oshinski AJ, Keskkula H, Paul DR. Polymer 1992;33:268-283.

[2] Oshinski AJ, Keskkula H, Paul DR. Polymer 1992;33:284-293.

[3] Takeda Y, Keskkula H, Paul DR. Polymer 1992;33:3173-3181.

[4] Usuki A, Kojima Y, Kawasumi M, Okada A, Fukushima Y, Kurauchi T, Kamigaito O. J Mater Res 1993;8:1179-1184.

[5] Okada A, Usuki A. J Mater Res 1995;C3:109-115.

[6] Cho JW, Paul DR. Polymer 2000;42:1083-1094.

[7] Fornes TD, Yoon PJ, Keskkula H, Paul DR. Polymer 2001;42:9929-9940.

[8] Goettler L, A., Powell C, E. US Patent No. WO 99/41299 1999;

[9] Goettler L, A., Joardar S, S., Middleton J, C. US Patent No. WO 00/09571 2000;

[10] Lu Y, Zhang G, Feng M, Zhang Y, Yang M, Shen D. J Polym Sci, Part B: Polym Phys 2003;41:2313-2321.

[11] Liu X, Wu Q, Zhang Q, Mo Z. J Polym Sci, Part B: Polym Phys 2002;41:63-67.

[12] Liu X, Wu Q, Berglund L. Polymer 2002;43:4967-4972.

[13] Wu T-M, Wu J-Y. J Macromol Sci, Phys 2002;B41:17-31.

[14] Zhang Q-x, Yu Z-z, Yang M, Ma J, Mai Y-w. J Polym Sci, Part B: Polym Phys 2003;41:2861-2869.

[15] Qin H, Su Q, Zhang S, Zhao B, Yang M. Polymer 2003;44:7533-7538.

[16] Yu Z-Z, Yang M, Zhang Q, Zhao C, Mai Y-W. J Polym Sci, Part B: Polym Phys 2003;41:1234-1243.

[17] Liu X, Wu Q. Macromol Mater Engng 2002;287:180-186.

[18] Nair SV, Goettler LA, Lysek BA. Polym Eng Sci 2002;42:1872-1882.

[19] Han B, Ji G, Wu S, Shen J. Eur Polym J 2003;39:1641-1646.

[20] Tanaka G, Goettler LA. Polymer 2001;43:541-553.

[21] Fornes TD, Yoon PJ, Hunter DL, Keskkula H, Paul DR. Polymer 2002;43:5915-5933.

[22] Inoue M. J Polym Sci, Part A: Polym Chem 1963;1:2697-2709.

[23] Fornes TD, Yoon PJ, Paul DR. Polymer 2003;44:7545-7556.

[24] Fornes TD, Paul DR. Polymer 2003;44:3945-3961.

CHAPTER 5

EFFECT OF PROCESSINGON THE EXFOLIATION OF PA-6 NANOCOMPOSITES

INTRODUCTION

The degree of exfoliation, or dispersion, of clay particles in nanocomposites prepared by melt processing depends on both the affinity between the polymer and the organoclay and the details of the melt blending process. Previous studies from our laboratories have shown that the type of extruder used and the amount of shear it produces have a significant effect on the morphology and properties of nylon 6 (PA-6) nanocomposites [1, 2]; hence, it is important to optimize the extruder processing conditions to obtain high degrees of platelet delamination and dispersion to achieve significant matrix reinforcement.

Nanocomposites formed by melt processing have been described extensively over the past few years; a considerable part of this literature examines the effect of the type of polymer matrix or organoclay chemical structure on the morphology and properties of these composites [3-17]. Others report on molecular modeling [18-22], and the effect of clay particles on the crystallization behavior of the matrix [14, 23, 24], while degradation and color formation in the composite materials [25-27], their thermal properties [6], and the use of composite theory modeling [28] are also analyzed. On the other hand, very few studies address the problem of optimizing the extruder mixing conditions [1, 2, 26]. The latter have shown that there needs to be a long enough residence time and an appropriate shear history to obtain good exfoliation of clay platelets and mechanical

property enhancements. The morphology and mechanical properties of PA-6 nanocomposites prepared by a single screw extruder have been compared to the properties of PA-6 nanocomposites formed in a twin screw extruder with the conclusion that a high degree of exfoliation was only obtained by twin screw extruders (TSE's); the single screw extruder used did not provide sufficient shear or residence time [1]. Dennis et al. made an extensive study of the effect of extruder type and screw design on the degree of platelet delamination and dispersion in a PA-6 matrix [2]. It was shown that excellent delamination and dispersion can be achieved in both counter- and co-rotating twin screw extruders with a well-optimized screw configuration and that medium shear intensity, rather than a high shear level, leads to the best platelet delamination and dispersion of PA-6 organoclay nanocomposites. In addition, recent studies in polymer nanocomposites targeted towards addressing specific questions regarding clay exfoliation require the use of polymer matrices and/or organoclays with specific characteristics [17, 29]; micro-compounders such as the one from DSM may be a good alternative for nanocomposite research especially when only small amounts of material are available.

The objectives of this study are to further explore the effect of extruder mixing conditions on the morphology and mechanical properties of PA-6 nanocomposites prepared by melt processing and to benchmark the degree organoclay dispersion, platelet delamination, and matrix reinforcement of PA-6 nanocomposites processed in a DSM micro-compounder versus the nanocomposites processed in two highly-optimized twin screw extruders. Detailed comparisons of various levels of shear, residence times, feed port location, and passes through the extruder are reported for PA-6 nanocomposites processed in these three extruders. A brief comparison to less exfoliated particles in polyolefin matrices is also made.

EXPERIMENTAL

To examine the effect of extruder mixing conditions on PA-6 nanocomposites, an extrusion grade of PA-6 and an organoclay based on $M_3(HT)_1$ were used. The polyamide was chosen in order to have high melt viscosity and promote the exfoliation of the organoclay, while the organoclay was selected based on several studies performed in our laboratories showing a high degree of exfoliation and one of the largest enhancements in the mechanical properties of PA-6 [5]. Specifications for these materials as well as explicit details on melt processing and characterization techniques are given in Chapter 3; conditions and specific information concerning this study follow.

PA-6 organoclay nanocomposites were prepared by melt compounding using a Werner and Pfleiderer ZSK 25 twin screw extruder (ZSK 25), a Haake twin screw extruder, and a DSM micro-compounder. The polymer fed into the DSM micro-compounder was cryogenically ground to ensure a good distribution of the organoclay in the polymer and to facilitate feeding. Table 5.1 shows the processing conditions used for each extruder and injection molder in this study. The processing conditions used here for each extruder were optimized to produce high levels of platelet delamination and dispersion of PA-6 nanocomposites [1, 4]. Dry extruded pellets from the ZSK 25 and Haake TSE's were injection molded into standard (ASTM D638, Type 1) tensile bars using an Arburg Allrounder 305-210-700 injection molder, while each 3 g batch produced in the DSM micro-compounder was injection molded into smaller bars (7.3 x 1 x 0.32 cm) using a DSM bench-top micro-injection molder.

TEM micrographs were obtained using a JEOL 2010F transmission electron microscope operating at an accelerating voltage of 120 kV. TEM samples for morphology characterization were cryogenically cut into ultrathin sections (30 to 50 nm thick) with a diamond knife at a temperature of -40ºC using a Reichert-Jung Ultracut E

microtome. These sections were taken from the central part of a tensile bar normal to the flow direction (FD) and normal to the transverse direction (TD), and they were viewed parallel to the flow and transverse directions, respectively, as shown in Figure 3.5.

Table 5.1 Equipment and processing conditions used in this study.

Equipment type	Manufacturer (designation used here)	Processing conditions
Modular intermeshing co-rotating twin screw extruder	Werner and Pfleiderer ZSK 25 (ZSK 25 polymer feeder)	Screw speed: 500 rpm Barrel temp.: 240ºC Die temp.: 230ºC Feed rate: 18.14 kg/h Feed conditions: dry blend of polymer and clay
	Werner and Pfleiderer ZSK 25 (ZSK 25 clay feeder)	Screw speed: 500 rpm Barrel temp.: 240ºC Die temp.: 230ºC Feed rate: 18.14 kg/h Feed conditions: separate polymer and clay feeders
	Haake (Haake)	Screw speed: 285 rpm Barrel temp.: 240ºC Die temp.: 240ºC Feed rate: 1.2 kg/h Feed conditions: dry blend of polymer and clay
Batch-type intermeshing co-rotating twin screw compounder	DSM micro-compounder (DSM)	Screw speed: 100 rpm Barrel temp.: 240ºC Die temp.: 240ºC Feed rate: 3.2 g/batch Feed conditions: dry blend of polymer and clay
Injection Molding machine	Arburg Allrounder 305-210-700	Barrel temperature range (from feed to nozzle): 240, 250, 255, and 260 ºC Injection pressure: 70 bar Molding pressure: 35 bar Mold temperature: 80 ºC
	DSM bench-top micro-injection molder	Cylinder temperature: 260 ºC Injection pressure: 4 bar Mold temperature: 80 ºC

RESULTS AND DISCUSSION

Effect of processing on the morphology and properties of PA-6 nanocomposites

The three extruders used in this study have different screw configurations, optimum feed rates, and residence time distributions that exert different levels of shear and residence times on the polymer/organoclay mixture during nanocomposite formation. The screw designs of the extruders used in this study are shown in Figure 5.1. The ZSK 25 TSE has an area of high shear in zone 3 and two turbine mixing elements (TME), one between zones 5 and 6 and the other in zone 9. It has two feed ports; the first in zone 1, for the polymer, and the second in zone 4, for the clay. This allows the polymer to melt, in the high shear area, before being mixed with the clay. The Haake TSE has two medium-shear areas at the end of zone 1 and in zone 3, and only one feed port for both polymer and clay. Details on how the screw elements affect the mixing characteristics of the polymer inside the extruder are given by Dennis et al. [2]. On the other hand, the DSM micro-compounder has no shear elements, one feed port for both polymer and clay, and the residence time can be varied through a recirculation channel. A residence time of 10 min was used in this study based on a series of preliminary tests showing that 10 min was enough time to melt the polymer and fully mix it with the organoclay.

The residence time distributions and the mean residence times for the Haake and ZSK 25 extruders were determined as described by Shon et al. [30], and the results are plotted in Figure 5.2. The residence time distributions for the ZSK 25 TSE were determined by adding 5 g of sodium montmorillonite into the polymer feeder or into the clay feeder, accordingly, and measuring ash contents of collected samples of PA-6 extrudate after passing through the twin screw extruder [26]. The mean residence time for the clay in the ZSK 25 extruder is approximately 0.95 min when adding the clay from the clay feeder, and 1.38 min when adding the clay from the polymer feeder. On the

other hand, the residence time distribution for the Haake TSE was determined by Cho et al. using aluminum pellets [1]; the mean residence time for this extruder is 3.4 min. The following results show the morphology and properties of PA-6 nanocomposites prepared using the extruders and conditions described above.

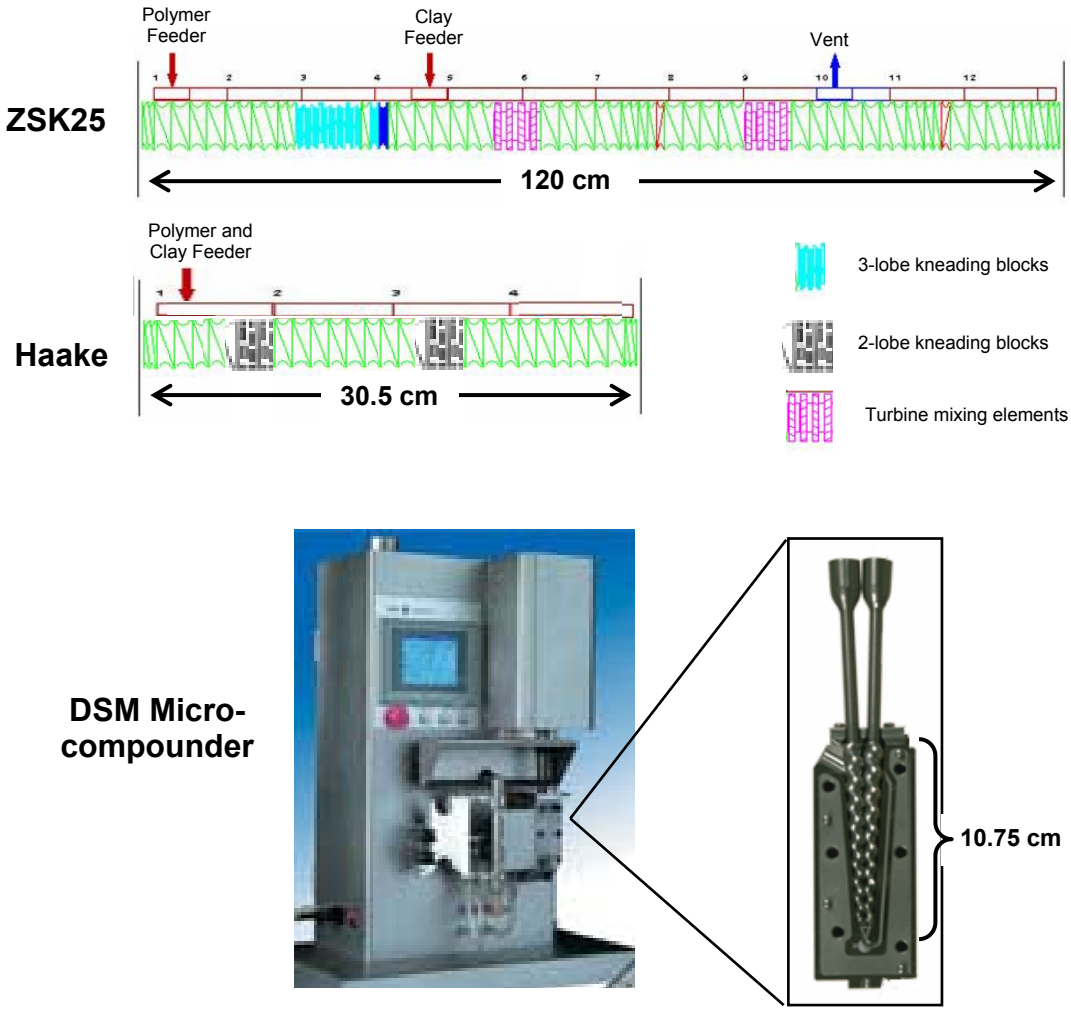

Figure 5.1 Diagrams of the compounders used in this work.

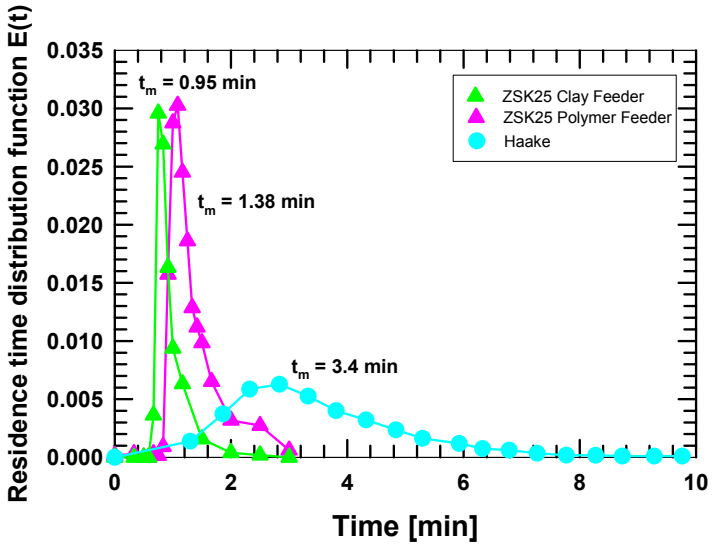

Figure 5.2 Residence time distributions for ZSK 25 adding the clay from the clay feeder, ZSK 25 adding the clay from the polymer feeder, and the Haake twin screw extruders.

Morphology

Figure 5.3 shows WAXS scans for various nanocomposites prepared in this study containing approximately 4.5 wt% MMT, along with a scan of the pure organoclay for comparison. None of the nanocomposites studied here show basal reflections, which suggests well-exfoliated structures in all cases.

TEM micrographs viewed in the flow direction are shown in Figure 5.4. It can be seen that all the composites have high degrees of exfoliation, regardless of the extruder used; however, differences in morphology can be observed between the different extruders and extrusion conditions. At low concentrations, Figure 5.4 shows that the composites formed in the ZSK 25 and the Haake extruders have organoclay particles with long lengths and high degrees of orientation, while the ones formed in the DSM micro-compounder show particles with slightly shorter lengths and a lower orientation. At high

concentrations, all the composites have a similar structure, i.e., mostly single platelets well dispersed in the matrix.

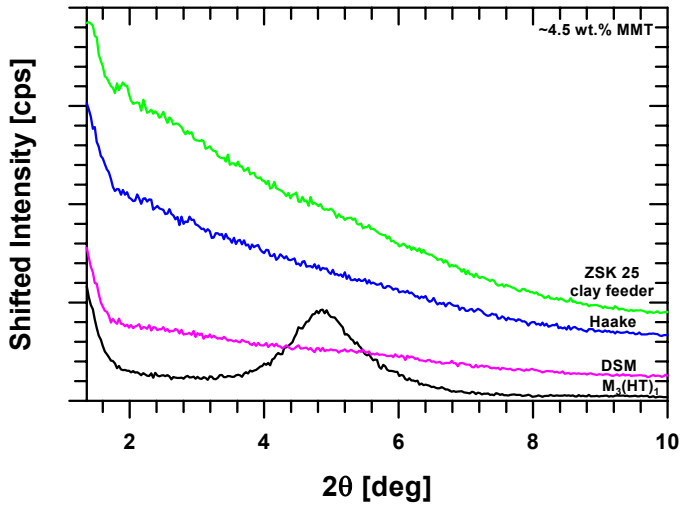

Figure 5.3 WAXS patterns for $M_3(HT)_1$ organoclay and PA-6/$M_3(HT)_1$ nanocomposites processed using different twin screw extruders and feeding conditions. MMT concentration is approximately 4.5 wt%.

These trends were quantified through particle analysis of TEM images as described in Chapter 3; a summary of the results is shown in Table 5.2. Histograms of particle length and thickness distributions at low and high concentrations are presented in Figures 5.5 and 5.6, respectively. In these figures, some of the distributions had a small number of particles with dimensions on either extreme of the size scales which did not show up significantly in the present plots. Since these particles may have some effect on the calculated averages reported in Table 5.2, their locations have been noted with arrows on the corresponding plots. These results show that at both concentrations, the composites formed in the ZSK 25, the Haake, and the DSM TSE's have similar particle length distributions, all with the majority of the particles having lengths between 30 and 60 nm. However, at low concentrations, the nanocomposites formed using the ZSK 25 and the Haake extruders have more particles with lengths above 70 nm.

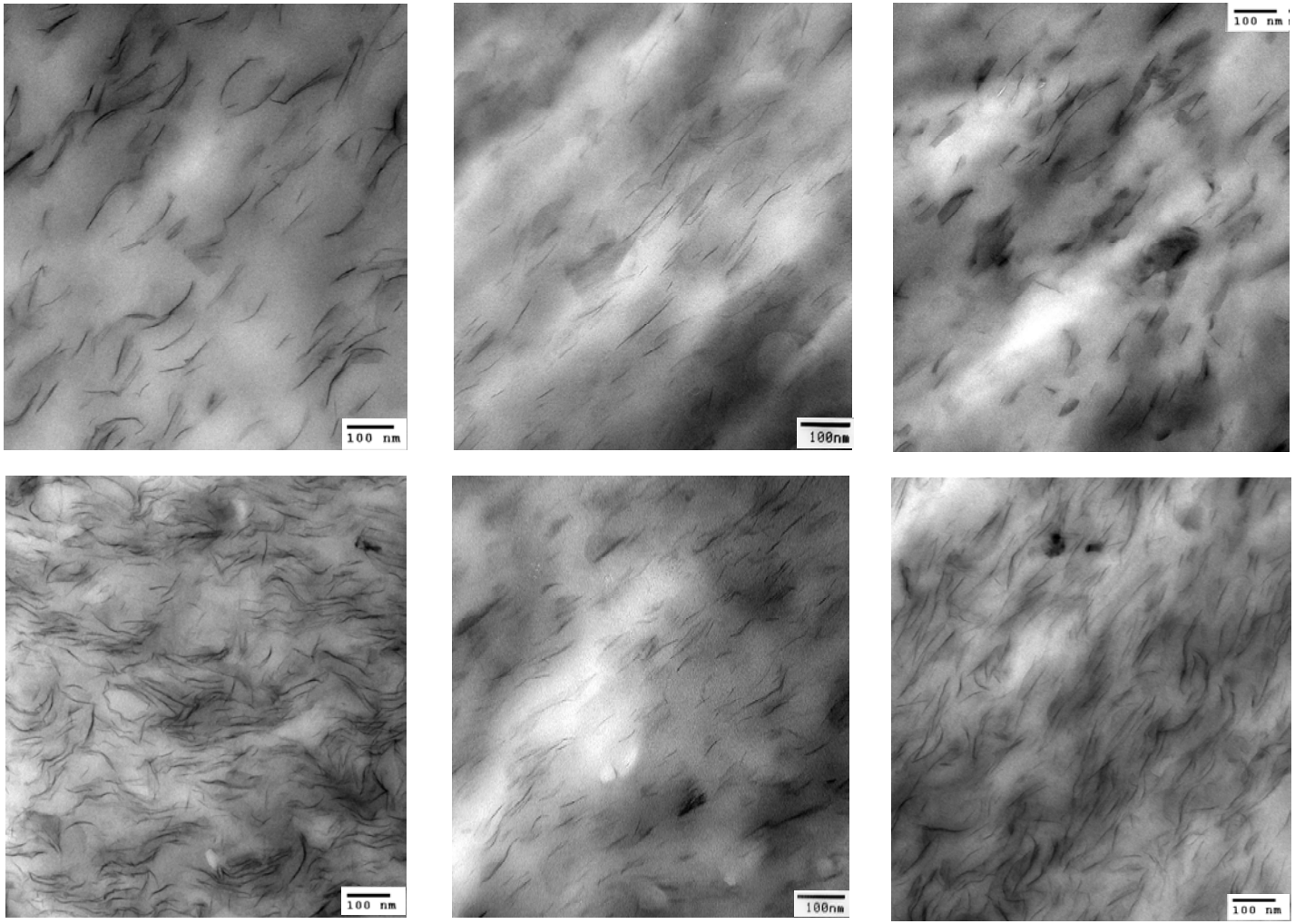

Figure 5.4 TEM micrographs of PA-6/$M_3(HT)_1$ nanocomposites, with organoclay concentrations of approximately 1.5 wt% MMT (above) and 4.5 wt% MMT (below), processed by different twin screw extruders.

Table 5.2 Particle analysis results for PA-6/$M_3(HT)_1$ nanocomposites. Extruder comparison/ Flow direction.

Extruder	Number of particles analyzed	Number average particle length $(\bar{\ell})_n$ [nm]	Weight average particle length $(\bar{\ell})_w$ [nm]	Number average platelets / particle	Weight average platelets / particle	Number average particle thickness [a] $(\bar{t})_n$ [nm]	Weight average particle thickness [a] $(\bar{t})_w$ [nm]
ZSK 25 clay feeder							
1.21 wt% MMT	1387	63	81	1.1	1.2	1.1	1.4
5.02 wt% MMT	5108	51	64	1.2	1.4	1.3	1.8
Haake							
1.28 wt% MMT	451	64	84	1.4	1.7	1.7	2.5
4.37 wt% MMT	1549	53	71	1.2	1.3	1.3	1.7
DSM							
0.89 wt% MMT	1044	50	63	1.1	1.2	1.2	1.5
4.06 wt% MMT	2796	56	70	1.1	1.2	1.1	1.4
ZSK 25 polymer feeder							
1.51 wt% MMT	892	35	44	1.3	1.5	1.4	2.0
4.68 wt% MMT	1720	37	47	1.2	1.4	1.3	2.0

Extruder	Number Average Aspect ratio [b] $(\bar{\ell})_n/(\bar{t})_n$	100% Exfoliation No. Average Aspect ratio	Weight Average Aspect ratio [c] $(\bar{\ell})_w/(\bar{t})_w$	100% Exfoliation Wt. Average Aspect ratio	Particle density [particles / μm^2]	Specific particle density (particle density @ 1 and 5.5 wt% MMT) [particles / μm^2]
ZSK 25 clay feeder						
1.21 wt% MMT	57	67	58	86	220	182
5.02 wt% MMT	39	54	36	68	758	830
Haake						
1.28 wt% MMT	39	68	34	89	153	120
4.37 wt% MMT	42	57	42	76	426	536
DSM						
0.89 wt% MMT	43	53	42	67	161	181
4.06 wt% MMT	50	59	50	74	414	560
ZSK 25 polymer feeder						
1.51 wt% MMT	25	37	22	47	238	158
4.68 wt% MMT	29	39	24	50	619	727

[a] No. average and wt. average thicknesses were obtained by converting each value of number of platelets per particle in the distribution to particle thickness as outlined by Fornes et al. [28], and taking the no. and wt. averages respectively.
[b] These values of the aspect ratio were computed from the number average platelet lengths and thicknesses
[c] These values of the aspect ratio were computed from the weight average platelet lengths and thicknesses

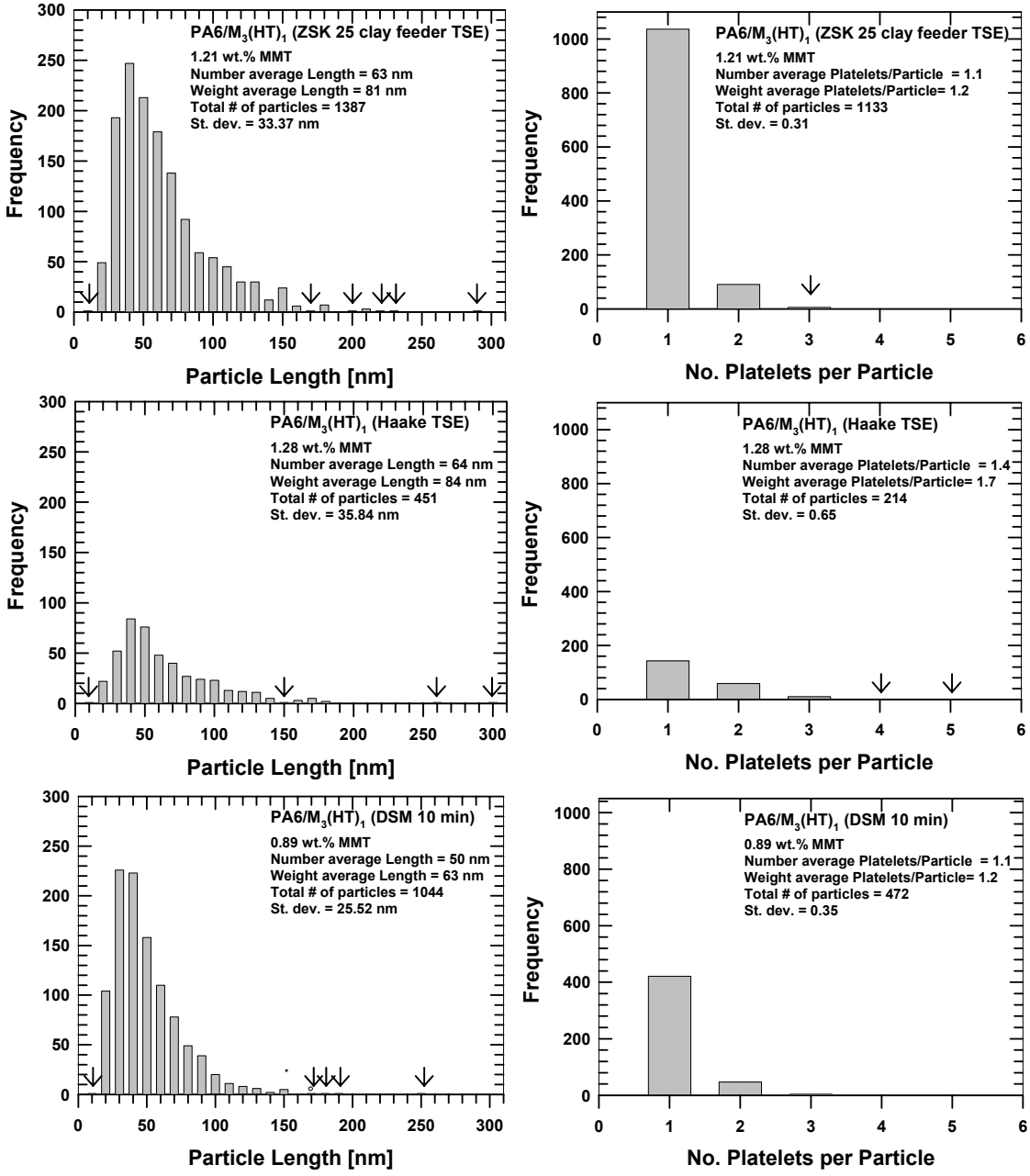

Figure 5.5 Histograms of particle length and thickness distributions for PA-6 nanocomposites at ~1.5 wt% MMT. The arrows in the figures indicate finite particle populations that do not appear at the scales shown here.

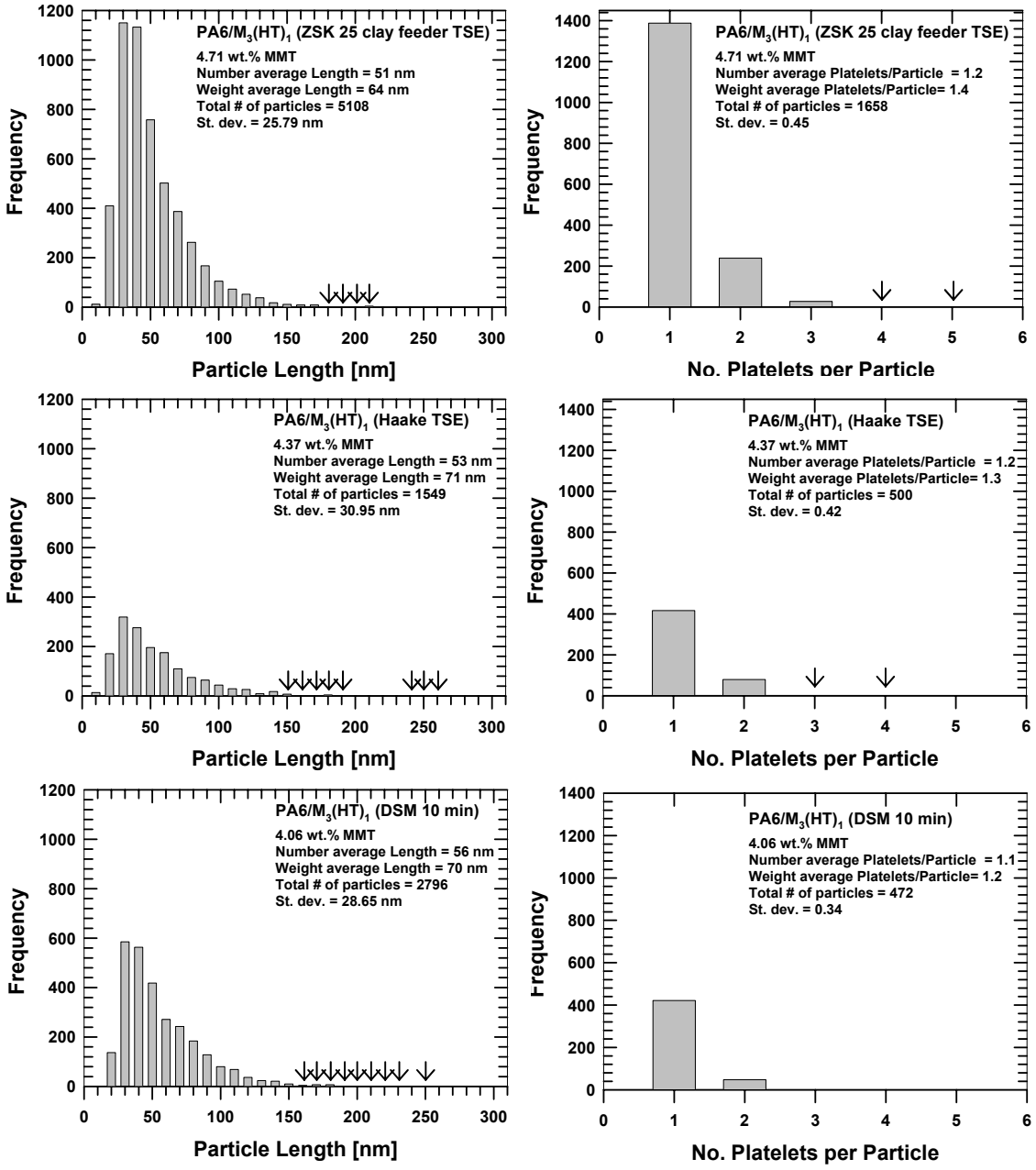

Figure 5.6 Histograms of particle length and thickness distributions for PA-6 nanocomposites at ~4.5 wt% MMT. The arrows in the figures indicate finite particle populations that do not appear at the scales shown here.

With respect to platelet delamination, the analysis shows that the particles in all the composites are primarily single platelets. The nanocomposites compounded in the Haake have slightly higher average thicknesses at low concentrations; nonetheless, more than 70% of the particles analyzed were single-platelet particles.

Additionally, at low concentrations, the ZSK 25 extruder leads to the highest aspect ratio, while slightly lower values were observed for the composites processed in the Haake and DSM TSE's. At high concentrations, the aspect ratio of the composites processed in the DSM micro-compounder is slightly higher than for the ZSK 25 and the Haake extruders. This might be due to the lower average particle thickness obtained for the nanocomposites made in the DSM micro-compounder. Since the values of average particle thickness are critical for aspect ratio calculations, in order to reflect the morphology seen through TEM imaging for composites with very high degrees of exfoliation such as PA-6 nanocomposites; the small differences between the numbers are many times larger than the inherent errors of the analysis. For example, in the nanocomposite systems analyzed here, more than 70% of the particles are single platelets in all cases. The remaining particles with more than one platelet are mostly skewed particles (Fig. 4.14) where the average thickness is less than the value obtained by calculation from the number of platelets per particle. For this reason, a 100% exfoliation aspect ratio was calculated, assuming that the average particle thickness is mainly equal to that of a single platelet. These results, also included in Table 5.2, show that the composites formed in the ZSK 25 and the Haake TSE's have the highest 100% exfoliation aspect ratio, while the composites processed in the DSM micro-compounder have a slightly lower 100% exfoliation aspect ratio. This is more in accordance with the TEM observations shown previously and with the mechanical property results shown next. These types of approximations should be taken into consideration for composite

theory modeling, especially when such small differences in morphology and mechanical properties are observed [8, 28].

Additionally, at low clay concentrations, the specific particle density is higher in the nanocomposites processed in the ZSK 25 extruder and in the DSM micro-compounder, followed by the ones formed in the Haake TSE which have a slightly lower particle density. On the other hand, at high concentrations, the ZSK 25 yields the highest specific particle density, while the Haake and DSM compounders lead to a lower particle density.

It is also important to add that as the clay concentration increases, the average particle length decreases slightly for the nanocomposites processed in the ZSK 25 and in the Haake extruders, while it remains almost the same in the DSM micro-compounder. The number of platelets per particle and the aspect ratio remain almost the same or decrease slightly with increasing clay concentration in most cases. As expected, the specific particle density increases in all cases as the clay concentration increases.

PA-6 nanocomposites were extruded using the ZSK 25 TSE by dry-blending the polymer and the organoclay prior to feeding both from the polymer feeder in zone 1 and compared to the nanocomposites described in the previous section formed by using separate feeders for the polymer and the organoclay in zones 1 and 4, respectively. WAXS results for the composites formed by dry-blending the polymer and the organoclay in the polymer feeder do not show any basal reflections, similar to what was shown in Fig. 5.3, which suggests a high degree of platelet delamination in these nanocomposites as well. The TEM micrographs viewed parallel to the flow direction shown in Figure 5.7 show that the particle lengths for these composites seem noticeably

smaller than the composites formed by adding the organoclay from the clay feeder and than the nanocomposites processed in the other extruders.

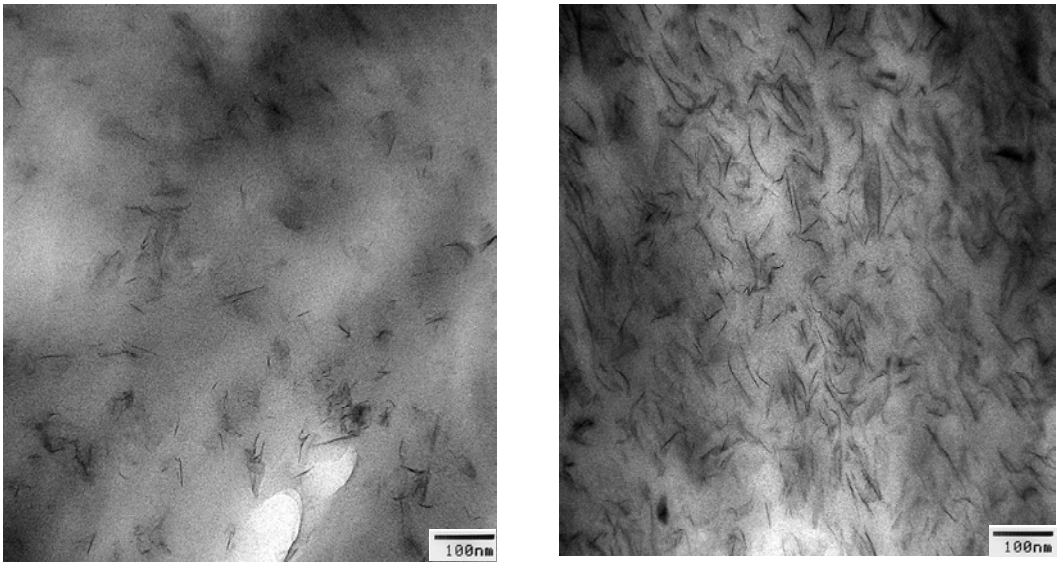

Figure 5.7 TEM micrographs of PA-6/$M_3(HT)_1$ nanocomposites processed in the ZSK 25 twin screw extruder by premixing the polymer and the organoclay and adding both in the polymer feeder.

The particle analysis results for these composites are also shown in Table 5.2; particle length and thickness distributions are shown in Figure 5.8. These results confirm our observations by showing a very narrow particle length distribution, where most of the particles have lengths between 20 and 50 nm; in addition, the particle length remains almost constant as the clay concentration increases. These results also show slightly higher average particle thicknesses for these composites, which also seems to be related to the presence of skewed particles as mentioned for the composites processed in the Haake extruder. The considerably lower average particle length obtained gives noticeably lower aspect ratios, at both concentrations, when compared to the ones

observed in the ZSK 25 extruder using the clay feeder and also with respect to the composites processed in the Haake and DSM extruders.

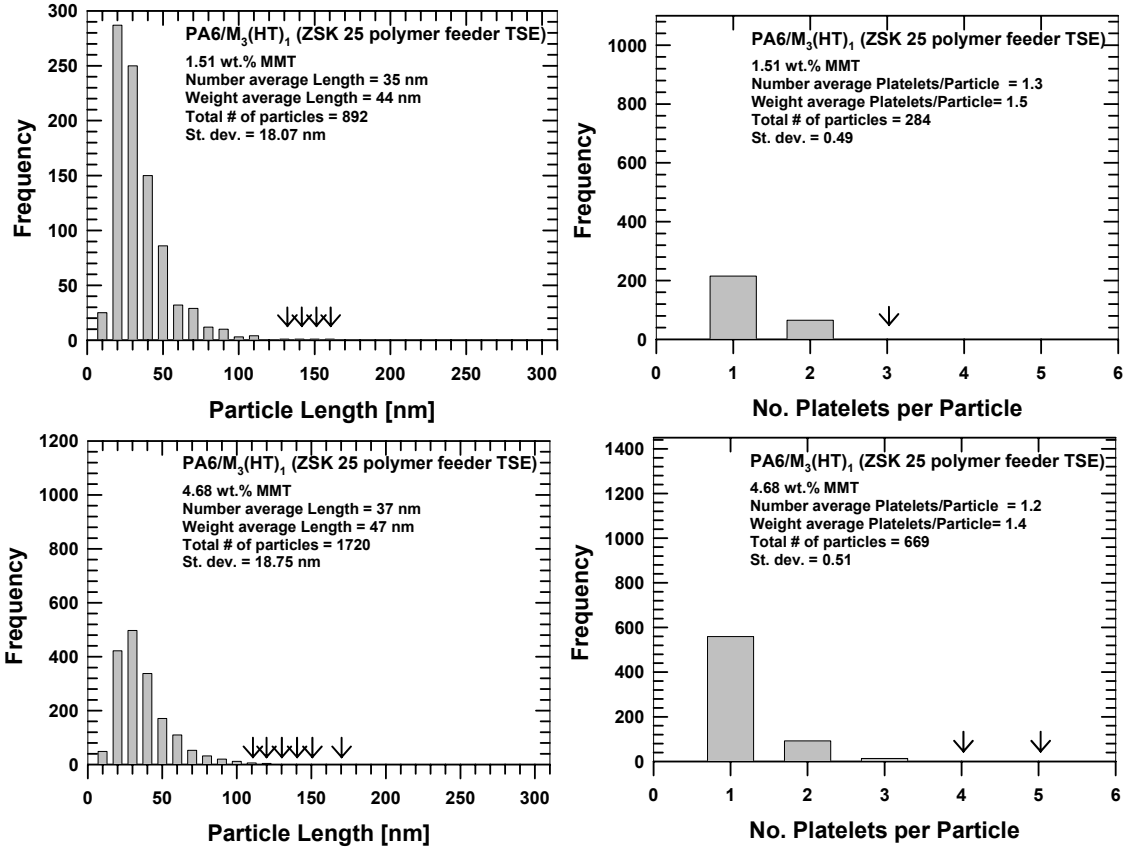

Figure 5.8 Histograms of particle length and thickness distributions for PA-6 nanocomposites processed in the ZSK 25 twin screw extruder by premixing the polymer and the organoclay. The arrows in the figures indicate finite particle populations that do not appear at the scales shown here.

The effect of residence time on the degree of platelet dispersion of PA-6 nanocomposites formed in the DSM micro-compounder was investigated by processing the nanocomposites at residence times of 10, 15, and 20 min. The WAXS scans for the nanocomposites showed no basal reflections, similar to what was shown in Fig. 5.3, and this again suggests well-exfoliated structures in all cases. Figure 5.9 shows TEM

micrographs viewed parallel to the flow direction for the composites formed in the DSM micro-compounder at residence times of 10 and 20 min. At both concentrations, a noticeably higher number of particles is observed when the residence time is increased from 10 to 20 min.

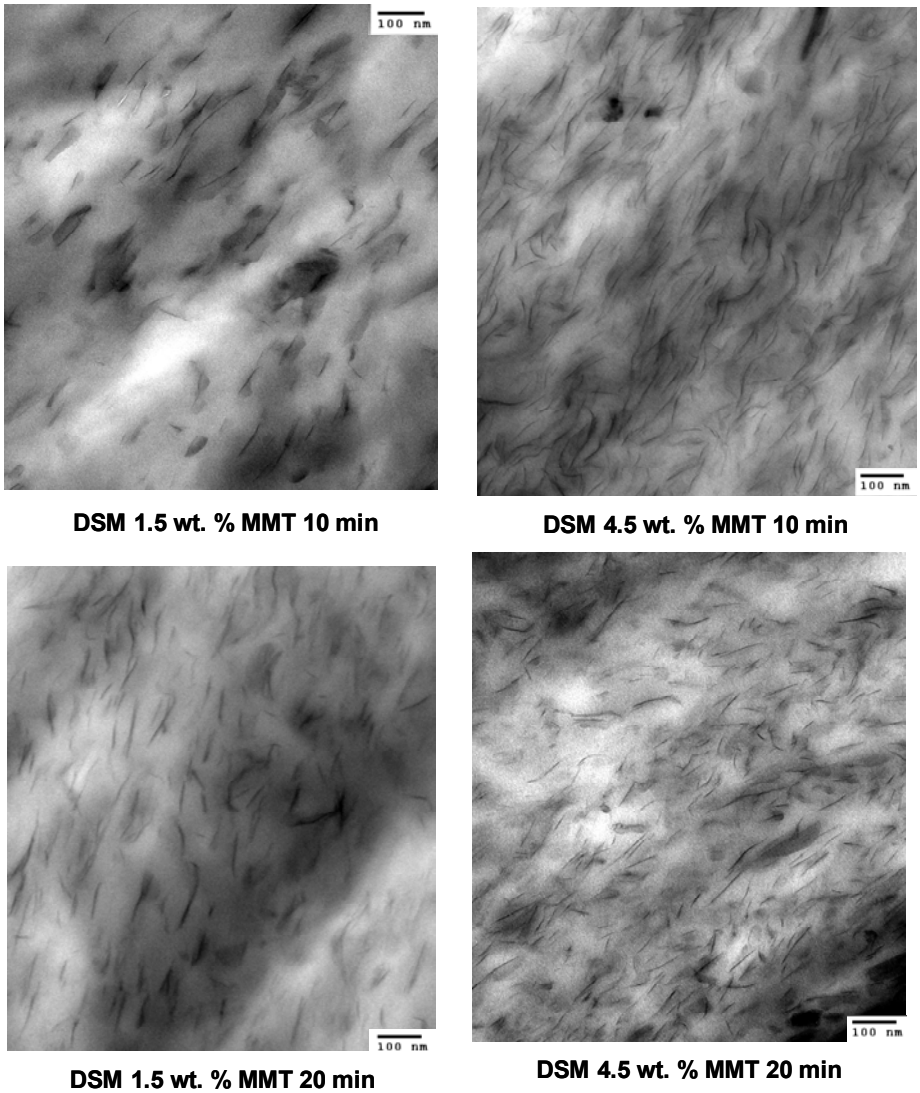

Figure 5.9 TEM micrographs of PA-6/$M_3(HT)_1$ nanocomposites processed in the DSM micro-compounder at residence times of 10 and 20 min.

The particle analysis results shown in Table 5.3 confirm an increase in particle density with increasing residence time at both concentrations. The particle length distributions shown in Figure 5.10 show a shift towards higher particle lengths with a longer residence time for low clay concentrations, while the number of particles with lengths between 20 and 40 nm increases with longer mixing times at higher clay concentrations. In spite of this, the range of particle lengths for the majority of the particles remains basically the same. Table 5.3 also shows there is no noticeable change in particle thickness at either concentration; most of the particles analyzed were single platelets at low and high concentrations and for both residence times. As a result, the aspect ratio increases with residence time at low concentrations, while it slightly decreases at high concentrations; this is mostly due to the changes in the average particle length mentioned earlier.

A somewhat analogous effect was achieved for the Haake and ZSK 25 extruders by re-extruding some of the nanocomposite samples one or two additional times, i.e., number of passes. To maintain consistency in this experiment, the effect of number of passes could only be explored in the ZSK 25 TSE when the polymer and organoclay were dry-blended and fed from the polymer feeder. The WAXS scans for these nanocomposites again show no basal reflections, which is indicative of the high degree of exfoliation obtained for this PA-6 nanocomposite system. Figures 5.11 and 5.12 show TEM micrographs for the nanocomposites processed in the Haake and ZSK 25 extruders after one and three passes. These figures show that the number of particles is higher in the nanocomposites extruded three times than when only extruded once. Figure 5.11 shows that at low concentrations, increasing the number of passes from one to three increases the number of particles similarly for both extruders, while at high

Table 5.3 Particle analysis results for PA-6/$M_3(HT)_1$ nanocomposites. Effect of residence time in DSM micro-compounder/ Flow direction.

Extruder	Number of particles analyzed	Number average particle length $(\bar{\ell})_n$ [nm]	Weight average particle length $(\bar{\ell})_w$ [nm]	Number average platelets / particle	Weight average platelets / particle	Number average particle thickness [a] $(\bar{t})_n$ [nm]	Weight average particle thickness [a] $(\bar{t})_w$ [nm]
DSM							
0.89 wt% MMT/ 10 min	1044	50	63	1.1	1.2	1.2	1.5
1.17 wt% MMT/ 20 min	1115	66	84	1.1	1.2	1.1	1.4
4.06 wt% MMT/ 10 min	2796	56	70	1.1	1.2	1.1	1.4
4.19 wt% MMT/ 20 min	2802	42	52	1.1	1.2	1.1	1.4

Extruder	Number Average Aspect ratio [b] $(\bar{\ell})_n/(\bar{t})_n$	100% Exfoliation No. Average Aspect ratio	Weight Average Aspect ratio [c] $(\bar{\ell})_w/(\bar{t})_w$	100% Exfoliation Wt. Average Aspect ratio	Particle density [particles / μm^2]	Specific particle density (particle density @ 1 and 5.5 wt% MMT) [particles / μm^2]
DSM						
0.89 wt% MMT/ 10 min	43	53	42	67	161	181
1.17 wt% MMT/ 20 min	58	70	60	89	202	172
4.06 wt% MMT/ 10 min	50	59	50	74	414	560
4.19 wt% MMT/ 20 min	39	45	37	55	410	538

[a] No. average and wt. average thicknesses were obtained by converting each value of number of platelets per particle in the distribution to particle thickness as outlined by Fornes et al. [28], and taking the no. and wt. averages respectively.
[b] These values of the aspect ratio were computed from the number average platelet lengths and thicknesses
[c] These values of the aspect ratio were computed from the weight average platelet lengths and thicknesses

concentrations, the composites formed using the Haake TSE show a more noticeable increase in number of particles as the number of passes increases (Fig. 5.12).

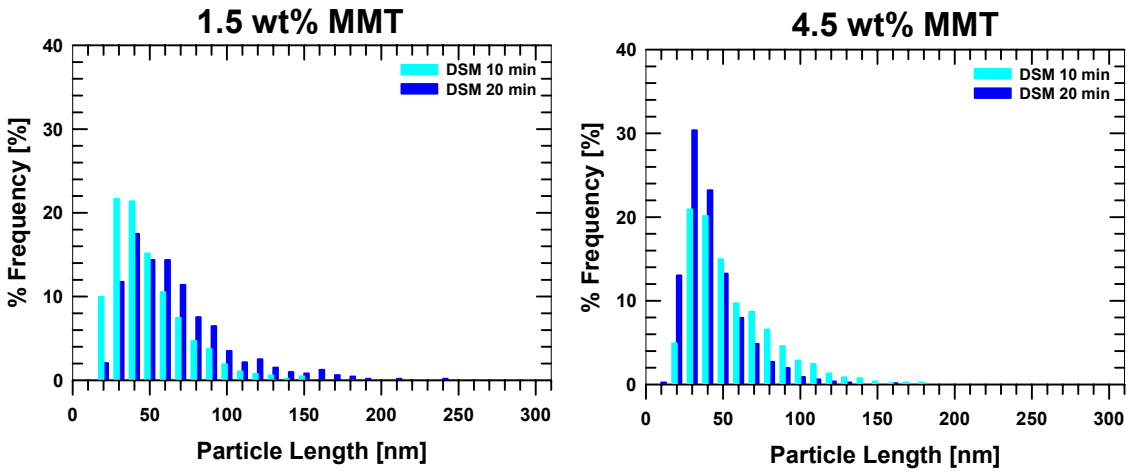

Figure 5.10 Histograms of particle length distribution for PA-6 nanocomposites processed in the DSM micro-compounder for 10 and 20 min.

The particle analysis results in Table 5.4 do not show large differences in average particle lengths as the number of passes was increased, on the other hand, the histograms in Figure 5.13 show that at low concentrations, the particle length distribution for the composites formed in the Haake TSE shifts towards lower particle lengths as the number of passes is increased, i.e., the lengths of the majority of the particles shift from 30-50 nm to 20-50 nm at high residence times, and there is a smaller number of particles with lengths over 100 nm. In addition, the particle length distribution for the composites prepared in the ZSK 25 TSE remains almost the same when increasing the number of passes, and most of its particles still have lengths in the range of 20-50 nm. Figure 5.13 also shows the distributions of particle lengths at high concentrations; these distributions indicate no significant change from one to three passes for either case. The particle thicknesses and aspect ratios remain almost unchanged in all cases as the number of

passes is increased, while a slight tendency towards lower thicknesses was observed in some cases (Table 5.4). It is also shown that the specific particle density increases in both cases as the number of passes is increased; this is consistent with a better dispersion obtained through longer mixing times.

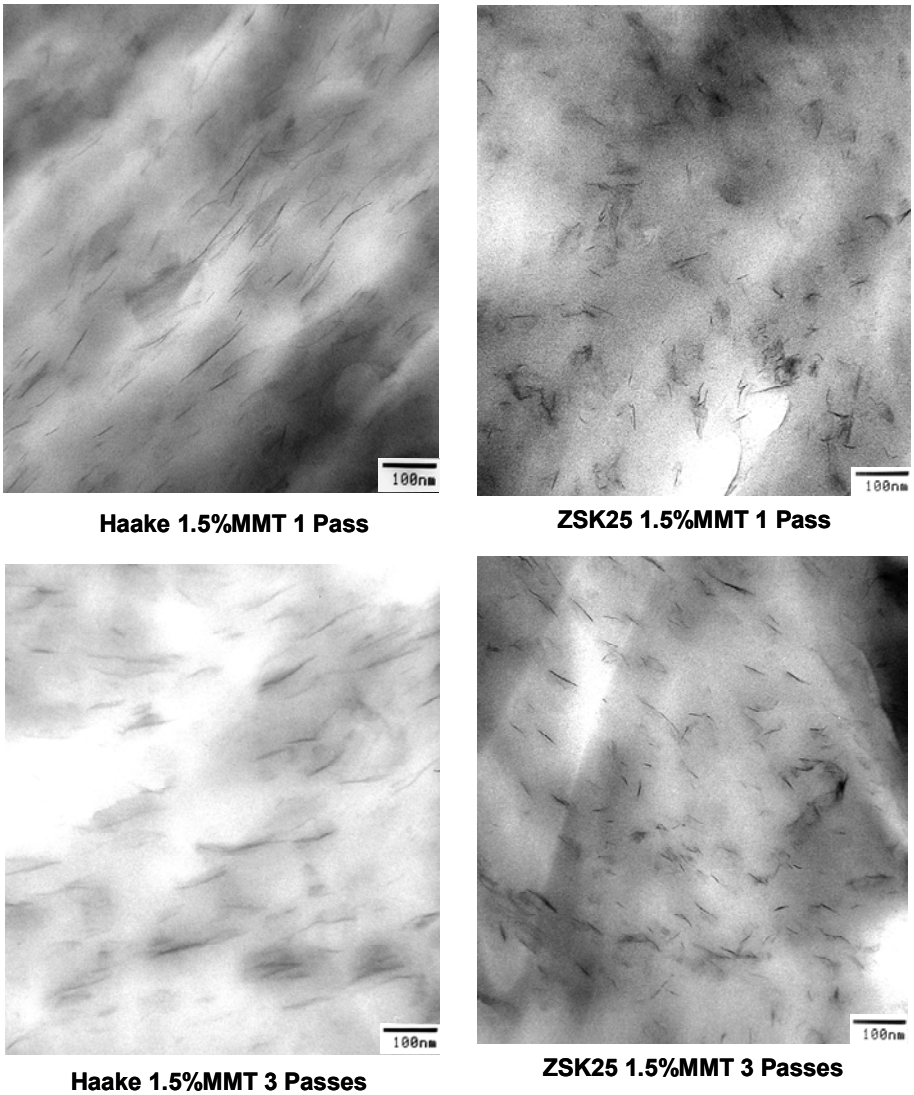

Figure 5.11 TEM micrographs of PA-6/$M_3(HT)_1$ nanocomposites with ~1.5 wt% MMT. Effect of number of passes for the Haake and ZSK25 (polymer feeder) TSE's.

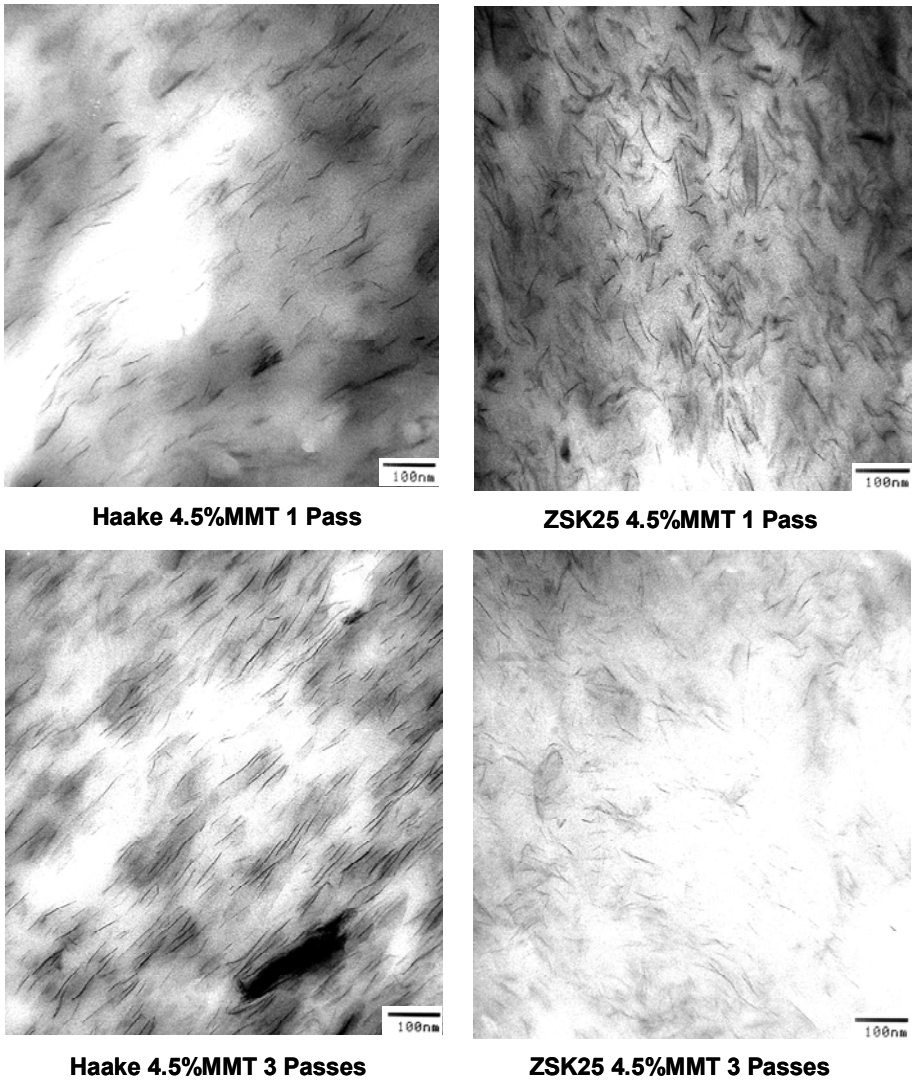

Figure 5.12 TEM micrographs of PA-6/$M_3(HT)_1$ nanocomposites with ~4.5 wt% MMT. Effect of number of passes for Haake and ZSK25 (polymer feeder) TSE's.

Mechanical properties

Figure 5.14 shows the effect of MMT concentration on Young's modulus, yield strength and elongation at break for the nanocomposites prepared in this study. These results show that the addition of organoclay leads to a substantial increase in Young's modulus for all the nanocomposites, even at low loadings. The nanocomposites processed using the ZSK 25 extruder with the clay feeder and using the Haake TSE

Table 5.4 Particle analysis results for PA-6/$M_3(HT)_1$ nanocomposites. Effect of number of passes in Haake and ZSK25 twin screw extruders/ Flow direction.

Extruder	Number of particles analyzed	Number average particle length $(\bar{\ell})_n$ [nm]	Weight average particle length $(\bar{\ell})_w$ [nm]	Number average platelets / particle	Weight average platelets / particle	Number average particle thickness [a] $(\bar{t})_n$ [nm]	Weight average particle thickness [a] $(\bar{t})_w$ [nm]
Haake							
1.28 wt% MMT/ 1 pass	451	64	84	1.4	1.7	1.7	2.5
1.29 wt% MMT/ 3 passes	882	49	62	1.2	1.3	1.3	1.7
4.37 wt% MMT/ 1 pass	1549	53	71	1.2	1.3	1.3	1.7
4.47 wt% MMT/ 3 passes	3033	51	67	1.2	1.3	1.3	1.7
ZSK 25 polymer feeder							
1.51 wt% MMT/ 1 pass	892	35	44	1.3	1.5	1.4	2.0
1.45 wt% MMT/ 3 passes	936	37	44	1.3	1.4	1.4	1.9
4.68 wt% MMT/ 1 pass	1720	37	47	1.2	1.4	1.3	2.0
4.71 wt% MMT/ 3 passes	2727	38	47	1.1	1.2	1.1	1.5

Extruder	Number Average Aspect ratio [a] $(\bar{\ell})_n/(\bar{t})_n$	100% Exfoliation No. Average Aspect ratio	Weight Average Aspect ratio [b] $(\bar{\ell})_w/(\bar{t})_w$	100% Exfoliation Wt. Average Aspect ratio	Particle density [particles / μm^2]	Specific particle density (particle density @ 1 and 5.5 wt% MMT) [particles / μm^2]
Haake						
1.28 wt% MMT/ 1 pass	39	68	34	89	153	120
1.29 wt% MMT/ 3 passes	39	52	36	66	234	181
4.37 wt% MMT/ 1 pass	42	57	42	76	426	536
4.47 wt% MMT/ 3 passes	41	55	39	71	566	696
ZSK 25 polymer feeder						
1.51 wt% MMT/ 1 pass	25	37	22	47	238	158
1.45 wt% MMT/ 3 passes	26	39	23	47	260	179
4.68 wt% MMT/ 1 pass	29	39	24	50	619	727
4.71 wt% MMT/ 3 passes	34	40	31	50	568	663

[a] No. average and wt. average thicknesses were obtained by converting each value of number of platelets per particle in the distribution to particle thickness as outlined by Fornes et al. [28], and taking the no. and wt. averages respectively.
[b] These values of the aspect ratio were computed from the number average platelet lengths and thicknesses
[c] These values of the aspect ratio were computed from the weight average platelet lengths and thicknesses

reveal the largest increase in Young's modulus, while the ones processed in the DSM micro-compounder lead to a lower increase in modulus. There is a substantial increase in the yield strength for the composites processed in the ZSK 25 and in the Haake extruder, and the results obtained for elongation at break show a very pronounced decrease in ultimate elongation for these composites. As mentioned in Chapter 3, the Young's modulus is the only tensile property that can be measured for the composites prepared in the DSM micro-compounder since the bars formed in the DSM micro-injection molder do not have tabs needed to measure failure properties.

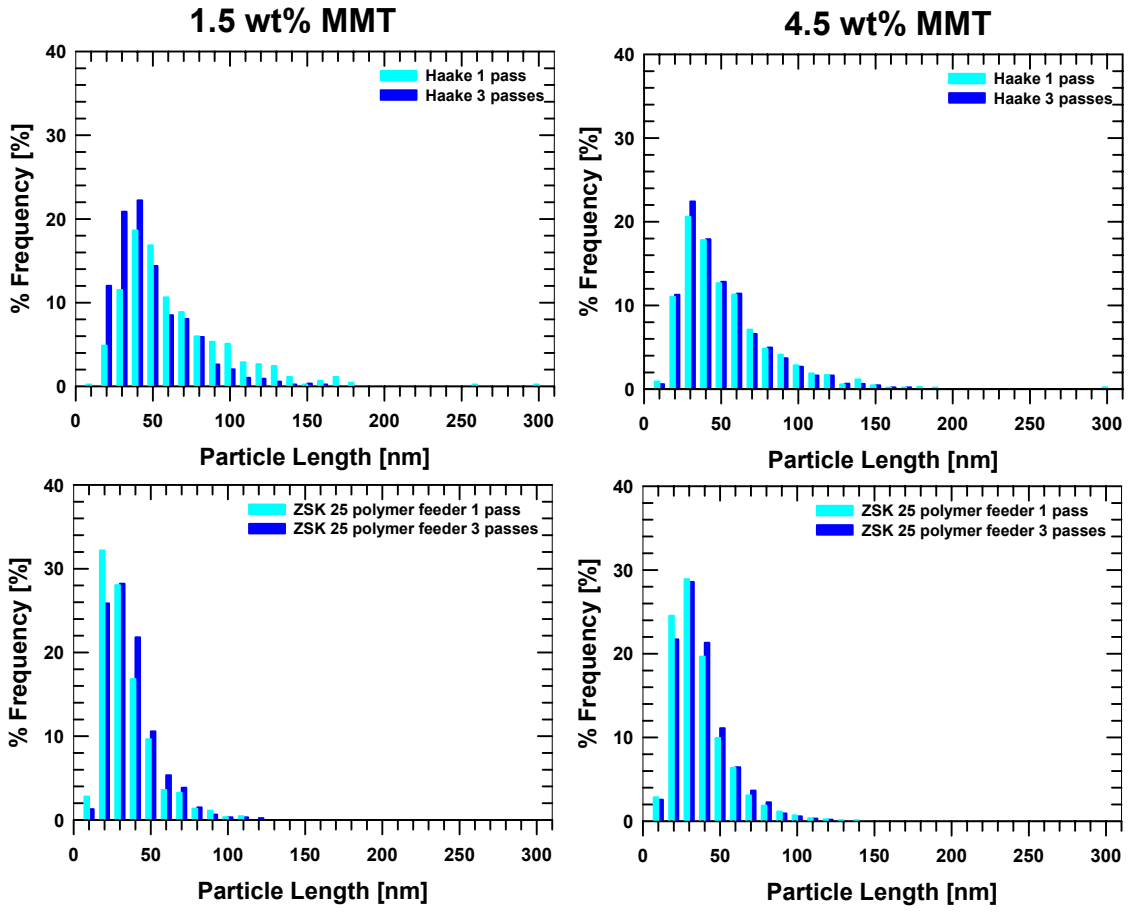

Figure 5.13 Histograms of particle length distribution for PA-6 nanocomposites processed in the Haake and ZSK 25 twin screw extruders for 1 and 3 passes.

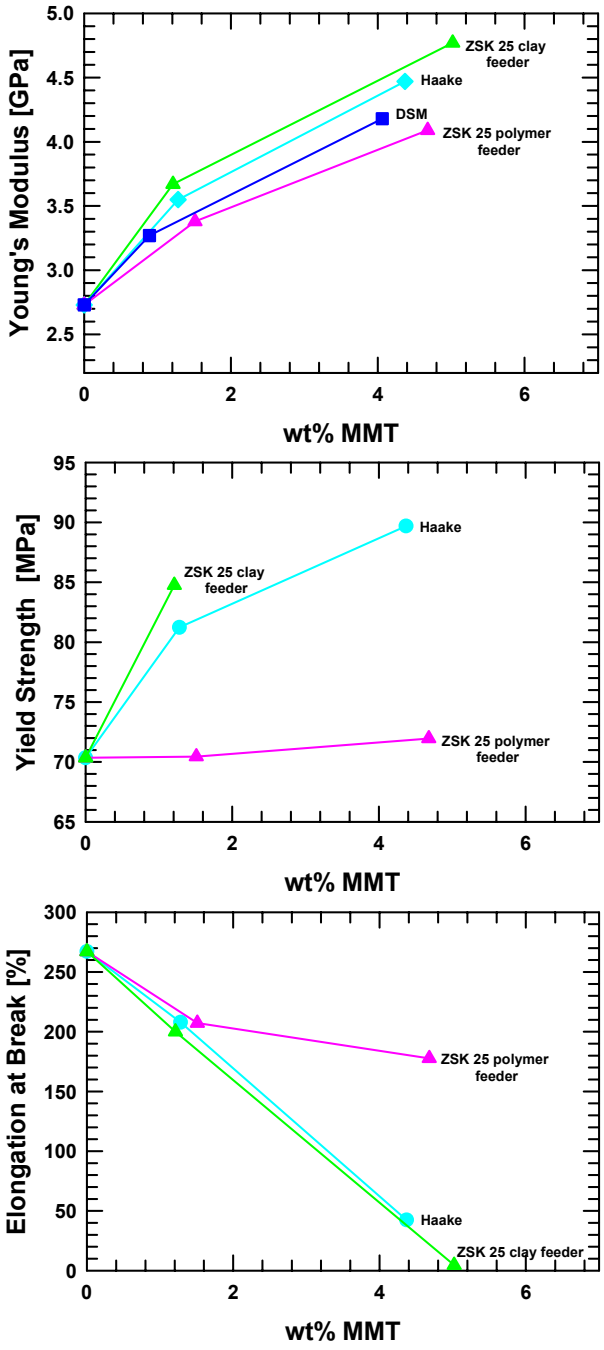

Figure 5.14 Mechanical properties of PA-6 nanocomposites processed using different twin screw extruders and feeding conditions.

The addition of a mixture of dry blended polymer and organoclay at the polymer feeder in the ZSK 25 extruder leads to the lowest increase in Young's modulus and yield strength, while a less pronounced decline is observed in elongation at break. This is most probably due to the lower aspect ratios, resulting from the smaller average particle lengths described in the previous section. The particle lengths from these composites may be close to the critical length required to reinforce the composite [31].

Figure 5.15 shows the Young's modulus for the nanocomposites prepared using the DSM micro-compounder at various residence times. Increasing the residence time in the DSM micro-compounder beyond the minimum 10 min does not lead to a noticeable increase in Young's modulus.

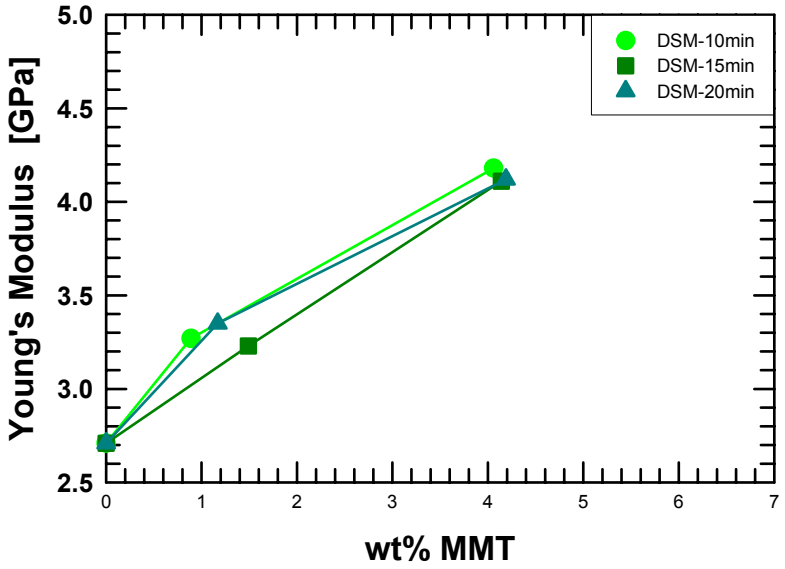

Figure 5.15 Young's modulus of PA-6 nanocomposites processed in the DSM micro-compounder. Effect of residence time.

Figure 5.16 shows the effect of number of passes on Young's modulus, yield strength, and elongation at break for the composites prepared in the Haake and ZSK 25 extruders by dry blending the polymer and the organoclay prior to feeding into the

extruder. Interestingly, there is a good correlation between the number of passes and the level of matrix reinforcement for these two cases: the Young's modulus and the yield strength increase while the elongation at break decreases proportionally as the number of passes is increased.

The mechanical property results shown above are consistent with the morphology deduced through WAXS, TEM, and particle analysis. All the composites prepared in this study show extremely high levels of exfoliation; the absence of X-ray basal reflections and a morphology primarily consisting of single-platelet particles is in accord with the large increase in modulus in all cases. In the cases presented here, the screw configurations used in the ZSK 25 by adding the organoclay from the clay feeder and in the Haake extruders seem to produce the best platelet dispersion and delamination. The longer particles formed cause the largest increase in modulus and yield strength and the greatest reduction in ultimate elongation. It appears that melting the polymer before coming into contact with the organoclay, followed by a low level of shear, and applying a medium level of shear throughout the extruder, for a longer residence time seems to be the most favorable extruder mixing conditions employed in this study. The lack of shear elements and the considerably longer residence times in the DSM micro-compounder seem to produce a slightly lower degree of clay dispersion and modulus enhancement.

For the cases presented here, blending the organoclay in the ZSK 25 extruder with solid polymer, as opposed to blending it with the molten polymer, leads to extremely short particle lengths and a lower matrix reinforcement possibly be due to the attrition of clay platelets under these conditions. Dennis et al. mention that shear is necessary to melt the polymer, breakup the clay particles, and promote contact between the organoclay

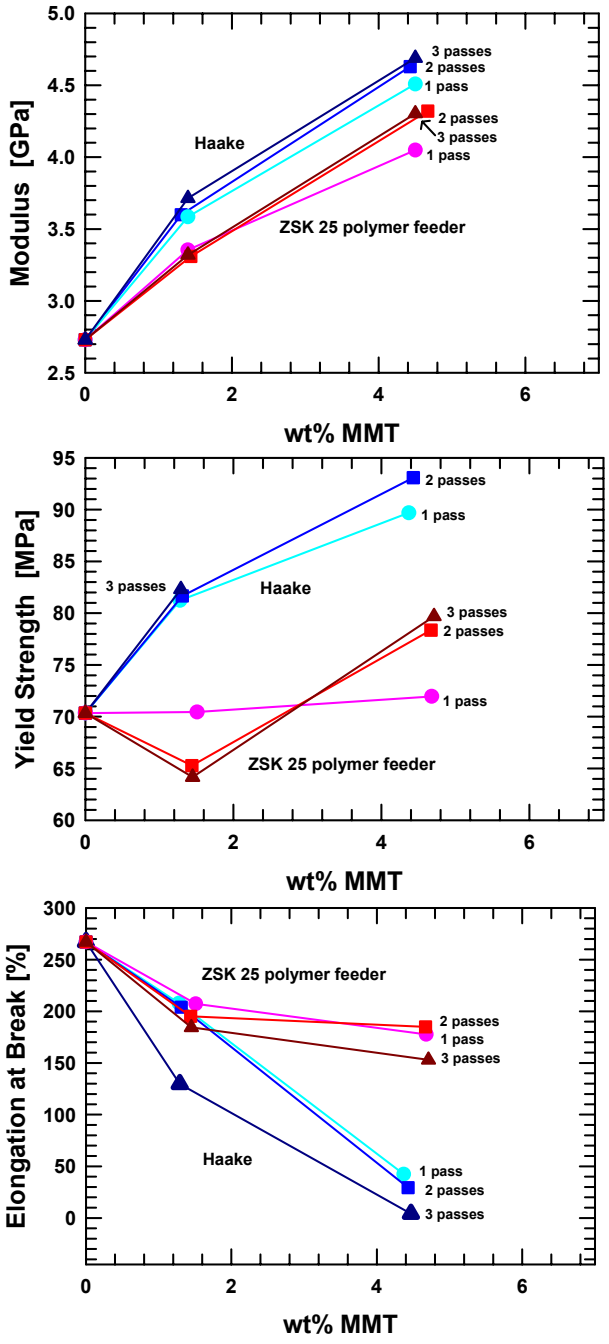

Figure 5.16 Mechanical properties of PA-6 nanocomposites for Haake and ZSK 25 extruders. Effect of number of passes.

and the polymer, but that a low-to-medium shear environment after the initial mixing is most favorable to promote platelet delamination. They suggest that a very high shear, dispersive mixing is not ideal for delamination of PA-6 nanocomposites [2]. It is well known that for glass fiber composites, mixing solid pellets with the fibers produces fiber attrition; hence, dry blending the solid polymer and the organoclay may be severe on the clay particles. Short particle lengths were not observed for the nanocomposites formed in the Haake TSE, even though the polymer and organoclay were also dry blended; therefore, these two extruder conditions have a different effect on the clay particles. In the case of the Haake extruder, the longer residence time may indicate that the polymer in the mixture may start to melt before it reaches the foremost shear element; this may reduce the force exerted on the clay particles. On the other hand, the ZSK25 extruder has a shorter residence time that may not allow the polymer to melt by the time the mixture reaches the first shear element. From extruder specifications and the mean residence times shown before, it is estimated that the polymer is conveyed for twice as much time before reaching the first shear element in the Haake TSE which may support what is implied above.

Dennis et al. conclude that increasing the residence time in the extruder generally improves delamination and dispersion of the organoclay, which in turn improves the mechanical properties of the composites [2]. Increasing the residence time in the DSM micro-compounder led to higher clay dispersion for PA-6 nanocomposites; however, longer mixing times did not produce significant changes in modulus enhancement. In addition to particle aspect ratio, the relative degree of orientation or alignment with respect to the test direction affects the degree of reinforcement; generally the alignment of particles is primarily affected by the molding process. Since the nanocomposites formed in the ZSK 25 and Haake TSE's were molded using the same injection molder

and under the same processing conditions, the differences observed in the morphology and properties of these nanocomposites must be largely due to the effects of the extruder mixing characteristics. On the other hand, the nanocomposites processed in the DSM micro-compounder were molded using the DSM bench-top micro-injection molder; therefore, the morphology and the lower modulus enhancement observed for these nanocomposites probably reflect both the lack of shear elements and longer residence time during compounding as well as the nature of the injection molding process, such as the lower injection pressure and shear for particle alignment. In spite of this, the DSM micro-compounder produces similar trends in morphology and modulus as the ones obtained with conventional twin screw extruders, suggesting that the DSM micro-compounder is a good alternative for nanocomposite research especially when only small amounts of material are available.

Increasing the number of passes in the extruder produces higher particle dispersion, giving rise to higher levels of reinforcement. Cho et al., also found that the mechanical properties of PA-6 nanocomposites were improved by a second and third pass through the extruder [1]. Increasing the number of passes produces an increase in matrix reinforcement, while morphological analysis shows an improvement in clay dispersion even when the particle size remains mostly the same. When the nanocomposites are extruded several times through the extruder, the material not only spends more time in the extruder increasing the mixing time, but it also goes through more than one melting cycle that may also have an effect on the mechanical properties of the nanocomposites.

Morphology characterization of PA-6 nanocomposites in different viewing directions

As mentioned earlier for nanocomposites formed by melt processing, when there is a very good affinity between the polymer and the organoclay, the degree of platelet dispersion and delamination is determined primarily in the extruder [2] while it might be expected that the orientation of the particles is determined mostly by the nature of the injection molding process [6]. Because of this, the morphology characterization from different viewing directions within the molded sample should provide insights on how the platelets are aligned during the mold-filling process. Generally, one expects the filler particles to align with the polymer flow direction, i.e., with the major axis of the platelets in the flow direction [6, 32-35]. In a paper comparing the thermal expansion behavior of PA-6 nanocomposites, Yoon et al. compared the morphology of PA-6/$(HE)_2M_1R_1$ nanocomposites as viewed in the TEM parallel to all three orthogonal directions, i.e., viewing parallel to the transverse (TD), normal (ND), and flow (FD) directions, as shown in Figure 3.5. They observed that in views parallel to the FD, the platelets seemed more randomly oriented, with a preferential alignment along the transverse direction; while in views parallel to the TD, the platelets were better aligned along the flow direction and tilted faces were observed probably from a tendency for rotation in the transverse direction [6]. They also mention that more exfoliated systems seem to have higher alignment of platelets, since single platelets may be easier to align than irregular particles. Particle analyses performed by Yoon et al. show that the average particle length was larger when viewed parallel to the transverse direction, suggesting that the clay particles may be anisotropic in dimensions within the plane and tend to orient with the major axis aligned with the dominant flow field, i.e., where the stresses are highest [6]. On the other hand, Lee et al. show that the opposite is observed in poorly exfoliated

systems like polypropylene/polypropylene modified with maleic anhydride (PP/PP-g-MA) nanocomposites, i.e., the particles show a higher alignment along the TD when viewed parallel to the flow direction, while the particles seemed more randomly oriented, with a preferential alignment towards the FD in views parallel to the transverse direction [15, 36]. Even though there is a difference in the alignment of clay particles from PA-6 and PP/PP-g-MA nanocomposites in views parallel to different directions, particle analysis performed by Lee et al. also showed that the average particle length in PP/PP-g-MA nanocomposites was larger when viewed parallel to the transverse direction [36]; this is in accord with the reasoning presented above regarding the alignment of the major axis of the particles with the dominant flow field.

Figure 5.17 and 5.18 show TEM micrographs viewed parallel to the transverse direction for various nanocomposites prepared in this study, at low and high concentrations, respectively. They should be compared with Figures 5.4 and 5.7, accordingly, since the latter show the same nanocomposites viewed parallel to the flow direction. These figures show high degrees of clay dispersion in all cases, which is consistent with the observations made in the previous sections. At low concentrations, the particles viewed parallel to the TD seem to have longer lengths than when viewed parallel to the FD in all cases. The nanocomposites prepared in the ZSK 25 extruder by adding the organoclay from the clay feeder show a good alignment of platelet edges in both orientations, while a slightly higher alignment towards the polymer flow direction can be seen when viewed parallel to the TD. Additionally, the composites prepared in the Haake TSE show good alignment, with long extended particles in both viewing directions. On the other hand, the nanocomposites prepared in the ZSK 25 extruder by dry blending the polymer and the organoclay in the polymer feeder show almost no alignment in any direction. The nanocomposites prepared in the DSM micro-

compounder present poor alignment in both orientations, with a slightly higher alignment when viewed parallel to the FD. Furthermore, at high concentrations, the particles seem to have more similar lengths in both views, while the orientation seems more random in most of the cases when viewed parallel to the FD. All the nanocomposites processed in the ZSK 25 TSE show noticeably higher alignment of platelet edges when viewed parallel to the TD with respect to the view parallel to the FD. Again, the composites processed in the Haake show good alignment in both orientations, with a slightly higher alignment of platelet edges when viewed parallel to the TD. The nanocomposites processed in the DSM micro-compounder also show similar particle alignment in both orientations, with a slightly higher alignment when viewed in the TD. It is important to note that no tilted faces were noticeable at low concentrations (Fig. 5.16), whereas tilted faces were observed at high concentrations.

These observations are in accord with what was observed by Yoon et al., where an overall higher particle alignment was observed in views parallel to the TD. More noticeable differences can be seen at high concentrations probably due to the greater interaction between adjacent platelets. The differences in processing conditions employed in the two injection molders clearly lead to different degrees of particle alignment, as can be observed from the lower alignment of particles for nanocomposites processed in the DSM micro-compounder and –injection molder. On the other hand, the nanocomposites prepared in the Haake TSE show good particle alignment in both orientations, contrary to the marked differences observed in the composites processed in the ZSK 25 TSE; the high shear experienced by the organoclay may have produced irregular particles that may not align with the polymer flow as effectively as regular particles. These results suggest that the morphology generated by the extruder may also play a significant role in subsequent particle alignment.

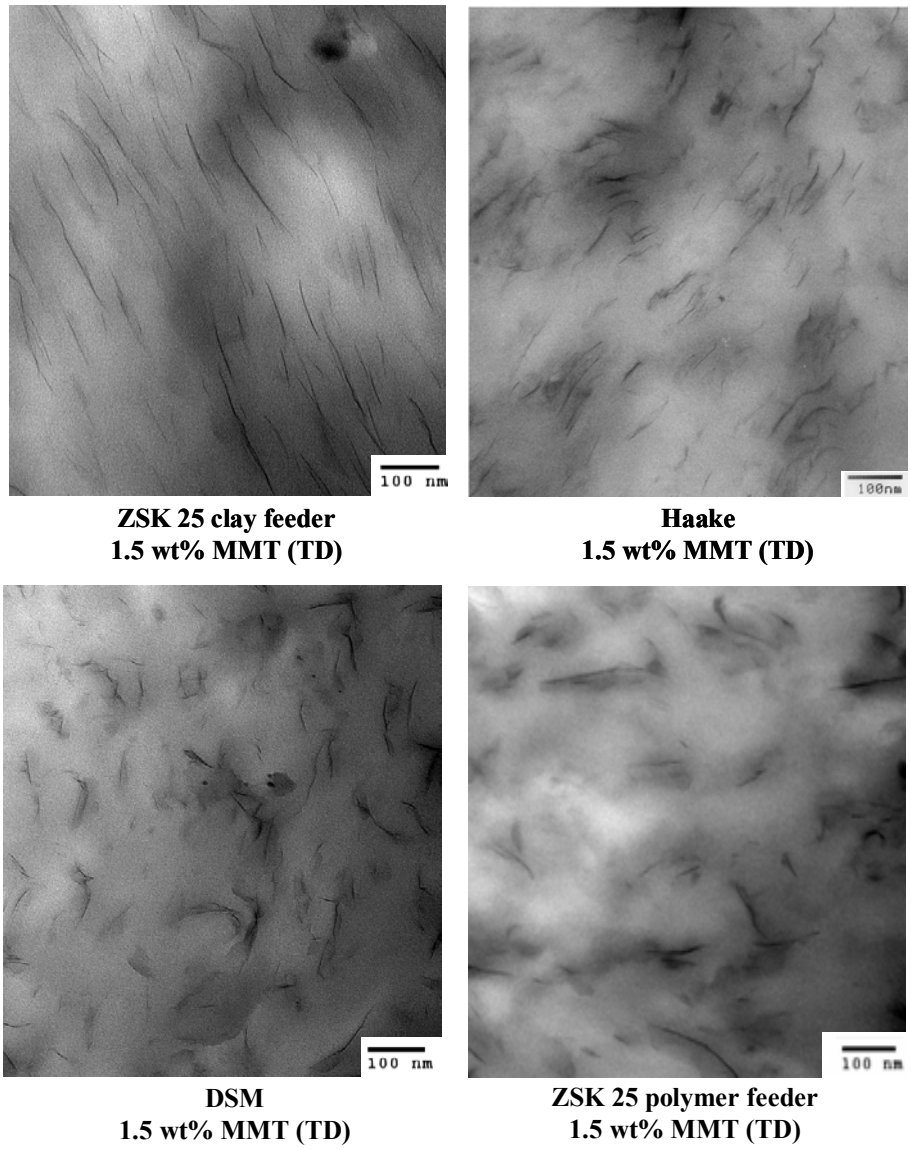

ZSK 25 clay feeder
1.5 wt% MMT (TD)

Haake
1.5 wt% MMT (TD)

DSM
1.5 wt% MMT (TD)

ZSK 25 polymer feeder
1.5 wt% MMT (TD)

Figure 5.17 TEM micrographs of PA-6/$M_3(HT)_1$ nanocomposites with approximately 1.5 wt% MMT. View parallel to the transverse direction (TD). Compare to Figures 5.4 and 5.7, accordingly, with view parallel to flow direction (FD).

Particle analysis results for TEM micrographs viewed parallel to the TD are shown in Table 5.5. Figure 5.19 shows a visual representation of the differences in particle lengths observed in the two viewing directions, where the particles are

represented as ellipsoids and are positioned with respect to the values of modulus and wt% MMT for each nanocomposite. In this figure, the horizontal axis of the ellipsoids is proportional to the number average particle length obtained from the analysis in the TD, while the vertical axis is proportional to the number average particle length obtained from the analysis in the FD (Fig. 5.19a). The values of average particle length for each orientation show that the particles are larger at low clay concentrations than at higher concentrations where the particles have essentially circular shapes, i.e., very similar average particle lengths in both directions. The ellipsoids obtained from the analysis of the nanocomposites prepared in the ZSK 25 extruder show the major axis parallel to the FD, i.e., higher average particle lengths were obtained in the analysis performed from views parallel to the TD. On the other hand, the ellipsoids obtained from the analysis of the nanocomposites processed in the Haake and DSM extruders show the opposite; the reason for this is not clear at this time. Nevertheless, this figure clearly shows that overall, the larger particles produce the highest enhancement in modulus, and this is particularly apparent at low clay concentrations (Fig. 5.19b). The results presented here show that even though there is a very small difference in particle dimensions from the two different directions, e.g., the difference in the values of particle length obtained in the analyses in the FD and the TD is less than 20 nm, the particles tend to align in most cases with their larger dimension in the direction of shear during specimen preparation by injection molding.

The average particle thicknesses obtained for views parallel to the TD are similar to those observed in the views parallel to the FD (Table 5.2). The aspect ratio values follow the same trend as the particle lengths, while higher particle densities are observed in the transverse direction for low clay concentration and in the flow direction for the higher clay concentrations. Lee et al. mention that for the less-exfoliated PP/PP-g-MA

system, the aspect ratio decreases with increasing clay concentration when viewed parallel to the transverse direction as a result of the increase in average particle thickness as the amount of clay is increased, while it remains almost unchanged when viewed parallel to the flow direction. They mention that this difference may be due to the bending of clay particles and/or the peeling-apart of platelet edges in clay particles as a result of the shear stress that is also present [36].

TEM analyses for PA-6 nanocomposites shown here and elsewhere suggest that single platelets behave differently in the presence of flow fields than the stacks of platelets seen in PP/PP-g-MA nanocomposite analyses. Figure 5.20 shows the Young's modulus for low density polyethylene (LDPE)/ Cloisite 6A ($M_2(HT)_2$-140) nanocomposites prepared by R.K. Shah using the Haake and ZSK 25 twin screw extruders under the same mixing conditions as described above for PA-6 nanocomposites. The processing conditions used were described by Shah et al. in a manuscript that evaluates the physical and barrier properties of blown films of LDPE and sodium ionomer poly(ethylene-*co*-methacrylic acid) nanocomposites prepared by melt mixing [37]. Even though no morphology characterization through WAXS, TEM, or particle analysis is available, this figure shows that the extruder mixing conditions described above lead to somewhat different trends in Young's modulus for LDPE nanocomposites than what was observed for PA-6 nanocomposites. The addition of clay produces an increase in modulus in all cases; however, the increase in modulus observed for the nanocomposites processed in the Haake extruder is more similar to the increase observed for the composites processed in the ZSK 25 when dry-blending the polymer and the organoclay in the polymer feeder than when adding the clay from the clay feeder. In addition, increasing the number of passes through the ZSK 25 extruder (dry-blending in the polymer feeder) seems to have no significant effect on the modulus of the

nanocomposites, while a higher number of passes leads to a decrease in modulus for the nanocomposites processed through the Haake extruder.

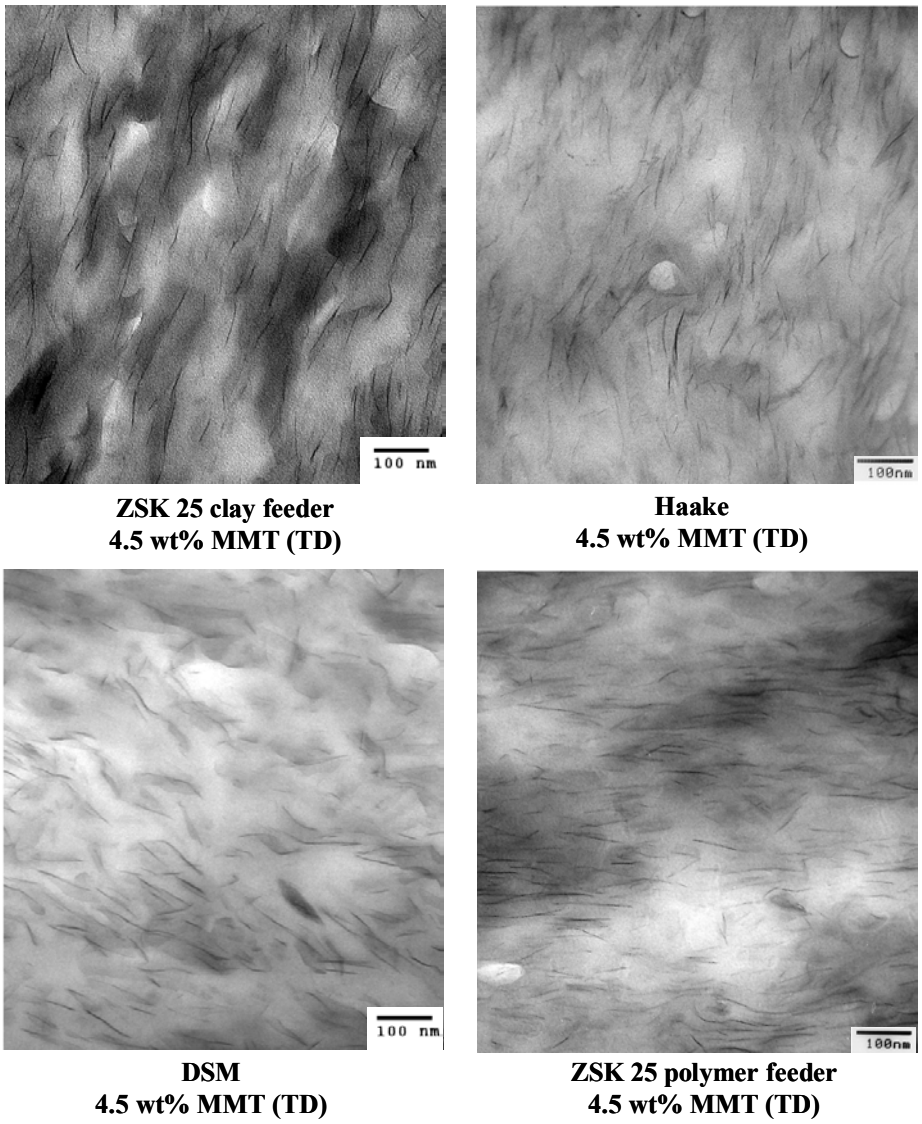

ZSK 25 clay feeder
4.5 wt% MMT (TD)

Haake
4.5 wt% MMT (TD)

DSM
4.5 wt% MMT (TD)

ZSK 25 polymer feeder
4.5 wt% MMT (TD)

Figure 5.18 TEM micrographs of PA-6/$M_3(HT)_1$ nanocomposites with approximately 4.5 wt% MMT. View parallel to the transverse direction (TD). Compare to Figures 5.4 and 5.7, accordingly, with view parallel to flow direction (FD).

Table 5.5 Particle analysis results for PA-6/$M_3(HT)_1$ nanocomposites. Transverse direction.

Extruder	Number of particles analyzed	Number average particle length $(\bar{\ell})_n$ [nm]	Weight average particle length $(\bar{\ell})_w$ [nm]	Number average platelets / particle	Weight average platelets / particle	Number average particle thickness [a] $(\bar{t})_n$ [nm]	Weight average particle thickness [a] $(\bar{t})_w$ [nm]
ZSK 25 clay feeder							
1.21 wt% MMT	1229	79	106	1.1	1.3	1.2	1.6
5.02 wt% MMT	3585	54	71	1.2	1.3	1.1	1.4
Haake							
1.28 wt% MMT	870	46	58	1.4	1.6	1.6	2.4
4.37 wt% MMT	1589	52	69	1.3	1.4	1.4	1.9
DSM							
0.89 wt% MMT	1255	43	56	1.1	1.2	1.2	1.5
4.06 wt% MMT	3402	50	65	1.1	1.2	1.1	1.4
ZSK 25 polymer feeder							
1.51 wt% MMT	2019	43	52	1.1	1.2	1.2	1.5
4.68 wt% MMT	2385	45	60	1.1	1.2	1.1	1.4

Extruder	Number Average Aspect ratio [b] $(\bar{\ell})_n/(\bar{t})_n$	100% Exfoliation No. Average Aspect ratio	Weight Average Aspect ratio [c] $(\bar{\ell})_w/(\bar{t})_w$	100% Exfoliation Wt. Average Aspect ratio	Particle density [particles / μm^2]	Specific particle density (particle density @ 1 and 5.5 wt% MMT) [particles / μm^2]
ZSK 25 clay feeder						
1.21 wt% MMT	66	84	66	113	195	242
5.02 wt% MMT	49	57	49	76	529	505
Haake						
1.28 wt% MMT	29	49	25	62	270	316
4.37 wt% MMT	37	55	35	73	413	425
DSM						
0.89 wt% MMT	37	46	37	60	186	313
4.06 wt% MMT	46	53	48	69	511	566
ZSK 25 polymer feeder						
1.51 wt% MMT	37	46	34	55	317	315
4.68 wt% MMT	40	48	42	64	636	612

[a] No. average and wt. average thicknesses were obtained by converting each value of number of platelets per particle in the distribution to particle thickness as outlined by Fornes et al. [28], and taking the no. and wt. averages respectively.
[b] These values of the aspect ratio were computed from the number average platelet lengths and thicknesses
[c] These values of the aspect ratio were computed from the weight average platelet lengths and thicknesses

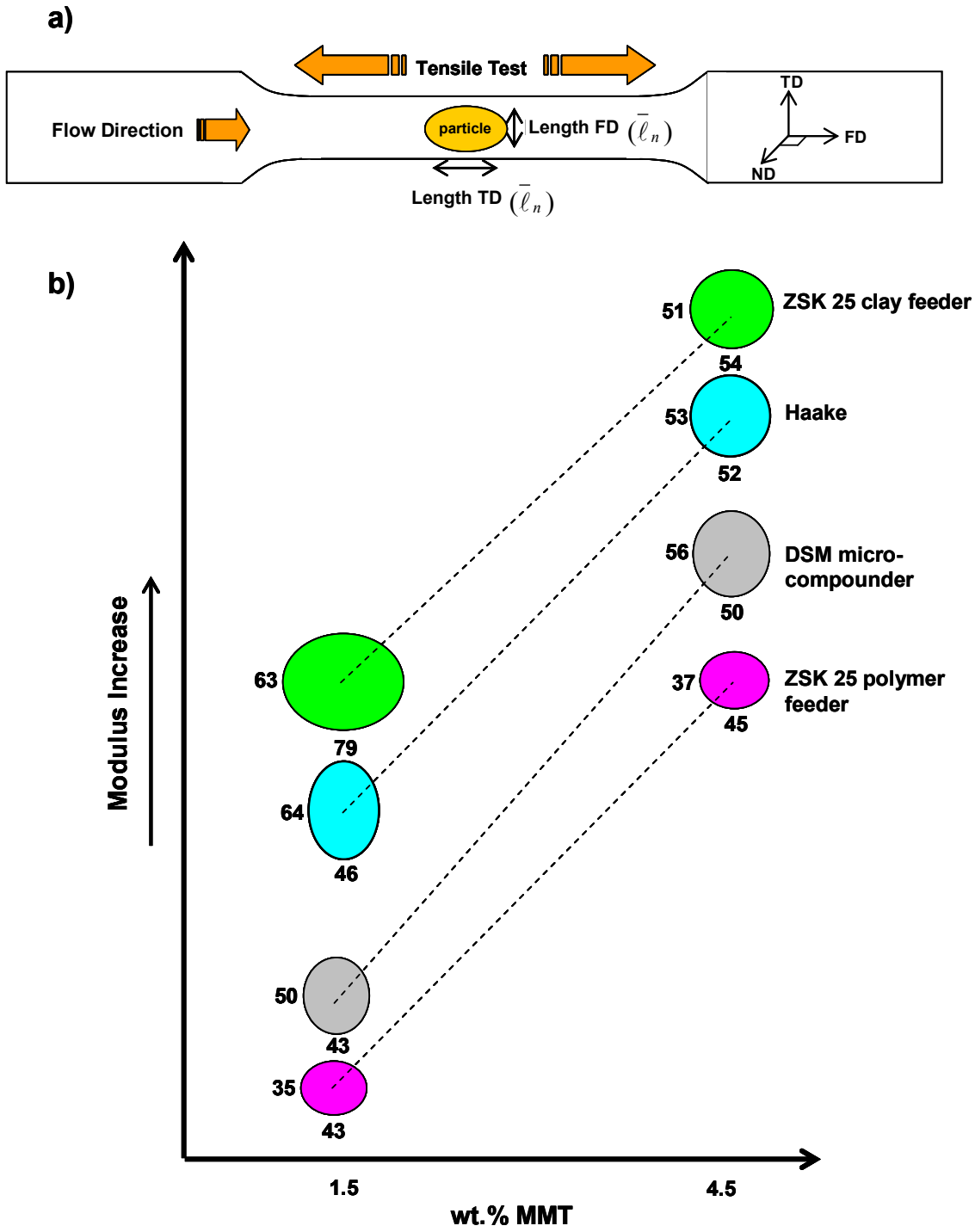

Figure 5.19 Representation of particles as ellipsoids with dimensions equal to number average particle length results from particle analysis in FD and TD directions. a) Illustration of the axis and orientations used to sketch the particles. b) particle representations of PA-6/ $M_3(HT)_1$ nanocomposites with respect to modulus enhancement and clay concentration.

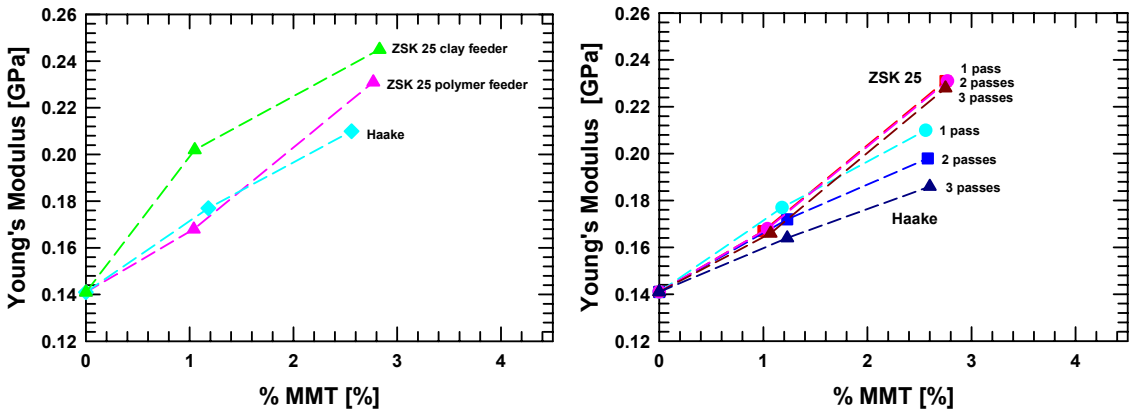

Figure 5.20 Young's modulus of LDPE/$M_2(HT)_2$-140 nanocomposites processed in the Haake and ZSK 25 twin screw extruders under the same mixing conditions as for PA-6 nanocomposites. a) Extruder comparison, and b) number of passes in ZSK 25 (dry-blending polymer and organoclay in polymer feeder) and Haake twin screw extruders.

Further analyses for these nanocomposites cannot be made since no TEM observations are available and other tensile properties such as elongation at break showed no clear trends. In spite of this, these results show that the extruder mixing conditions have different effects for systems that present lower degrees of exfoliation. Dennis et al. mention that when there is poor affinity between the polymer and the organoclay, the process can be optimized to give composites with small particles but that the chemical compatibility between each resin and the organoclay is of paramount importance [2].

CONCLUSION

Nanocomposites prepared from $M_3(HT)_1$ organoclay and an extrusion grade of PA-6 were melt blended using three different twin screw extruders to explore the effect of mixing conditions, feed port location, residence time, and number of extrusion passes on the morphology and mechanical properties. The ZSK 25 twin screw extruder had two

feed ports, one for the polymer and another for the organoclay. It had a region of high shear after the polymer feed port to melt the polymer before coming into contact with the organoclay, and two low shear regions after the clay feed port to provide a low, distributive mixing for nanocomposite formation. The Haake twin screw extruder had two medium-intensity shear areas distributed along the length of the barrel and only one feed port for both polymer and clay. The DSM micro-compounder had no shear elements, one feed port, and the residence time could be varied through a recirculation channel.

From observations of morphology and mechanical property data it was concluded that the configurations used in the ZSK 25 and the Haake TSE's produce the best platelet dispersion and matrix reinforcement. The lack of shear elements and longer residence time (10 min) in the DSM micro-compounder seemed to produce a slightly lower degree of dispersion and a lower modulus enhancement for PA-6 nanocomposites. On the other hand, the high shear intensity used to melt the polymer in the ZSK 25 when a dry blend of polymer and organoclay was introduced to the polymer feeder produced extremely short particle lengths, possibly due to clay platelet attrition by the solid polymer which led to the lowest matrix reinforcement. In addition, increasing the residence time in the DSM micro-compounder from 10 to 15 and 20 min produced higher particle dispersion and orientation, but did not produce a clear increase in Young's modulus. This might reflect both the lack of shear elements and longer residence time during compounding as well as the nature of the injection molding process, such as the lower injection pressure and shear for particle alignment. In spite of this, the DSM micro-compounder produced similar morphological and modulus trends as the ones obtained with conventional twin screw extruders, which shows that the DSM micro-compounder is a good alternative for

nanocomposite research and development especially when only small amounts of material are available.

Increasing the number of passes through the Haake and ZSK 25 twin screw extruders leads to higher particle dispersion giving rise to greater matrix reinforcement. Both the increase in mixing time in the extruder as well as the re-melting process experienced by the material might have an effect on matrix reinforcement.

The differences in morphology seen by TEM in two orthogonal directions is in accord with the observations presented by Yoon et al. [6] where the particles seemed to align in most cases with the larger dimension parallel to the polymer flow direction. The differences observed in TEM analyses suggest that the extrusion process may also play a role in particle alignment of the final molded composite. Different trends in Young's modulus were observed for polyolefin nanocomposites which suggest that the chemical compatibility between the polymer matrix and the organoclay is of paramount importance.

REFERENCES

[1] Cho JW, Paul DR. Polymer 2000;42:1083-1094.

[2] Dennis HR, Hunter DL, Chang D, Kim S, White JL, Cho JW, Paul DR. Polymer 2001;42:9513-9522.

[3] Kim DH, Fasulo PD, Rodgers WR, Paul DR. *Article in preparation*

[4] Fornes TD, Yoon PJ, Keskkula H, Paul DR. Polymer 2001;42:9929-9940.

[5] Fornes TD, Yoon PJ, Hunter DL, Keskkula H, Paul DR. Polymer 2002;43:5915-5933.

[6] Yoon PJ, Fornes TD, Paul DR. Polymer 2002;43:6727-6741.

[7] Yoon PJ, Hunter DL, Paul DR. Polymer 2003;44:5323-5339.

[8] Chavarria F, Paul DR. Polymer 2004;45:8501-8515.

[9] Finnigan B, Martin D, Halley P, Truss R, Campbell K. Polymer 2004;45:2249-2260.

[10] Fornes TD, Paul DR. Macromolecules 2004;37:7698-7709.

[11] Fornes TD, Hunter DL, Paul DR. Polymer 2004;45:2321-2331.

[12] Hotta S, Paul DR. Polymer 2004;45:7639-7654.

[13] Shah RK, Paul DR. Polymer 2004;45:2991-3000.

[14] Finnigan B, Martin D, Halley P, Truss R, Campbell K. J Appl Polym Sci 2005;97:300-309.

[15] Lee HS, Fasulo PD, Rodgers WR, Paul DR. Polymer 2005;46:11673-11689.

[16] Shah RK, Hunter DL, Paul DR. Polymer 2005;46:2646-2662.

[17] Chavarria F, Paul DR, Polymer 2006.

[18] Vaia RA, Giannelis EP. Macromolecules 1997;30:8000-8009.

[19] Vaia RA, Giannelis EP. Macromolecules 1997;30:7990-7999.

[20] Balazs AC, Singh C, Zhulina E. Macromolecules 1998;31:8370-8381.

[21] Tanaka G, Goettler LA. Polymer 2001;43:541-553.

[22] Vaia RA, Krishnamoorti R, *Polymer Nanocomposites: Synthesis, Characterization, and Modeling*. Krishnamoorti R,Vaia RA, Eds., ACS Symposium Series. Oxford University Press, Washington, D.C., 2001.

[23] Fornes TD, Paul DR. Polymer 2003;44:3945-3961.

[24] Liu L, Qi Z, Zhu X. J Appl Polym Sci 1999;71:1133-1138.

[25] Fornes TD, Yoon PJ, Paul DR. Polymer 2003;44:7545-7556.

[26] Yoon PJ, Hunter DL, Paul DR. Polymer 2003;44:5341-5354.

[27] Shah RK, Paul DR. Polymer 2006;47:4075-4084.

[28] Fornes TD, Paul DR. Polymer 2003;44:4993-5013.

[29] Stretz HA. Ph.D. Thesis, The University of Texas at Austin, 2005.

[30] Shon K, Chang D, White JL. International Polymer Processing XIV 1999;1:44-50.

[31] Courtney TH, *Mechanical Behavior of Materials*. Mc Graw Hill, Second, 2000, pp. 733.

[32] Yalcin B, Cakmak M. Polymer 2004;45:2691-2710.

[33] Clarke SM, Rennie AR, Convert P. Europhysics Letters 1996;35:233-238.

[34] Yamamoto S, Matsuoka T. J. Chem. Phys. 1997;107:3300-3308.

[35] Yalcin B, Valladares D, Cakmak M. Polymer 2003;44:6913-6925.

[36] Lee HS, Fasulo PD, Rodgers WR, Paul DR. Polymer 2006;47:3528-3539.

[37] Shah RK, Krishnaswamy RK, Takahashi S, Paul DR. Polymer 2006;47:6187-6201.

CHAPTER 6

ORGANOCLAYS WITH REDUCED-CATION EXCHANGE CAPACITY: EFFECT ON MORPHOLOGY AND PROPERTIES OF NANOCOMPOSITES

INTRODUCTION

As mentioned earlier, high levels of exfoliation require favorable polymer-organoclay interactions and optimum processing conditions. Under the best possible processing conditions, the affinity of the polymer for the polar clay surface and/or for the non-polar organic modifier is very important for obtaining high clay platelet dispersion and mechanical property enhancement. Processing conditions aid in reducing clay particle size and in ensuring good contact between the polymer and the organoclay, but good chemistry is required to produce exfoliation [1]. Previous studies from our laboratories show that the best clay dispersion and mechanical property enhancement for nylon 6 (PA-6) nanocomposites is obtained when using a one-tailed organoclay that permits access of the polymer chains to the silicate surface, while the opposite is observed for nanocomposites made from polypropylene/polypropylene modified with maleic anhydride (PP/PP-g-MA) systems and various polyethylene copolymers, i.e., higher clay dispersion and mechanical property enhancement are observed when using organic modifiers with more than one tail that provide a higher coverage of the polar clay surface and, therefore, less access of the polymer to the silicate surface [2-4]. An independent way to assess the effect of organoclay surface coverage on morphology and properties of nanocomposites is to reduce the cation exchange capacity (CEC) of the clay. A smaller number of exchangeable cations in the clay will reduce the amount of alkyl

ammonium ions that can be exchanged onto the silicate surface and, hence, reduce the degree of organoclay surface coverage.

It is widely known that the layer charge of smectites can be reduced by a process known as the Hoffman-Klemen effect, where heating lithium-montmorillonite (Li-MMT) at temperatures between 200 and 300ºC causes the transition of exchangeable lithium (Li^+) ions to a non-exchangeable state. Lithium fixation is produced by the partial migration of Li^+ ions from the clay galleries into the silicate layers reducing the total layer charge [5]. The extent of Li^+ fixation depends on the type of smectite, the temperature of heating, and its duration [6-10]. Alternatively, different levels of charge reduction can be obtained at the same temperature in bi-ionic lithium-sodium montmorillonites (Li-Na-MMT's) by varying the amount of exchangeable Li^+ and Na^+ ions prior to heating the clay samples [11]. The smaller size of the Li^+ ions allows them to migrate into the MMT layers, while the larger Na^+ ions mainly stay at the interlayer spacing.

Layer charge reduction produces a decrease in the clay basal spacings, as well as in the solvation and swelling ability of the clay [7-16]. Calvet and Prost showed that the limiting value of exchangeable cations necessary to expand previously-heated montmorillonite in water was 50%, since water molecules cannot reach the internal surface when this value is lower [7]. Similar conclusions were reached by Brindley and Ertem, where they state that full expansion in water ceases when the exchangeable cations fall below 60 mequiv/ 100 g of clay [11]. Komadel et al. and Hrobarikova et al. show that the swelling ability of lithium-calcium montmorillonite (Li-Ca-MMT) is

considerably reduced after heating at temperatures above 150ºC [9, 10]. Some authors suggest that this might be due to the collapse of interlayers from heterogeneous charge distribution in pristine MMT as well as the non-homogeneous charge reduction that can be produced by ion segregation in bi-ionic montmorillonites [13-16].

To our knowledge, the effect of charge reduction on the morphology and mechanical properties of melt-processed nanocomposites has not been studied. The one report on reduced-CEC polymer nanocomposites was based on the formation of thin-film composites in a polyimide matrix by chemical methods [17]. The object of this study is to explore the effect of CEC reduction on the morphology and Young's modulus of PA-6 and PP/PP-g-MA organoclay nanocomposites prepared by melt processing. Considering the arguments about the affinity of the polymer for the silicate surface versus the optimal number of alkyl tails on the surfactant mentioned above, it might be expected that a lower CEC may aid in the exfoliation of nanocomposites made with PA-6 while this most likely would reduce the degree of exfoliation that could be achieved in PP/PP-g-MA nanocomposites.

EXPERIMENTAL

To examine the effects of CEC reduction, an extrusion grade of PA-6 and different PP/PP-g-MA blends were melt-processed with reduced-CEC organoclays to form nanocomposites. The PA-6 and the PP/PP-g-MA system used here were chosen based on previous studies performed in our laboratory that showed high platelet dispersion and mechanical property enhancement of their nanocomposites [3, 18, 19]. The relative amounts of PP and PP-g-MA contained in the nanocomposites were established in order to have a 1:1 ratio of PP-g-MA to organoclay. Specifications of

these materials as well as explicit details of the melt processing and characterization techniques are given in Chapter 3; conditions and specific information regarding this study follow.

PA-6 and PP/PP-g-MA nanocomposites were formed in a 5 mL DSM micro-compounder and DSM bench-top micro-injection molder described in Chapter 3. A screw speed of 100 rpm and a residence time of 10 min were used; PA-6 nanocomposites were formed using a barrel temperature of 240ºC, an injection molder cylinder temperature of 260ºC, and a mold temperature of 80ºC, while PP/PP-g-MA nanocomposites were formed using a barrel temperature of 185ºC, an injection molder cylinder temperature of 210ºC, and a mold temperature of 40ºC. The injection pressures were 4 and 3 bar for PA-6 and PP/PP-g-MA nanocomposites, respectively.

The stiffness of the composites was characterized by the Young's modulus from the injection molded samples obtained by testing a total of three specimens five times each, and averaging the responses; these five repetitions were performed under 1% strain where no hysteresis could be detected [20, 21]. Standard deviations were typically of the order of 1 to 10% for the samples based on PA-6, and 1 to 4% for the samples based on PP/PP-g-MA.

Transmission electron microscopy (TEM) micrographs were obtained using a Phillips EM208 transmission electron microscope with an accelerating voltage of 80 kV. Samples for TEM were cryogenically cut into ultra thin sections (50 to 70 nm thick) with a diamond knife at temperatures of -40 and -60ºC for PA-6 and PP/PP-g-MA nanocomposites, respectively, using an RMC PowerTome XL ultramicrotome with a CR-X universal cryosectioning system. These sections were taken from the central part of the injection molded bar normal to the transverse direction (TD) and viewed in the TEM parallel to the transverse direction, as shown in Figure 3.5.

CEC reduction of sodium montmorillonite

Three reduced-CEC montmorillonite clays, i.e., clays A, B, and C, were supplied by the CSIRO laboratories in Australia. They were formed by exchanging specific percentages of the Na^+ ions contained in sodium montmorillonite with Li^+ ions through a cation exchange reaction between sodium montmorillonite and lithium chloride (LiCl), followed by heating at 150ºC for 48 h to induce Li^+ fixation. The initial amounts of LiCl for each sample were calculated considering that 1 g of clay contained approximately one mmol of exchangeable Na^+ and were targeted to have 1:3, 2:3, and 1:1 ratios of Li^+ to Na^+ ions in the exchange reaction. The cation exchange reactions were performed by dissolving the LiCl in 3 L of filtered de-ionized water (milli-Q water) and adding 150 g of sodium montmorillonite. The mixture was stirred for 48 h and later centrifuged in a Spintron GT-155 centrifuge at 2000 rpm for 6 h. After this, 200 mL of the supernatant were decanted and the remaining mixture was re-suspended by shaking with an additional 400 mL of milli-Q water. The suspension was again centrifuged, keeping the contents refrigerated to promote the separation of the clay from solution. A second supernatant was decanted and the remaining suspension was washed several times to remove any excess Li^+, Na^+, and/or Cl^- ions. The residual slurry was oven dried for 16h; the temperature was then increased to 150ºC for 48 h to induce Li^+ fixation and obtain layer charge reduction. Table 6.1 shows details for the clays provided by CSIRO as well as the initial amounts of LiCl added for each clay.

Table 6.2 shows Inductively Coupled Plasma (ICP) analysis results also provided by CSIRO of Li^+ and Na^+ concentrations from the two supernatants extracted after the cation exchange reaction. This table shows that the solvation of Na-MMT leaches a high concentration of Na^+ ions into solution. The supernatants extracted from the clay solutions containing Li^+ ions show a higher concentration of Na^+ ions than the one

observed from the solvation of Na-MMT, and this concentration increases as the initial lithium concentration is increased. These results also show that the Li^+ concentration in the first supernatant from clay A is lower than the corresponding standard lithium solution, which suggests that a portion of the Li^+ ions are removed from solution after the cation exchange reaction. Further analyses of the results provided by CSIRO were not performed due to problems presented when separating the clay from the supernatant and, hence, it was very difficult to estimate the exact amount of clay remaining after the extractions. X-ray analysis results before and after heating provided by CSIRO for clay C show a slight decrease in d-spacing from 1.26 to 1.23 nm after heating at 150ºC for 48 hours.

Table 6.1 Clays Provided by CSIRO.

Clay (designation used here)	Composition	Target Li^+:Na^+ ratio	Amount of LiCl added	Heating Treatments
A	Li-Na-MMT	1:3	2.0 g (47.2 mmol)	48 h at 150ºC
B	Li-Na-MMT	2:3	3.9 g (92.0 mmol)	48 h at 150ºC
C	Li-Na-MMT	3:3	5.9 g (139.2 mmol)	48 h at 150ºC

The measured cation exchange capacities of the reduced-CEC clays as-received from CSIRO are shown in Table 6.3; the measurements were carried out by Southern Clay Products in Gonzalez, TX as described in Chapter 3. These results suggest that only a minor CEC reduction was obtained and that the CEC values were very similar in all three clays. For this reason, subsequent heating trials were performed, in order to determine if a higher CEC reduction could be achieved by increasing the temperature and duration of heating; these results are also shown in Table 6.3. The heating trials

performed show that heating a sample of clay B for another 48 h at 150ºC led to no significant change in CEC; similarly, heating a sample of clay A for 2 h at 250ºC produced almost no change in CEC either. The lowest CEC values obtained for each clay in these trials were 77, 73, and 65 mequiv/ 100 g of clay for clays A, B, and C, respectively, by heating for 24 h at 250ºC. The results also show that heating another sample of clay C for 36 h at 300ºC led to the same CEC reduction as when heating at 250ºC for 24 h. These values correspond to CEC reductions of approximately 16, 21, and 30%, respectively, which are lower than what was targeted by exchanging 25, 40 and 50% of the Na^+ ions by Li^+ ions in Na-MMT. It is important to add that all samples in Table 6.3 showed good dispersion in water and that WAXS scans from these samples at 50% relative humidity and of glycolated films showed the typical d_{001} spacings for Na-MMT, i.e., 1.2 and 1.7 nm, respectively [22].

Table 6.2 ICP analysis results for CSIRO clays [a, b].

Sample	Lithium [ppm]	Sodium [ppm]
Milli-Q water- background	< 0.2	< 5.0
Li^+ Standard solution (Li^+ concentration equivalent to B)	83	< 5.0
Na-MMT– supernatant (solvation of Na-MMT)	< 0.2	425
Clay A – 1st supernatant	45	677
Clay A – 2nd supernatant	33	505
Clay B – 1st supernatant	102	775
Clay B – 2nd supernatant	67	512
Clay C – 1st supernatant	179	884
Clay C – 2nd supernatant	93	445

[a] Results obtained by CSIRO, Australia.
[b] ~ 2mL of supernatant was taken for each measurement, and these samples were pre-filtered through a 0.45 micron syringe filter prior to analysis.

Table 6.3 CEC results for CSIRO clays and for heating trials.

	Cation Exchange Capacity (% of CEC reduction) [meq./ 100 g of clay]		
Clay:	A	B	C
CSIRO clay: As received	88 (4%)	85 (7%)	88 (4%)
Heating trials:			
1. Heated at 150ºC for 48 h	---	86.5 (6%)	---
2. Heated at 250ºC for 2 h	84 (9%)	---	---
3. Heated at 250ºC for 24 h	77 (16%)	73 (21%)	65 (30%)
4. Heated at 300ºC for 36 h	---	73 (21%)	---

Based on the results obtained from the heating trials, the CEC in these clays could not be lowered past a certain value even after heating at high temperatures for up to 36 h. Reports in the literature show that heating Li-Na-MMT clays at a temperature of 220ºC for 24 h can lead to reductions in CEC of over 60% [7, 12, 13]. Possible reasons for not reaching lower CEC's could be (1) the incomplete exchange of Li^+ for Na^+ ions during the cation exchange reaction, (2) the Li^+ ions did not effectively migrate inside the clay galleries remaining mostly at the clay surface, and/or (3) the extent of Li^+ fixation into the clay layers during heating was lower than expected. Some authors suggest that the presence of other ions such as Ca^+ or Na^+ may inhibit Li^+ fixation upon heating [10], and that variations in charge location due to heterogeneity in the charge density of the pristine clay [15, 16] may also affect CEC reduction.

Even though the CEC reduction was not as high as expected, subsequent heating was performed on these clays in order to have 3 different levels of CEC reduction, i.e., a

low, an intermediate, and the highest achievable CEC reduction. Since the CEC measurements from the heating trials showed very similar CEC values for clays A and B, clay B was heated at 80ºC for 1 h with the aim of achieving the lowest level of CEC reduction (Clay D) and clay A was heated at 250ºC for 24 h in order to obtain an intermediate CEC reduction (Clay E). Additionally, clay C was heated at 250ºC for 24 h with the aim of achieving the highest level of CEC reduction (Clay F). Preliminary CEC measurements on the twice-heated clays showed that the reduction in CEC was still low in all three clays. For this reason, a third heating treatment was performed to make sure the CEC was reduced; clays E and F were heated at 300ºC for an additional 24 h, while clay D was heated at the same temperature for 2 h. A summary of the heating treatments performed on each clay is described in Table 6.4. Further CEC measurements were not performed due to the small amounts of reduced-CEC clays supplied by CSIRO; however, the layer charge will be estimated for each clay from the number of equivalents of surfactant contained in the organoclays, by calculating the percentages of MMT and organic from the percentage of loss on ignition (LOI) measurements.

Table 6.4 Composition and heating treatments performed for the reduced-CEC clays used to form organoclays.

Clay (designation used here)	Composition	Heating Treatments	Charge Reduction
D	Clay B	a) 1 h at 80ºC b) 2 h at 300 ºC	Low
E	Clay A	a) 24 h at 150ºC b) 24 h at 300 ºC	Medium
F	Clay C	a) 24 h at 150ºC b) 24 h at 300 ºC	High

Two different types of organoclays containing $M_3(HT)_1$ and $M_2(HT)_2$ organic modifiers were produced from each reduced-CEC clay, i.e., clays D, E, and F; control samples for each type of organoclay with no CEC reduction were also made from Na-MMT for comparison. The organoclays were formed by dispersing the clays in water and mixing at high velocities to form slurries with concentrations of 1% solids. The slurries were later heated to 80ºC and mechanically stirred. Chloride salts of the corresponding quaternary ammonium surfactants were added to each clay and the solutions were left to react for 1.5 h. The reaction products were vacuum filtered, washed with methanol to remove the excess surfactant and then washed with distilled water to remove the remaining methanol. The wet clays were oven dried at 60ºC for 16 h, and then milled to produce organoclay powders. The amount of alkyl ammonium chloride in each reaction was kept constant in order to have 95 milliequivalents of surfactant per 100 g of clay (an MER of 95), which is the amount used for the preparation of the commercial organoclays that will also be used for comparison, i.e., Cloisite 20A and SPX 1137 described in Table 3.2.

Table 6.5 shows the percent LOI obtained for the organoclays described above, along with the percent of organic and the number of equivalents of surfactant calculated from the LOI values. These results show that the organoclays containing a surfactant with two long alkyl tails have a higher organic content than the organoclays that have a surfactant with only one long alkyl tail. Also, for both types of organoclays, the organic content of the control is higher than those of the organoclays with a reduced-CEC, where it decreases with higher CEC reduction. The organoclays with low and medium CEC reductions show a very similar organic content, while the organoclays with the highest CEC reduction show the lowest. In addition, the organic contents obtained for the commercial organoclays are higher than those for the control organoclays for both cases.

Table 6.5 LOI results, percentage of organic content, and number of equivalents of surfactant for the organoclays used in this study.

Clay	Charge Reduction of Clay	Surfactant: $M_2(HT)_2$ LOI [%]	Surfactant: $M_2(HT)_2$ Percent of organic* [%]	Surfactant: $M_2(HT)_2$ Equivalents of surfactant*,[a] [mequiv/ 100 g of clay]	Surfactant: $M_3(HT)_1$ LOI [%]	Surfactant: $M_3(HT)_1$ Percent of organic* [%]	Surfactant: $M_3(HT)_1$ Equivalents of surfactant*,[b] [mequiv/ 100 g of clay]
Control	None	37.8	33.4	95.1	25.1	19.9	82.3
D	Low	34.2	29.6	79.8	23.9	18.6	76.1
E	Med	33.0	28.4	75.0	24.1	18.9	77.5
F	High	30.3	25.5	64.8	21.2	15.7	61.8
Commercial organoclays:							
Cloisite 20A	None	38[c]	33.7	96.2			
SPX 1137	None				28[c]	23	99.2
Control(NP)[d]	None	38.8	34.5	99.8	26.8	21.7	92.1

[a] $MW_{M2(HT)2}$ = 528 g/ mol
[b] $MW_{M3(HT)1}$ = 301 g/ mol
[c] Values reported by SCP
[d] LOI and estimated layer charge results prior to purification of organoclays
Layer charge ≈ Equivalents of surfactant = % organic(1000/ MWsurf)*(100/ % MMT)
% organic = 100 – % MMT
% MMT = (100 – LOI)/0.935

In the commercial production of organoclays, the milliequivalent exchange ratio of 95 mequiv/ 100 g of clay used for these organoclays is slightly higher than the reported CEC for this montmorillonite, i.e., 92 mequiv/ 100 g of clay. This is done to ensure a reaction yield higher than 98%. Taking this into account, the percentage of organic in a fully exchanged organoclay with no CEC reduction should be around 33% and around 22% (± 0.5%) for $M_2(HT)_2$ and $M_3(HT)_1$ organic modifiers, respectively. Table 6.5 shows that the percent of organic calculated for the control organoclays is within the estimated range for the two-tailed control organoclay, while it is slightly lower for the organoclay containing the one-tailed organic modifier. The percents of organic obtained for the reduced-CEC organoclays are well below the estimated range for both types of organoclays and different percentages of organic can be observed with varying CEC reduction. For both types of organic surfactants, the percent of organic calculated for the

commercial organoclays is slightly higher than the value obtained for the control organoclays, yet very close to the estimated range of percent of organic for a fully exchanged organoclay.

The main differences between the commercial and control organoclays stem from the differences in the conditions of the cation exchange reaction, e.g., the concentration of solids in the clay slurry before addition of the alkyl ammonium surfactant, and from the purification procedure performed for the control and reduced-CEC organoclays to remove the excess surfactant contained in the clay galleries. LOI measurements performed for the control organoclays prior to purification (also in Table 6.5) show that in the case of the two-tailed surfactant, the organic content before purification is slightly higher to that estimated for the two-tailed commercial organoclay, while a slightly lower value was obtained in the case of the one-tailed organic modifier with respect to the one-tailed commercial organoclay. In addition, the organic content in the control organoclays before purification is higher than after purification for both types of organic modifiers. Xie et al. report a decrease in organic content for commercial $M_2(HT)_2$ organoclays after washing three times with methanol [23]. They also mention that organoclays formed using an MER higher than 95 showed a larger decrease in organic content than those formed using an MER of 95 after washing with methanol; in both cases, the organic content after washing was slightly lower than the expected value of 33%. The slightly lower organic content observed here for the control organoclay with the one-tailed organic modifier may imply that the yield of the cation exchange reaction with the alkyl ammonium surfactant was lower than expected, or that the washing procedure may have introduced a fraction of acidic protons that may have reduced the effective CEC of the aluminosilicates [23].

The number of equivalents of surfactant calculated by dividing the mass of organic modifier inside the clay galleries by its molecular weight provides an estimate of the average clay layer charge; that is, assuming a high enough alkyl ammonium exchange yield, the number of equivalents of surfactant should be close to the clay layer charge. The results of this calculation are also shown in Table 6.5. It can be seen that the estimated clay layer charge obtained from the reduced-CEC organoclays is lower than that obtained from the control organoclays, which in turn is lower than the values obtained from the commercial organoclays. These values are similar for each reduced-CEC clay, i.e., clays D, E, and F, and are independent of the surfactant used. The values for the commercial organoclays are also similar; however, the estimated clay layer charge obtained from the control organoclays shows a higher variation than that observed for the reduced-CEC and commercial organoclays.

The d-spacings obtained for these organoclays are shown in Table 6.6, while the actual X-ray scans are shown in Figure 6.1. The d-spacings for the two-tailed organoclays are significantly higher than those for the one-tailed organoclays. There is a slight decrease in d-spacing from the commercial to the control organoclays, and a more noticeable decrease is observed as the CEC is reduced. Furthermore, the intensities of the primary diffraction peaks (d_{001}) are sharper in the control organoclays than those observed for the commercial organoclays; the removal of excess surfactant in the control organoclay may produce higher homogeneity in the layer spacings and increased peak intensity. Figure 6.1 also shows that the peaks from the reduced-CEC organoclays are wider and at lower d-spacings than the peaks from the organoclays with no CEC reduction. The d-spacings for the organoclays with low charge reduction are close to

those obtained with the medium charge reduction organoclays, while the d-spacings for the organoclays with high charge reduction are noticeably lower.

Table 6.6 D-spacing results for the organoclays used in this study.

Clay	Charge Reduction of Clay	d-spacing [nm]	
		Surfactant: $M_2(HT)_2$	Surfactant: $M_3(HT)_1$
control	None	2.51	1.81
D	Low	2.35	1.69
E	Med	2.39	1.77
F	High	2.19	1.48
Commercial Organoclays:			
Cloisite 20A		2.55	---
SPX 1137		---	1.82

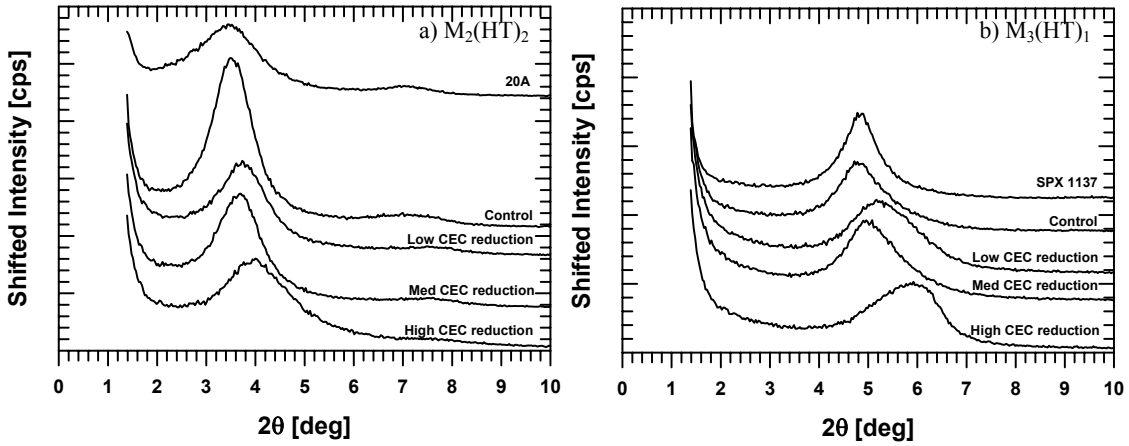

Figure 6.1 WAXS scans for the organoclays used in this study.

Paul et al. showed through experimental and molecular dynamics simulation studies that the d-spacing increases linearly with the mass ratio of intercalated surfactant to clay as the surfactant structure and the CEC are varied [24]. Figure 6.2 shows a single

linear relationship between the d-spacing and the mass ratio of intercalated surfactant to clay for all organoclays prepared in this study independent of the type of organic modifier used. The organoclays made from the two-tailed surfactant occupy the upper portion of this linear relationship while the organoclays made from the one-tailed surfactant form the lower one. For each type of organic modifier, the commercial organoclays are located in the upper part of the linear relationship, followed by the control organoclays. The points representing the organoclays with low and medium CEC reductions fall lower in this linear relationship while the organoclays with the highest CEC reduction are the lowest points in both cases.

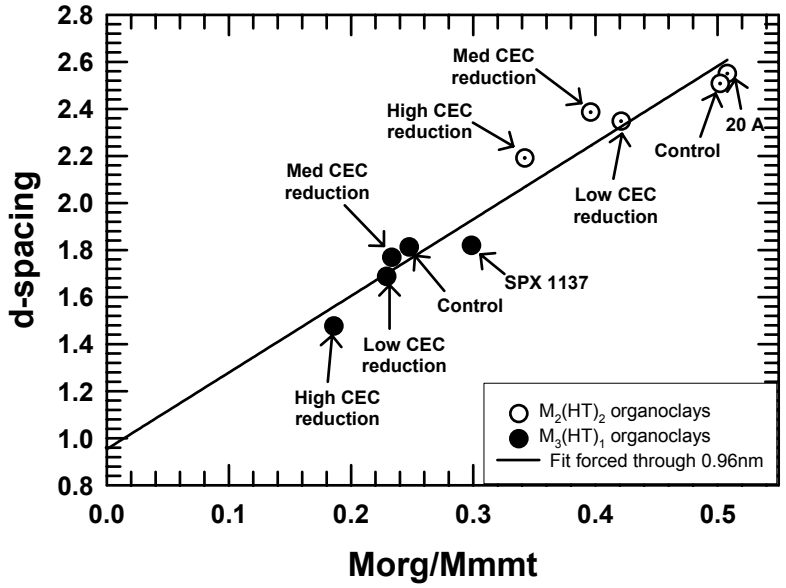

Figure 6.2 Relationship between organoclay d-spacing and mass ratio of intercalated surfactant to clay for the organoclays analyzed in this study.

The above results show that the amount of organic modifier contained in the clay galleries is larger for the organoclays exchanged with the two-tailed surfactant than for

those containing a one-tailed surfactant; this is consistent with the higher molecular weight of the two-tailed organic modifier. In addition, for both types of organoclays, the amount of organic modifier is largest for the commercial organoclays while the control organoclays have a slightly lower amount of organic modifier. The reduced-CEC organoclays have a noticeably lower value that tends to decrease with extent of CEC reduction; this suggests that a reduction in CEC was achieved for the heated clays, and that different levels of CEC reduction were obtained. Even though the organoclays with low and medium CEC reductions present very similar organic contents, a clear decrease was observed for the organoclays containing the highest CEC reduction with respect to the control and commercial organoclays. For a specific organic modifier, a lower amount of surfactant in the galleries may be the result of several factors, e.g., a lower reaction yield, the removal of excess surfactant through purification, and/or a reduction in the cation exchange capacity. The results presented here suggest that the purification procedure performed in the control and reduced-CEC organoclays may be the main factor contributing to the differences observed between the control and commercial organoclays even though other factors like exchange yield or reaction conditions may also have an effect. In the case of the reduced-CEC organoclays the results show an even lower amount of organic modifier, while the broader X-ray diffraction peaks observed for these organoclays also suggest a distribution of gallery spacings both, from platelet to platelet and along the same platelet which may stem from heterogeneities in layer charge and charge distribution. In addition, the diffraction peaks from the control organoclays were sharper, which suggests that these heterogeneities may have been produced by the CEC-reduction process, where ion segregation may have lead to an uneven CEC reduction. The differences in morphology and Young's modulus observed for PA-6 and PP/PP-g-MA nanocomposites formed from these organoclays are shown next.

Morphology

Figure 6.3 shows WAXS scans for the various PA-6 nanocomposites made in this study containing approximately 4.5 wt% MMT, along with the scans of each organoclay for comparison. Figure 6.3a shows that all the PA-6 nanocomposites containing $M_3(HT)_1$ are absent of any basal reflections, which suggests exfoliated structures. The curves for the nanocomposites made from the control organoclay and the organoclay containing the highest charge reduction show very subtle reflections around 2θ values of 3º and 6º, respectively; the reason for this is not clear at this time, but TEM pictures shown later confirm the presence of well-exfoliated morphologies in all PA-6/$M_3(HT)_1$ nanocomposites including these two cases. On the other hand, the X-ray scans from select PA-6/$M_2(HT)_2$ nanocomposites shown in Figure 6.3b have basal reflections, indicating the presence of clay agglomerates; the peaks for these nanocomposites are shifted to higher d-spacings than those from the pure organoclays which is consistent with some degree of intercalation into the clay galleries. Figure 6.3b also shows that the increase in d-spacing for both nanocomposites is very similar with respect to their corresponding organoclays.

Figure 6.4 shows representative TEM micrographs for PA-6/$M_3(HT)_1$ nanocomposites with concentrations of approximately 4.5 wt% MMT. All systems have extremely high levels of exfoliation and no significant differences in particle size or in number of particles could be observed, except for a small number of slightly larger particles that appear occasionally in the composites made from the reduced-CEC organoclays. TEM micrographs of select PA-6/$M_3(HT)_1$ nanocomposites with concentrations of approximately 1.5 wt% MMT are shown in Figure 6.5. A higher number of particles with longer lengths is observed for the nanocomposites made from

the control organoclay, while the composites made from the commercial organoclay and the organoclay with the highest CEC reduction show a slightly lower number of particles with shorter lengths. Additionally, TEM micrographs of PA-6/ $M_2(HT)_2$ nanocomposites with high clay concentrations made from the control organoclay and the organoclay with a low CEC reduction are shown in Figure 6.6. A significantly lower degree of exfoliation is observed in these nanocomposites with respect to the ones prepared with the one-tailed organoclays, which is consistent with the WAXS results shown above, as well as with previous studies by Fornes et al. [2]. The morphologies from the composites shown in this figure are very similar, with slight indications of higher platelet dispersion for the nanocomposite made from the control organoclay.

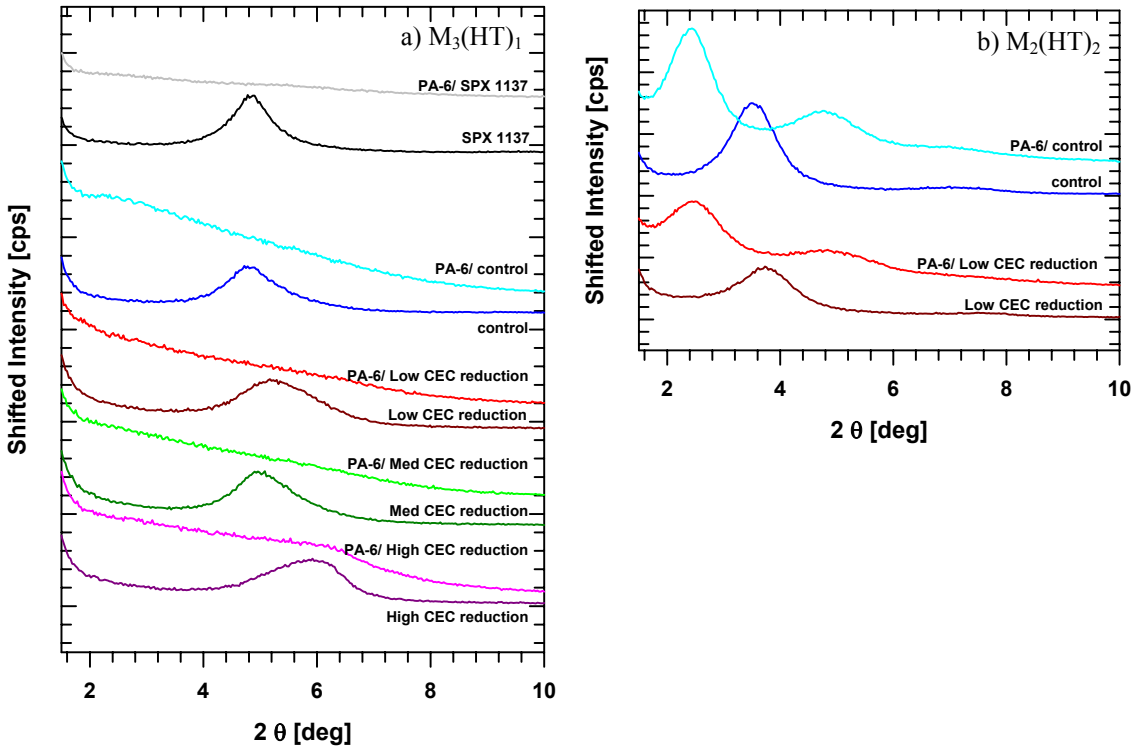

Figure 6.3 WAXS scans for pure organoclays and their respective PA-6 nanocomposites containing ~4.5 wt% MMT.

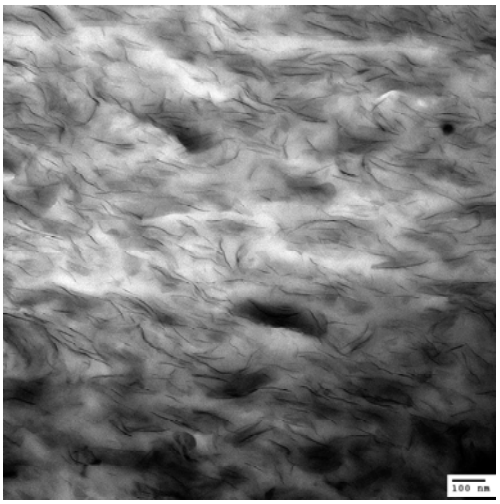

PA-6/ SPX 1137

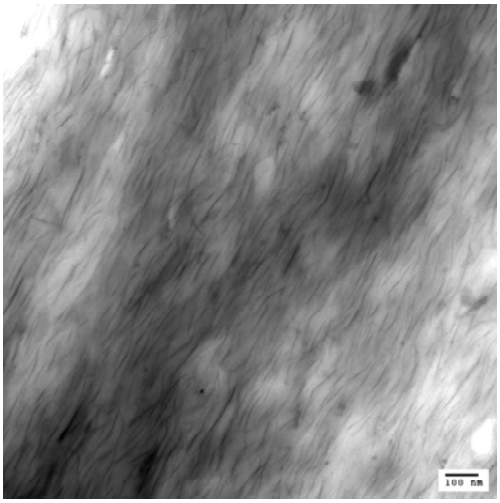

PA-6/$M_3(HT)_1$ control

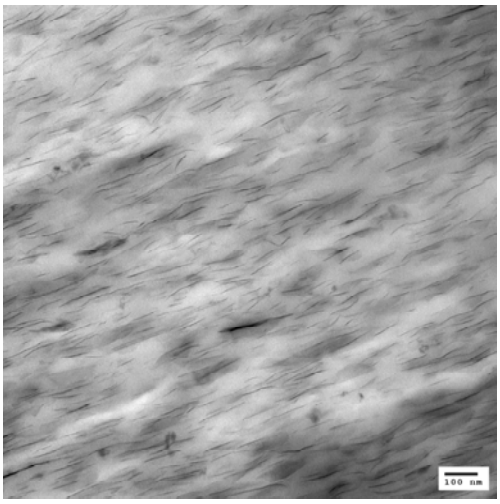

PA-6/$M_3(HT)_1$ Low CEC reduction

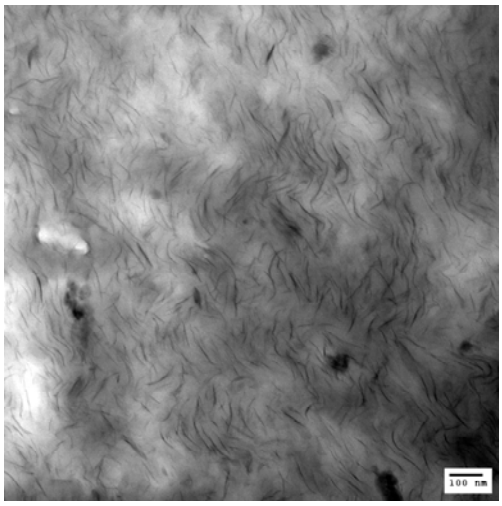

PA-6/$M_3(HT)_1$ Med CEC reduction

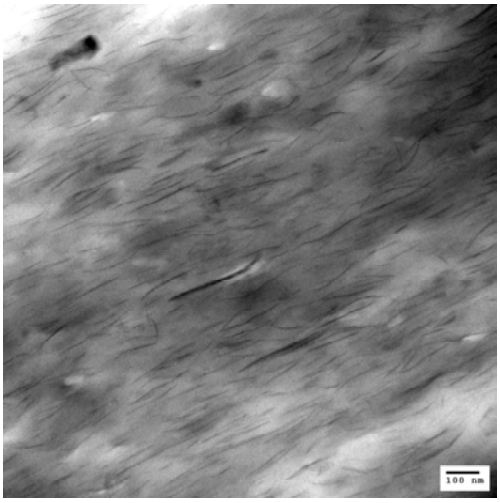

PA-6/$M_3(HT)_1$ High CEC reduction

Figure 6.4 TEM micrographs of PA-6/ $M_3(HT)_1$ nanocomposites with high clay concentrations.

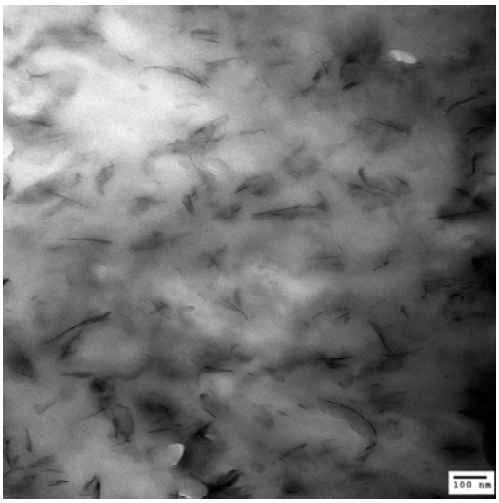

PA-6/ SPX1137

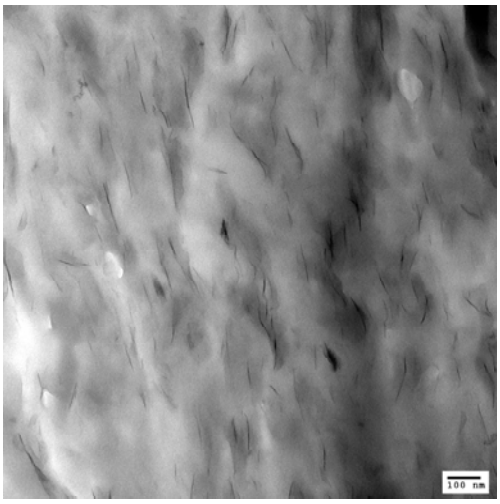

PA-6/$M_3(HT)_1$ High CEC reduction

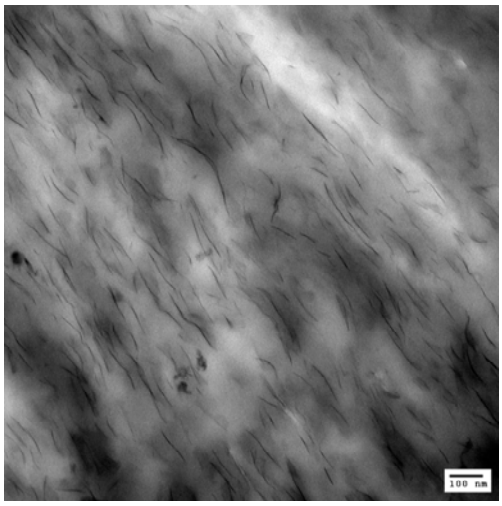

PA-6/ $M_3(HT)_1$ control

Figure 6.5 TEM micrographs of PA-6/ $M_3(HT)_1$ nanocomposites with low clay concentrations.

In the case of PP/PP-g-MA nanocomposites, the WAXS scans are shown in Figure 6.7. All of the samples show basal reflections indicating the presence of large stacks of platelets. The peaks are broader and shifted to lower d-spacings than those of the pure organoclays, which suggests a decrease in the inter-platelet distance probably from early stages of surfactant degradation during melt processing [25]. TEM micrographs of these nanocomposites are shown in Figures 6.8 and 6.9. Figure 6.8 shows

nanocomposites with concentrations of approximately 4.5 wt% MMT; the nanocomposites made from organoclays with reduced CEC show very large organoclay particles that are not seen in the nanocomposites containing the commercial and control organoclays. When comparing the nanocomposites made from the commercial and the control organoclays, both nanocomposites have fairly small and regular morphologies; the nanocomposites containing the control organoclay show larger particles, but of considerably smaller sizes than those observed for the composites made from the reduced-CEC organoclays. TEM micrographs of select nanocomposites at lower concentrations (Figure 6.9) show a uniform morphology. The nanocomposites containing the commercial organoclay show large particles with high platelet order. Slightly larger, more disordered particles are seen in the samples made from the control organoclay, while the composites made from the organoclay with a high CEC reduction show even larger particles with low platelet order.

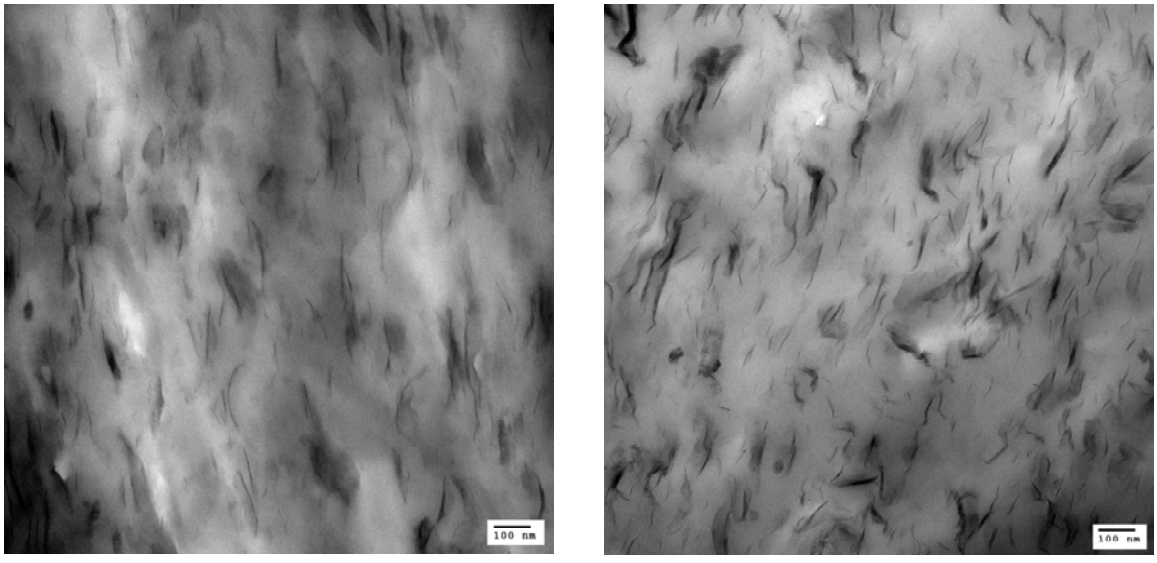

PA-6/ $M_2(HT)_2$ control **PA-6 $M_2(HT)_2$ Low CEC reduction**

Figure 6.6 TEM micrographs of PA-6/ $M_2(HT)_2$ nanocomposites with high clay concentrations.

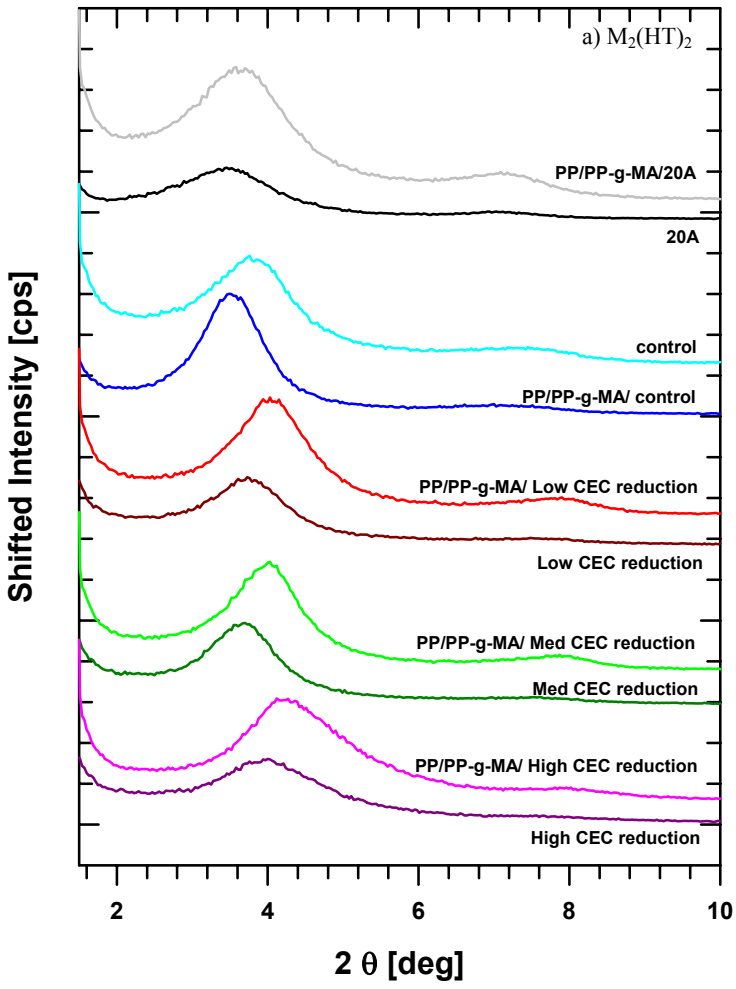

Figure 6.7 WAXS scans for pure organoclays and their respective PP/ PP-g-MA/ $M_2(HT)_2$ nanocomposites containing ~4.5 wt% MMT.

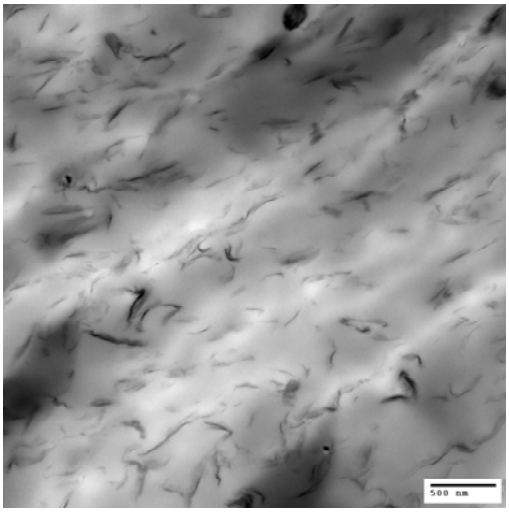

PP/PP-g-MA/20A

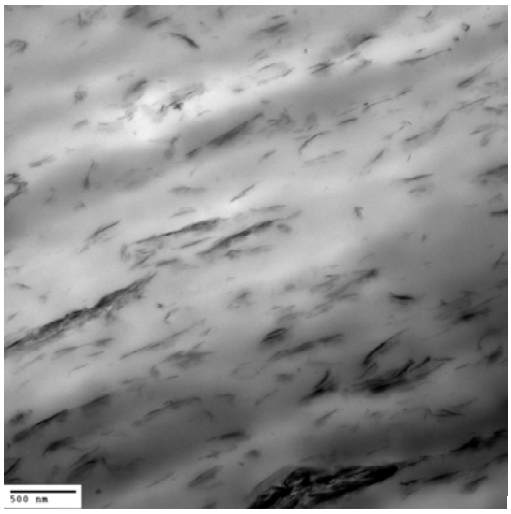

PP/PP-g-MA/$M_2(HT)_2$ control

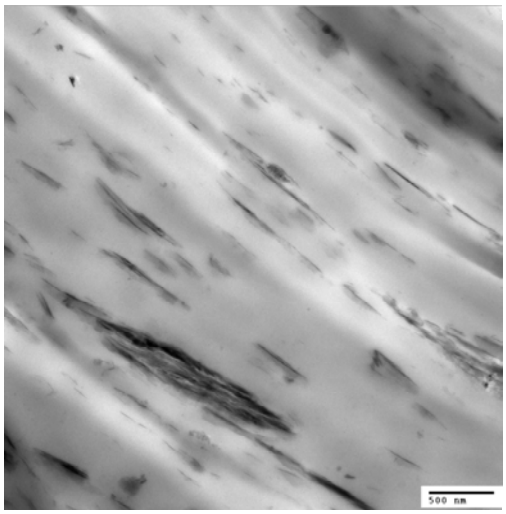

PP/PP-g-MA/$M_2(HT)_2$ Low CEC reduction

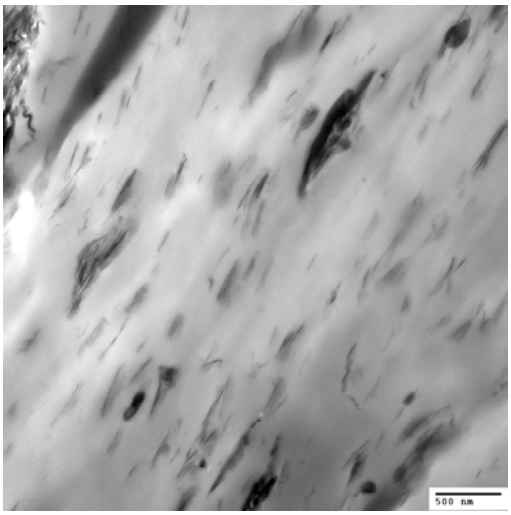

PP/PP-g-MA/$M_2(HT)_2$ Med CEC reduction

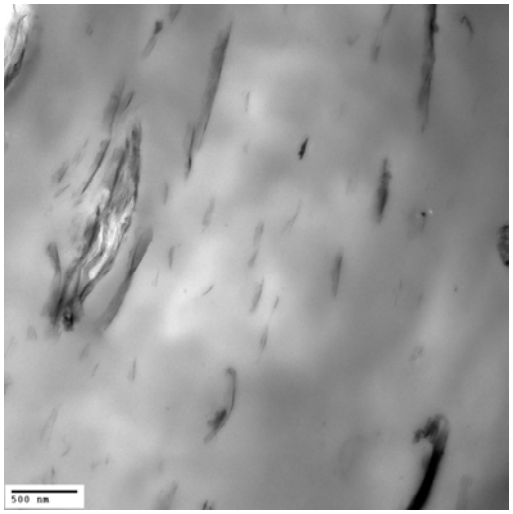

PP/PP-g-MA/$M_2(HT)_2$ High CEC reduction

Figure 6.8 TEM micrographs of PP/ PP-g-MA/ $M_2(HT)_2$ nanocomposites with high clay concentrations.

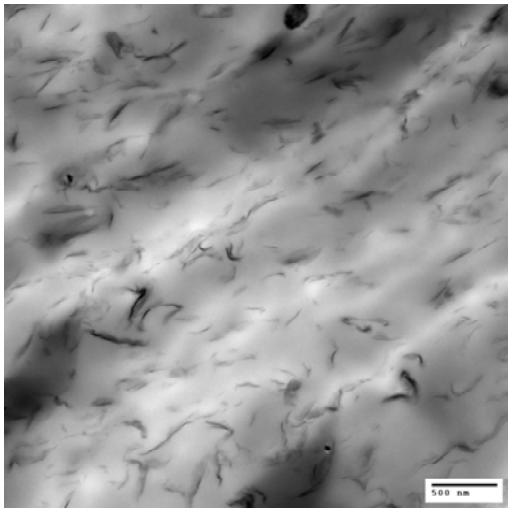

PP/PP-g-MA/20A

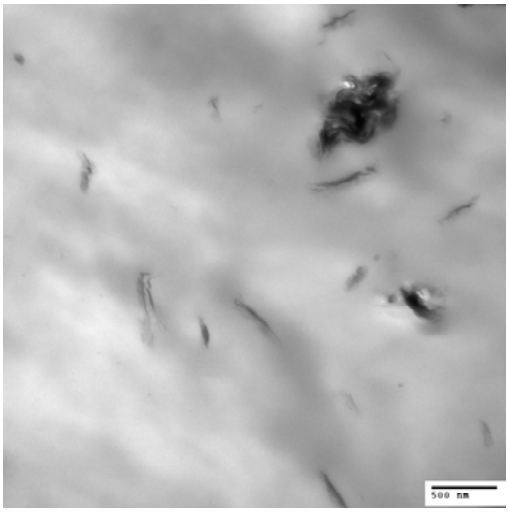

PP/PP-g-MA/ $M_2(HT)_2$ High CEC reduction

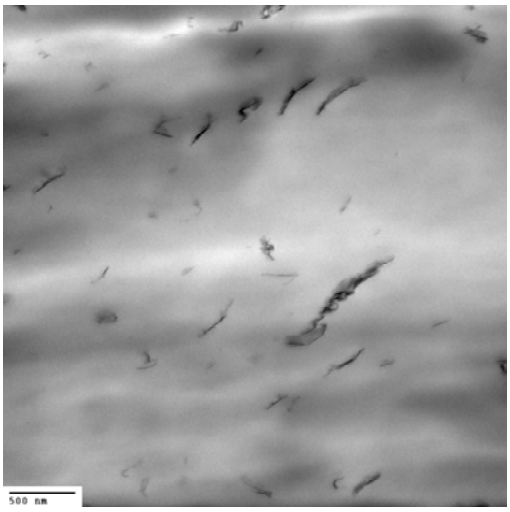

PP/PP-g-MA/ $M_2(HT)_2$ control

Figure 6.9 TEM micrographs of PP/ PP-g-MA/ $M_2(HT)_2$ nanocomposites with low clay concentrations.

Mechanical properties

Figure 6.10 shows the effect of clay concentration on Young's modulus for the nanocomposites prepared in this study. The modulus increases in all cases as the clay concentration is increased, even at low loadings. For PA-6 nanocomposites, the largest increase in Young's modulus is observed for the composites containing $M_3(HT)_1$

organoclays (Figure 6.10a). Here, the control organoclay produces the largest increase in modulus followed by the corresponding commercial organoclay, while the nanocomposites made from the reduced CEC organoclays fall below the moduli of the nanocomposites made from this organoclay. The organoclays containing low and medium CEC reduction lead to very similar modulus values, both lower than that of nanocomposites made from the organoclay with the highest CEC reduction. On the other hand, Figure 6.10b shows that no significant difference was observed in the Young's modulus for PA-6 nanocomposites made from the $M_2(HT)_2$ control organoclay and the corresponding organoclay containing low CEC reduction. Figure 6.10c shows the modulus of PP/PP-g-MA nanocomposites containing the $M_2(HT)_2$ organoclays. The modulus is highest for the composites made from the commercial organoclay, while no significant difference in modulus was observed between the nanocomposites containing the control and reduced-CEC organoclays.

The morphology and modulus results presented here show that PA-6 nanocomposites formed from the one-tailed control organoclay present a higher clay dispersion and modulus enhancement than those containing the corresponding commercial organoclay. Conversely, the two-tailed commercial organoclay produced higher clay dispersion and modulus enhancement for PP/PP-g-MA nanocomposites than the corresponding control organoclay. The removal of the small amounts of excess organic modifier may increase the affinity between the PA-6 and the organoclay; at the same time, it may result in a lower hydrophobicity of the organoclay leading to a lower affinity with the non-polar matrix. On the other hand, the evidence reported here shows that the reduced-CEC organoclays lead to lower exfoliation and modulus enhancement for both PA-6 and PP/PP-g-MA nanocomposites, while no clear correlation could be

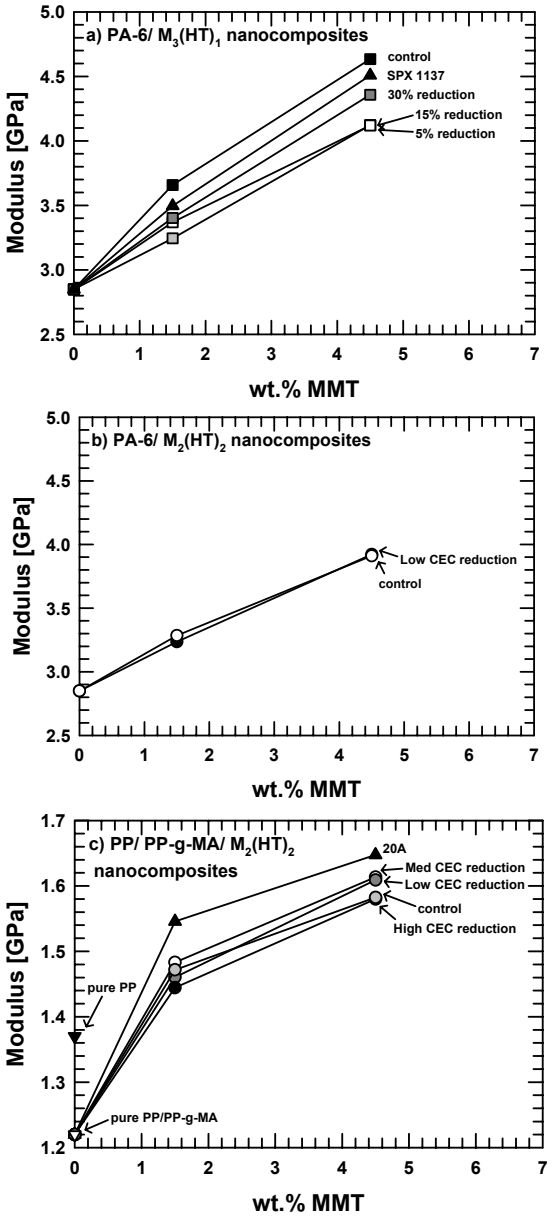

Figure 6.10 Young's modulus for PA-6 and PP/ PP-g-MA nanocomposites.

found with respect to the amount of CEC reduction. Even though the reduced-CEC organoclays contain an even lower amount of organic modifier, the 'macroscopic' measurements of CEC and LOI do not reflect the differences in layer charge and charge

distribution from gallery to gallery and/or within the same galleries that may be present and that could influence the exfoliation of the organoclay in the polymer matrix. Even if a direct measurement of these variations is not clear at this point, signs of heterogeneities were apparent from the X-ray diffraction results.

Most of the literature referenced in this study reports a different procedure for CEC reduction of Na-MMT by lithium fixation than the one employed here. That procedure is based on the method reported by Brindley and Ertem (1971) that involves mixing Li-MMT and Na-MMT in different proportions depending on the percentage of Li^+ desired, and dispersing the mixture in water [11]. Since Li-MMT and Na-MMT can be completely dispersed in water, an even distribution of Li^+ and Na^+ ions inside the clay galleries may be assumed and subsequent drying and heating are performed [11]. The kinetic process involved in the adsorption of Li^+ and Na^+ ions in solution into the surface of the clay platelets is assumed to be an equilibrium process where there is no selectivity for Li^+ over Na^+ or vice versa; therefore, after eventual ion exchange equilibration there should be equal amounts of Li^+ and Na^+ ions on each platelet. The method for the CEC reduction used here is mainly employed for the CEC reduction of Ca-MMT, since this clay does not expand in water beyond 1.9 nm [11]. Only one other study was found that used a procedure similar to the one used here [12], but they describe a more dilute suspension for the Li-Na cation exchange reaction and it was performed under dialytic equilibrium with $NaNO_3$. No problems of clay separation from suspension were mentioned in this reference which may suggest that a more diluted suspension might reduce or eliminate the problems described by CSIRO concerning clay separation from the supernatants. The possible differences between these methods are not known at this point, but the results shown above do confirm that high CEC reduction, as described in the other references, could not be achieved through this method.

CONCLUSIONS

Structure-property relationships for PA-6 and PP/PP-g-MA nanocomposites prepared by melt processing from a series of reduced-CEC organoclays are presented here. Three reduced-CEC MMT clays were supplied by CSIRO in Australia. Since CEC measurements on the as-received clays showed only a minor CEC reduction, subsequent heating based on preliminary tests was performed to target 3 different levels of CEC reduction, a low, and intermediate, and a high CEC reduction. Two different types of organoclays were produced containing $M_3(HT)_1$ and $M_2(HT)_2$ organic modifiers, along with controls for each type of organoclay made from Na-MMT for comparison. Purifications with methanol were performed for these organoclays to remove the excess surfactant in the clay galleries that could be present from the cation exchange reaction with the alkyl ammonium surfactants. X-ray analysis and percentage LOI calculations for these organoclays showed a reduction in the inter-gallery spacing and in the amount of organic modifier contained in the clay with increasing levels of CEC reduction. A lower inter-gallery spacing and amount of organic modifier was also observed for the control organoclays after purification with respect to the corresponding commercial organoclays.

The morphology and modulus results presented here show that the reduced-CEC organoclays formed in this study lead to a lower degree of exfoliation and modulus enhancement for both PA-6 and PP/PP-g-MA nanocomposites, while no clear correlation could be found with respect to the amount of CEC reduction. This was attributed to differences in layer charge and charge distribution that could have been produced during the charge reduction process. The control organoclay containing the one-tailed surfactant lead to a higher clay dispersion and modulus enhancement of PA-6 nanocomposites with respect to the commercial organoclay, while the two-tailed commercial organoclay lead

to higher clay dispersion and modulus enhancement in the case of PP/PP-g-MA nanocomposites; a smaller amount of organic surfactant in organoclays with no CEC reduction may increase its affinity with PA-6 while it may decrease its affinity with a non-polar matrix.

More work is needed to truly explore this effect, since questions regarding the CEC reduction process and charge heterogeneity could not be fully addressed. In addition, the small amounts of charge-reduced clay obtained from the current CEC-reduction process limited the extent of clay and nanocomposite characterization.

These preliminary observations on the CEC reduction process give important insights for future work on this subject. A more detailed study revisiting the CEC reduction process and subsequent characterization of the resulting clays should be carried out.

REFERENCES

[1] Dennis HR, Hunter DL, Chang D, Kim S, White JL, Cho JW, Paul DR. Polymer 2001;42:9513-9522.

[2] Fornes TD, Yoon PJ, Hunter DL, Keskkula H, Paul DR. Polymer 2002;43:5915-5933.

[3] Lee HS, Fasulo PD, Rodgers WR, Paul DR. Polymer 2005;46:11673-11689.

[4] Shah RK, Hunter DL, Paul DR. Polymer 2005;46:2646-2662.

[5] Komadel P, Madejova J, Bujdak J. Clays and Clay Minerals 2005;53:313-334.

[6] Hoffman U, Klemen R. Zeitschrift fur anorganische und allegemeine Chemie 1950;262:95-99.

[7] Calvet R, Prost R. Clays and Clay Minerals 1971;19:175-186.

[8] Bujdak J, Slosiarikova H, Cicel B. Journal of Inclusion Phenomena and Molecular Recognition in Chemistry 1992;13:321-327.

[9] Komadel P, Hrobarikova J, Smrcok L, Koppelhuber-Bitschnau B. Clay Minerals 2002;37:543-550.

[10] Hrobarikova J, Madejova J, Komadel P. Journal of Materials Chemistry 2001;11:1452-1457.

[11] Brindley GW, Ertem G. Clays and Clay Minerals 1971;19:399-404.

[12] Maes A, Stul MS, Cremers A. Clays and Clay Minerals 1979;27:387-392.

[13] Meier LP, Nuesch R. Journal of Colloid and Interface Science 1999;217:77-85.

[14] Clemenz DM, Mortland MM. Clays and Clay Minerals 1974;22:223-229.

[15] Lagaly G. Clays and Clay Minerals 1979;27:1-10.

[16] Stul MS, Mortier WJ. Clays and Clay Minerals 1974;22:391-396.

[17] Delozier DM, Orwoll RA, Cahoon JF, Ladislaw JS, J.G. SJ, Connell JW. Polymer 2003;44:2231-2241.

[18] Fornes TD, Yoon PJ, Keskkula H, Paul DR. Polymer 2001;42:9929-9940.

[19] Kim DH, Fasulo PD, Rodgers WR, Paul DR. *Article in preparation*

[20] Stretz HA. Ph.D. Thesis, The University of Texas at Austin, 2005.

[21] Chavarria F, Shah RK, Paul DR. *Article in preparation*.

[22] Greene-Kelly R. Journal of Soil Science 1953;4:233-237.

[23] Xie W, Gao Z, Pan W-P, Hunter DL, Singh A, Vaia RA. Chem Mater 2001;13:2979-2990.

[24] Paul DR, Zeng QH, Yu AB, Lu GQ. Journal of Colloid and Interface Science 2005;292:462-468.

[25] Shah RK, Paul DR. Polymer 2006;47:4075-4084.

CHAPTER 7

MORPHOLOGY AND PROPERTIES OF THERMOPLASTIC POLYURETHANE NANOCOMPOSITES: EFFECT OF ORGANOCLAY STRUCTURE

INTRODUCTION

The affinity of the polymer with the surface of the clay and/or with the organic surfactant of the organoclay is essential to promote favorable interactions between these species and, hence, obtain high levels of exfoliation. The affinity between the polymer matrix and the organoclay is determined, to some extent, by the polarity of the polymer and the type of organic modifier used to form the organoclay. Recent studies from our laboratory have shown that a polar polymer such as nylon 6 (PA-6), exhibits a higher level of exfoliation with an organoclay based on a surfactant with one alkyl tail, while nanocomposites made from non-polar polymers, such as polypropylene, polyethylene, and various copolymers show completely opposite trends, i.e., organoclays based on surfactants with two or more alkyl tails lead to more exfoliated nanocomposites than a one-tailed organoclay [1-4]. Since a one-tailed organoclay provides less coverage of the silicate surface than a two-tailed organoclay, these results suggest that PA-6 has a higher affinity for the polar surface of the clay than for the largely non-polar surfactant, while the opposite is true for non-polar matrices.

Thermoplastic polyurethanes (TPU's) have similar functional groups as PA-6 but rather different repeat unit structures. There is a growing literature on polyurethane nanocomposites describing, among other things, the effect of methods of preparation, polyurethane and organoclay structure, and hard segment concentration on degree of clay dispersion or exfoliation, microphase morphology, hydrogen bonding, rheology,

mechanical properties, thermal stability, flame retardancy, water sorption, and barrier properties [5-18]. There are very few reports on polyurethane nanocomposites prepared by melt processing [12, 13] in spite of the obvious advantages of this approach [19-21].

The objective of this study is to explore the effect of the surfactant chemical structure on the morphology and mechanical properties of TPU nanocomposites prepared by melt processing. Detailed comparisons of the structure of the organic treatment (such as number of alkyl tails, saturation of the alkyl chain, different side groups, and length of the alkyl chain) are reported here for nanocomposites formed from a medium-hardness TPU. A more limited study of nanocomposites based on high-hardness TPU is also reported. Mechanical properties and morphology characterization are used to evaluate the structure and performance of these composites.

EXPERIMENTAL

Two commercial grades of thermoplastic polyurethane were selected for this work; one was a medium-hardness polyester-based TPU from Dow Plastics and the other was a high-hardness polyether-based TPU from BASF. The medium- and high-hardness thermoplastic polyurethanes will be referred to as M-H and H-H TPU's, respectively. Several amine based organoclays were chosen to determine the effect of the number of long alkyl tails, $M_3(HT)_1$ vs. $M_2(HT)_2$, saturation of the primary tail, M_3T_1 vs. $M_3(HT)_1$, the effect of hydroxy ethyl functional groups, $(HE)_2M_1T_1$ vs. M_3T_1, and length of the alkyl tail, $(HE)_2M_1T_1$ vs. $(HE)_2M_1C^*_1$. Specifications for these materials as well as explicit details on melt processing and characterization techniques are given in Chapter 3; conditions and specific information concerning this study follow.

TPU nanocomposites were prepared by melt compounding in a Haake twin screw extruder at a screw speed of 280 rpm, a feed rate of 1200 g/h, and a temperature of 190

ºC. Dried extruded pellets were injection molded using a barrel temperature range of 200 to 215 ºC from feed to nozzle, respectively, for the M-H TPU materials, while a range of 180 to 200 ºC was used for the H-H TPU materials. A mold temperature of 50 ºC, injection pressure of 70 bar, and holding pressure of 65 bar were used for both materials.

Tensile stress at 300% elongation was reported, due to its standard use in the polyurethane literature; it will be referred to as the 300% stress. The values reported here represent an average of five specimens for modulus, and three to four specimens for elongation at break and 300% stress; standard deviations were typically of the order of 3% for modulus, and 1 to 30% for elongation at break. The values reported for 300% stress were obtained from the most representative stress-strain curve for each sample.

TEM micrographs were obtained using a JEOL 2010F transmission electron microscope operating at an accelerating voltage of 120 kV and a Phillips EM208 transmission electron microscope with an accelerating voltage of 80 kV. Samples for TEM were cryogenically cut into ultra thin sections (50-70 nm thick) with a diamond knife at a temperature of -40 ºC using an RMC PowerTome XL ultramicrotome with a CR-X universal cryosectioning system. These sections were taken from the central part of a tensile bar normal to the flow direction (FD) and viewed in the TEM parallel to the flow direction, as shown in Figure 3.5. Scanning transmission electron microscopy (STEM) images were obtained using a JEOL 2010F transmission electron microscope operating in the dark-field, scanning mode at an accelerating voltage of 200 kV.

The TEM images shown in this manuscript are representative of the morphologies of the nanocomposites observed through TEM; hence, the particle analysis results from the procedure described below may not be in exact accord with the observations from a single image since they represent averages over a much larger sample area. The analyses

were done to ensure an objective and accurate representation of the morphology of the nanocomposite systems.

RESULTS AND DISCUSSION

Effect of organic modifier for the M-H TPU

Morphology

Figure 7.1 shows WAXS scans for various nanocomposites made in this study containing ~2.3 wt% MMT, along with a scan of each organoclay for comparison. In every case, the nanocomposite scans show basal reflections indicating that all the nanocomposites contain tactoids of organoclay with high enough order and concentration to diffract X-rays. There is an increase in the d-spacing of all the nanocomposites with respect to that of the pure organoclays, except for the samples containing the $(HE)_2M_1C^*_1$ surfactant. The increase in d-spacing for the nanocomposites made with $M_3(HT)_1$ is from 1.8 to 2.9 nm, while those for $M_2(HT)_2$ show a slightly smaller increase from 2.55 to 3.41 nm. M_3T_1 shows an increase in d-spacing from 1.75 to 2.96 nm and $(HE)_2M_1T_1$ shows a weaker and more diffuse peak that seems to be centered around 3.05 nm, with respect to 1.77 nm of the organoclay. According to conventional interpretations, this suggests some degree of polymer intercalation into the organoclay galleries. It should be noted that the WAXS patterns in Fig. 7.1 show only one basal reflection for the organoclays, while more high-order reflections were observed for the nanocomposite samples. The organoclay scans were made from powders while the nanocomposite scans were made from the surface of injection molded samples. The greater orientations in the latter leads to multiple reflections while the more random orientations of the organoclay powders do not.

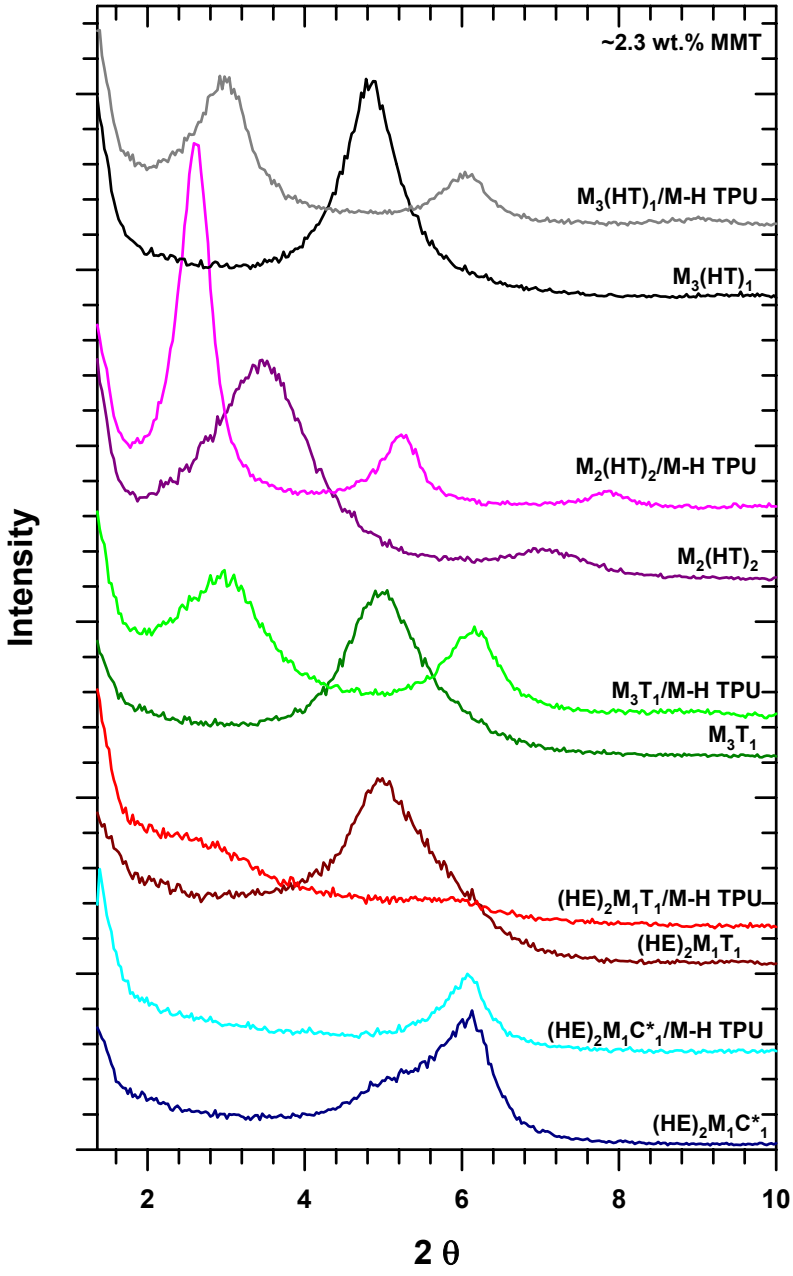

Figure 7.1 WAXS patterns for pure organoclays and their respective M-H TPU nanocomposites containing ~2.3 wt% MMT

TEM micrographs shown in Figures 7.2 and 7.3 provide additional insight about the morphology of these nanocomposites. At low concentrations, all the composites have a similar structure, except for the sample containing $(HE)_2M_1T_1$, which shows a noticeably higher number of particles. At high concentrations, the nanocomposites from $(HE)_2M_1T_1$ also have the highest number of particles with the smallest size. The nanocomposites containing $M_3(HT)_1$ and M_3T_1 have a somewhat lower number of particles of slightly larger size; while the samples containing $(HE)_2M_1C^*_1$ show a mixture of small particles and larger agglomerates. The two-tailed organic modifier ($M_2(HT)_2$) produces the lowest number of particles with the largest size. At the same clay concentration, the particle count is an indicator of the extent of exfoliation of clay platelets in the polymer matrix. As mentioned before, samples with a low particle count have large particles with high platelet agglomeration and, as the particle count increases, the particle size decreases as a result of the breakup of large particles, producing better dispersion.

The number of long alkyl tails on the surfactant in the organoclay affects the morphology of these TPU nanocomposites (Fig. 7.2a and b). $M_2(HT)_2$ leads to a small number of large, extended tactoids, while $M_3(HT)_1$ produces a higher number of small, elongated tactoids. The unsaturated surfactant, M_3T_1, produces a very similar morphology as that obtained from the saturated organoclay, $M_3(HT)_1$, but there seems to be a larger number of particles and more alignment in the nanocomposites made from the saturated organoclay (Figures 7.2b and c). The surfactant with hydroxy ethyl functional groups, $(HE)_2M_1T_1$, leads to the smallest tactoids and many particles are single platelets. There is a higher particle count, or a higher degree of clay dispersion in the samples containing hydroxy ethyl groups than in the ones containing methyl substituents (Fig. 7.3a and b). The length of the alkyl tail also seems to affect clay dispersion, as seen in

Figures 7.3b and c; the shorter alkyl tail does not produce as high clay dispersion as the longer alkyl.

These qualitative trends in Figures 7.2 and 7.3 were quantified by particle analysis of TEM images; the results are shown in Table 7.1. The complex shapes of the clay particles in TPU nanocomposites made thickness estimation very difficult, so values of aspect ratios for these samples could not be obtained. Nevertheless, measurements of particle lengths and densities give insight about the degree of platelet dispersion of these nanocomposites. At low concentrations, the particle lengths are very similar for all the samples, while the specific particle density is highest in the samples made with $(HE)_2M_1T_1$, as seen in the TEM micrographs. At high concentrations, the samples made from $M_2(HT)_2$ have the highest particle length, while the ones made from $(HE)_2M_1T_1$ have the lowest. The specific particle density is again highest for the nanocomposites made from the $(HE)_2M_1T_1$ organoclay, suggesting the highest degree of dispersion, while $M_2(HT)_2$ produces an extremely low particle density consistent with the large agglomerates seen in TEM. High matrix reinforcement might be expected from a high particle density; however, the aspect ratio of the filler particles is the true parameter needed to assess the degree of reinforcement.

The complex shapes of the clay particles in TPU nanocomposites were explored by comparing bright-field TEM and dark-field STEM images. When using the dark-field STEM technique, the MMT platelets appear white, while the polymer matrix, holes in the specimen, or any other low-atomic-density constituent are seen as a black background. Figure 7.4 confirms that the small gray areas seen around some of the particles in the bright-field TEM images are in fact clay. In a specific example, Figure 7.4c shows that the grey area surrounding the particle in Fig. 7.4b is white, which suggests the presence

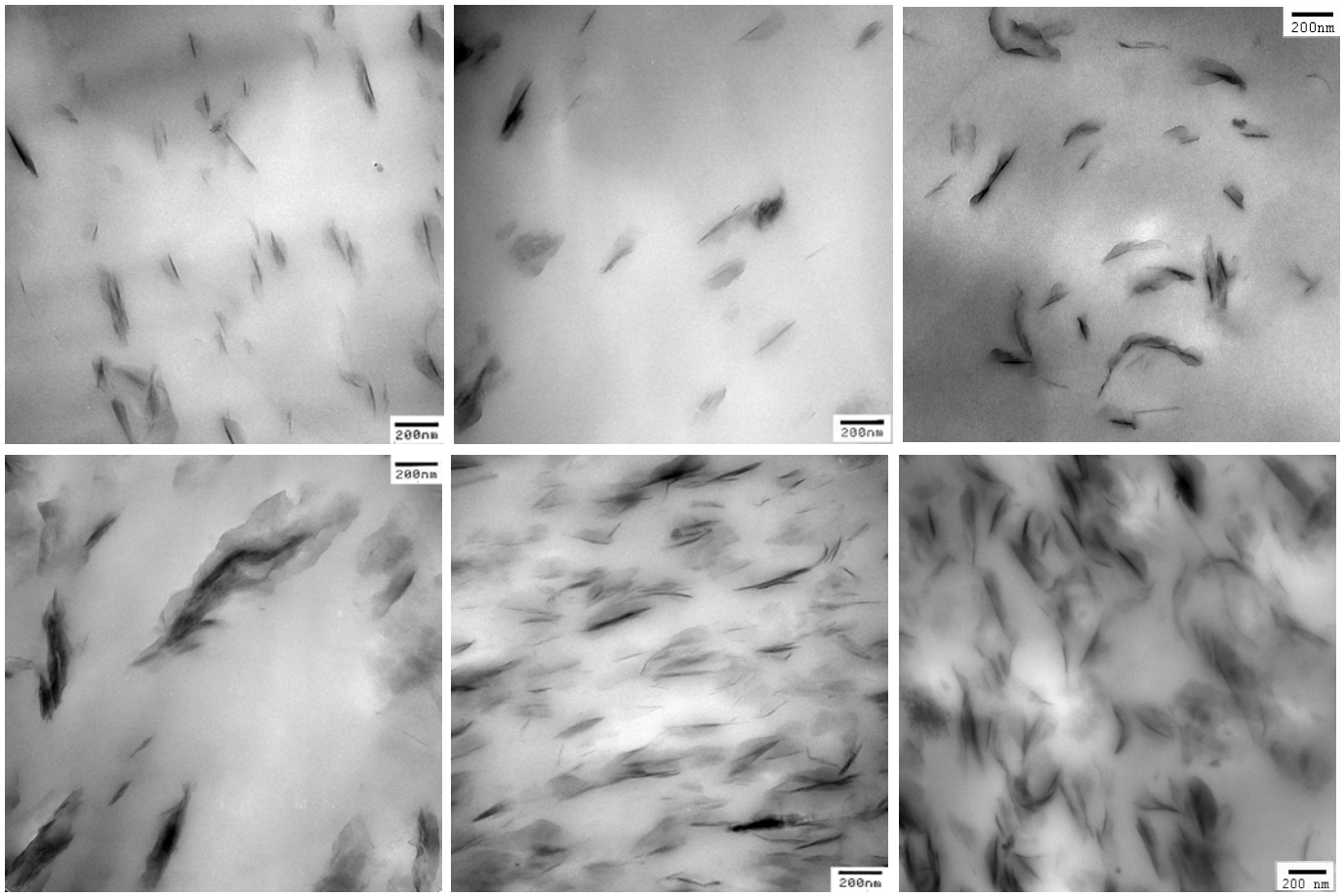

a) $M_2(HT)_2$ **b) $M_3(HT)_1$** **c) M_3T_1**

Figure 7.2 TEM micrographs for nanocomposites based on M-H TPU and organoclays a) $M_2(HT)_2$, b) $M_3(HT)_1$, and c) M_3T_1; with concentrations ranging from 0.48 to 0.94 wt% MMT (above) and from 4.61 to 6 wt% MMT (below).

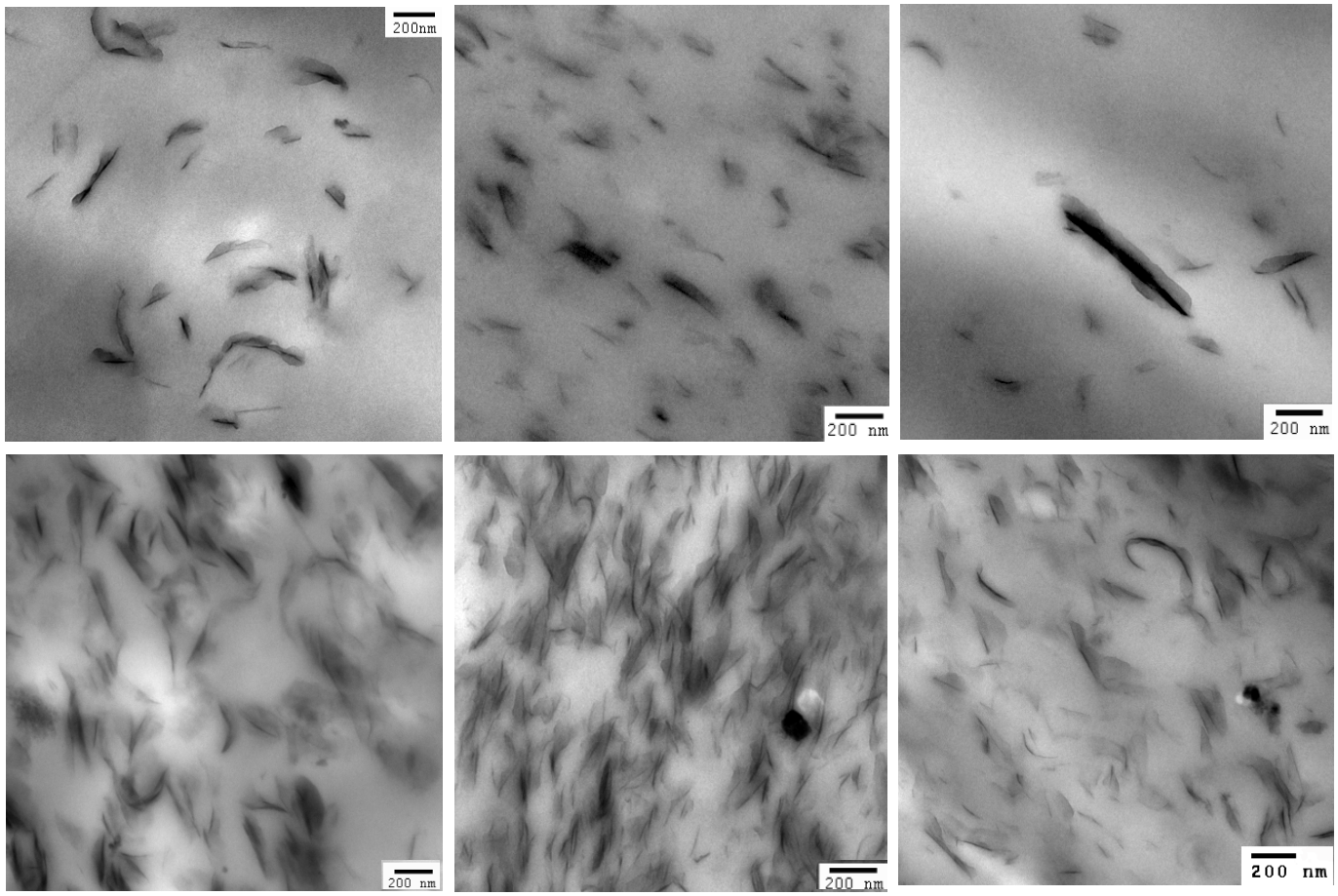

Figure 7.3 TEM micrographs for nanocomposites based on M-H TPU and organoclays a) M_3T_1, b) $(HE)_2M_1T_1$, and c) $(HE)_2M_1C^*_1$; with concentrations ranging from 0.9 to 0.95 wt% MMT (above) and from 5.46 to 6 wt% MMT (below).

of one or more MMT platelets. In bright-field TEM, sharp lines show platelet edges, i.e., the platelets are aligned with the electron beam, while grey areas of different intensities show one or more skewed or misaligned platelets.

Table 7.1 Particle analysis results of M-H TPU nanocomposites.

Organoclay nanocomposites	No. of Particles Analyzed	Particle Length [nm]		Particle Density [particles/μm^2]	Specific Particle Density [particles/μm^2]
		Number Average	Weight Average		
$M_3(HT)_1$					
0.48 wt% MMT	159	138 ± 3	172 ± 11	8 ± 2	16 ± 4
5.05 wt% MMT	842	141 ± 7	183 ± 12	43 ± 4	47 ± 5
$M_2(HT)_2$					
0.61 wt% MMT	233	113 ± 7	144 ± 7	11 ± 3	19 ± 4
4.61 wt% MMT	182	215 ± 31	327 ± 31	10 ± 1	12 ± 1
M_3T_1					
0.94 wt% MMT	541	142 ± 6	180 ± 12	9 ± 1	10 ± 1
6.00 wt% MMT	1311	191 ± 7	248 ± 16	22 ± 1	21 ± 1
$(HE)_2M_1T_1$					
0.9 wt% MMT	946	114 ± 10	142 ± 10	28 ± 4	31 ± 5
5.46 wt% MMT	1376	118 ± 2	149 ± 2	93 ± 12	93 ± 12
$(HE)_2M_1C^*_1$					
0.95 wt% MMT	546	135 ± 7	184 ± 19	10 ± 1	10 ± 1
5.68 wt% MMT	897	133 ± 12	132 ± 17	56 ± 7	54 ± 7

A careful analysis of the TEM images has led us to suggest a series of possible platelet orientations that might explain the clay morphologies seen by TEM. Images containing particles with a grey area on only one side of a sharp line may be a the result of a platelet oriented within the microtomed section as suggested in Figure 7.5; the sharp line being the edge of the platelet aligned with the electron beam, and the gray area being the skewed body. Particles with grey areas on both sides of sharp edges suggest more complex configurations of what was described in Figure 7.5. Figures 7.6 and 7.7 illustrate how grey areas on both sides might involve having a particle with one or many platelets separated on the far side of the sample, or a particle with many platelets skewed towards one side.

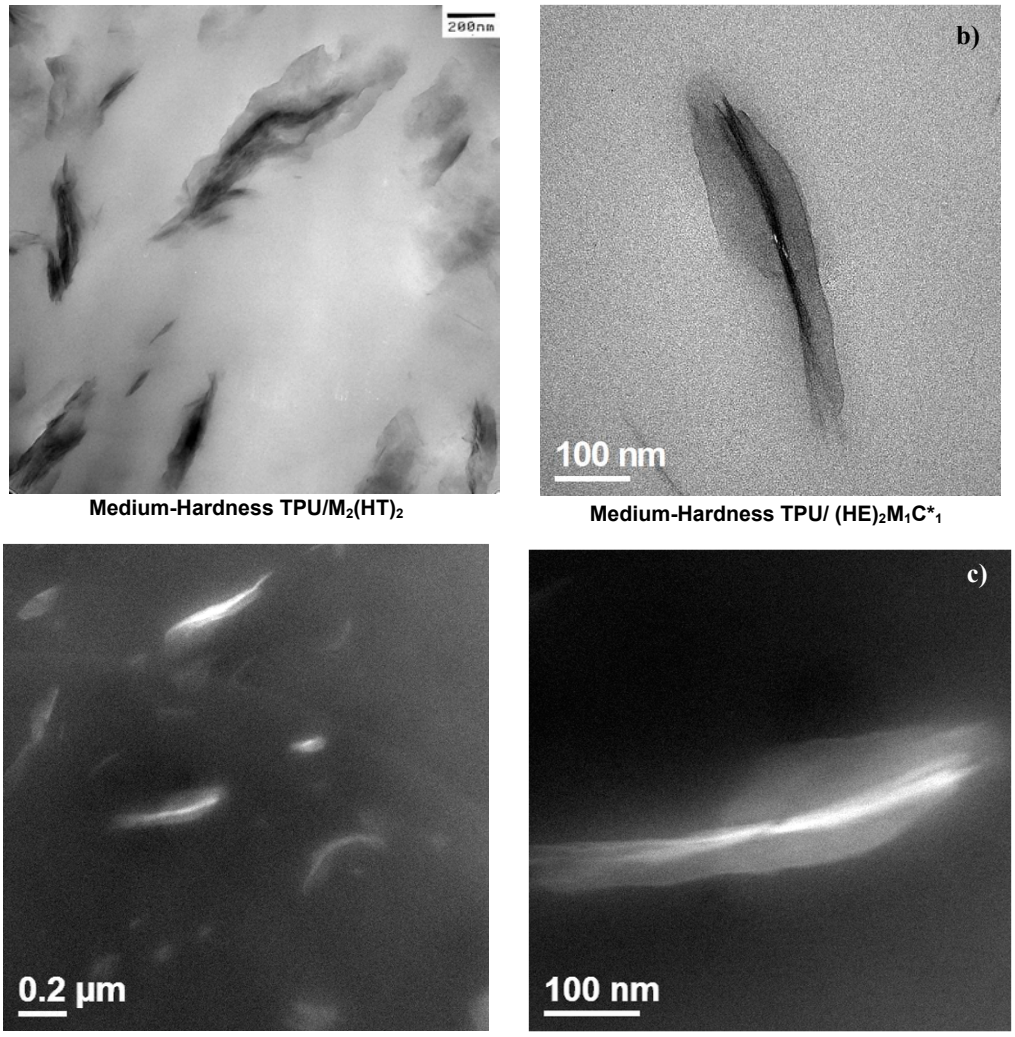

Figure 7.4 Dark-field analysis of M-H TPU nanocomposite particles. Above: bright-field TEM images of M-H TPU nanocomposites (low magnification showing many particles (left) and high magnification showing one particle (right)). Below: dark-field STEM images of M-H TPU nanocomposites (low magnification showing many particles (left) and high magnification showing one particle (right)).

As shown before, TEM images of some TPU nanocomposites have particles containing sharp dark areas in the center, surrounded by large grey areas. It is proposed that these images represent particles with aligned platelets in the center, surrounded by a smaller number of disordered platelets with no edges on the electron beam path. TEM micrographs taken with the view parallel to the 'normal direction' (i.e. in the FD-TD plane) show the same morphology, indicating that this condition might be present in all directions (Fig. 7.8).

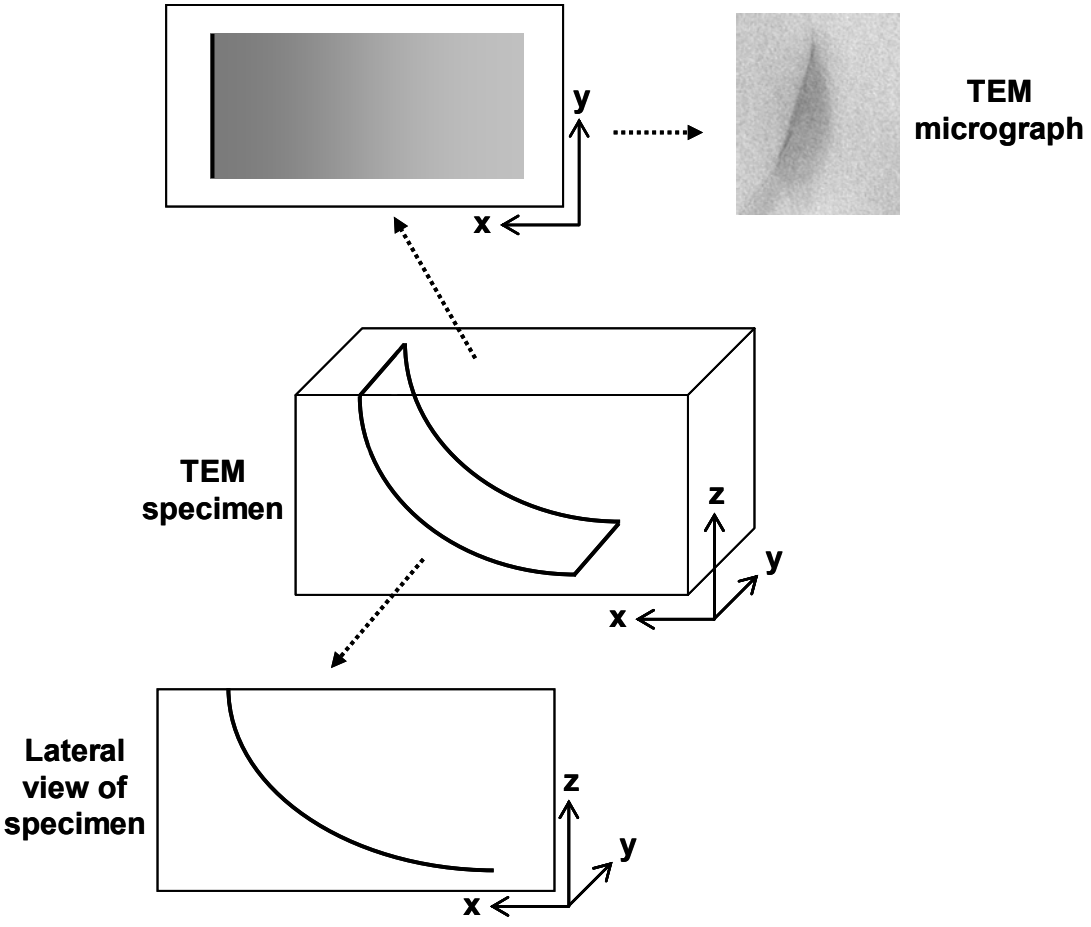

Figure 7.5 Schematic illustration of possible platelet orientation for a TEM image of a clay particle with a grey area on one side of a particle.

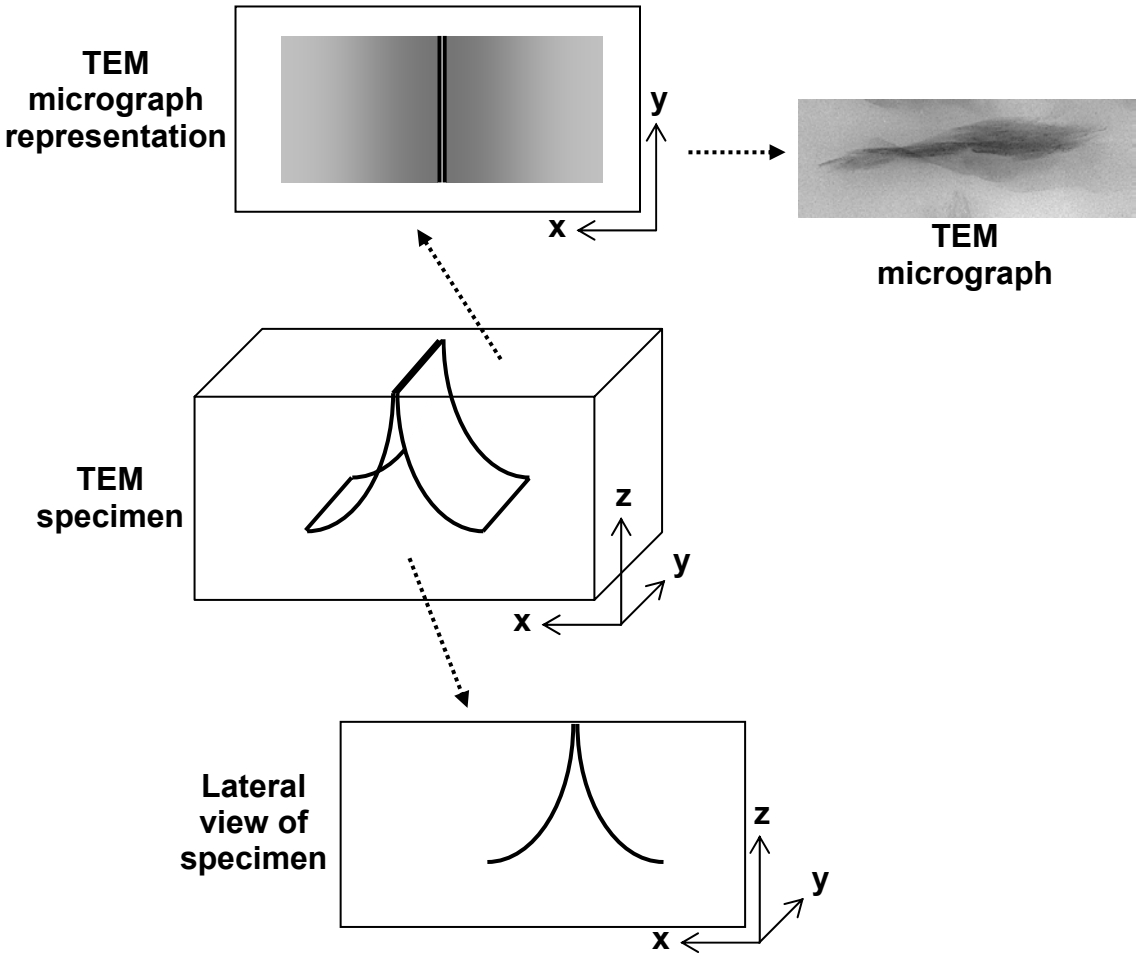

Figure 7.6 Schematic illustration of possible platelet orientation for a TEM image of a clay particle with grey areas on both sides of the particle: particle with one or many platelets separated on the far side of the sample.

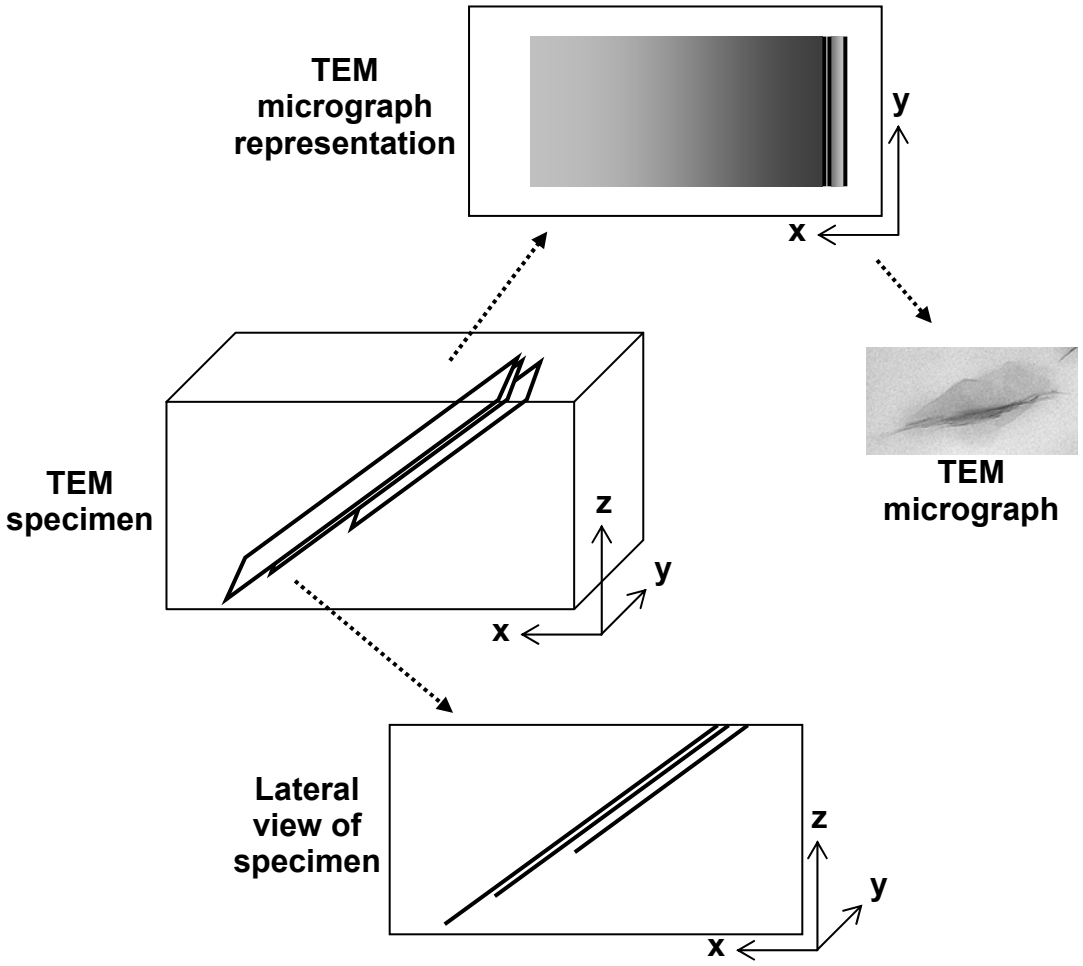

Figure 7.7 Schematic illustration of possible platelet orientation for a TEM image of a clay particle with grey areas on both sides of the particle: particle with many platelets, all skewed towards one side.

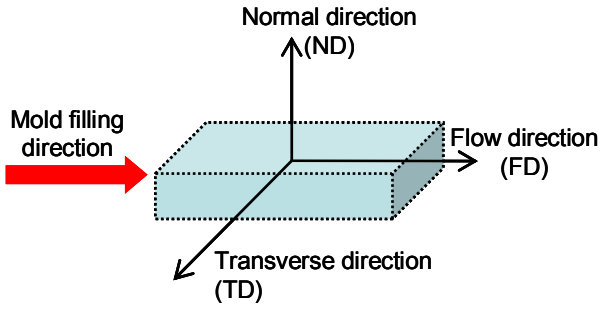

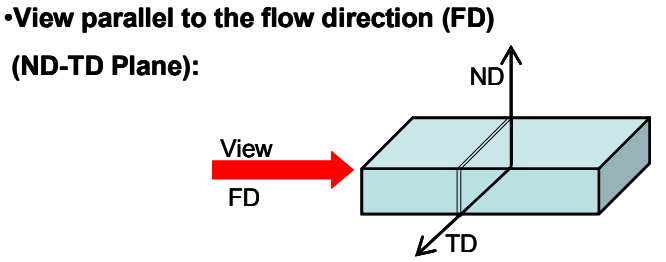

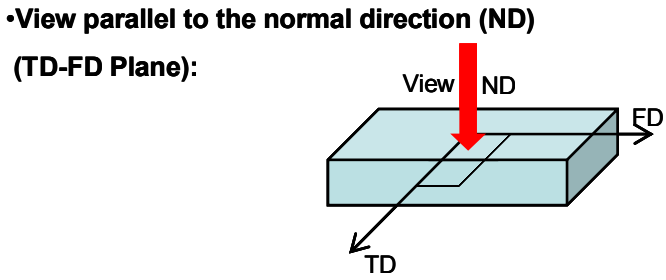

Medium-Hardness TPU/$M_2(HT)_2$

(view parallel to ND)

Figure 7.8 TEM image of TPU/$M_2(HT)_2$ nanocomposites (view parallel to the normal direction).

Mechanical Properties

Figure 7.9 shows representative stress-strain curves for the nanocomposites prepared in this study and illustrate three distinctive types of behaviors. Addition of clay produces an increase in the modulus at small strains in all cases; however, the different organoclays affect the large strain behavior in different ways and may even produce limitations on elongation. In the stress-strain curve for the nanocomposites made from $(HE)_2M_1T_1$, the stress is increased at all strains as the concentration of clay increases (Fig. 7.9a). This was also observed for the stress-strain curves of the nanocomposites made with $(HE)_2M_1C^*_1$, and M_3T_1, but to a lesser extent. The opposite behavior is observed in the stress-strain diagram for the nanocomposites made with $M_2(HT)_2$ (Fig. 7.9c), as the clay concentration is increased, the stress levels at high strains are reduced. An intermediate behavior is seen for the nanocomposites made with $M_3(HT)_1$, where the stress at low clay concentrations is higher than that of the pristine TPU, but lower at high clay concentrations (Fig. 7.9b). This suggests that at high strains, the $(HE)_2M_1T_1$ organoclay continues to reinforce the TPU even at high clay concentrations, $M_3(HT)_1$ provides high strain reinforcement only at low clay concentrations, while $M_2(HT)_2$ does not reinforce the polyurethane matrix at high strains. The elongated tensile bars show signs of permanent set and stress whitening; both increase as the clay concentration increases. The permanent set is highest for the samples made from $M_2(HT)_2$, followed by the ones made with $M_3(HT)_1$. Samples made from $(HE)_2M_1T_1$, M_3T_1, and $(HE)_2M_1C^*_1$ all have similar permanent set, lower than the samples made from $M_2(HT)_2$ and $M_3(HT)_1$. On the other hand, stress whitening is highest for the samples made from $(HE)_2M_1T_1$, followed by the samples made from M_3T_1 and $(HE)_2M_1C^*_1$. The samples from $M_3(HT)_1$ show somewhat less stress whitening, while those made from $M_2(HT)_2$ have the lowest

stress whitening. A more detailed study would be needed to sort out all the operative mechanisms behind these observations, but this is beyond the scope of this work.

Figure 7.10 shows the Young's modulus and stress at 300% strain, respectively, for the nanocomposites prepared in this study. The addition of clay produces an increase in the Young's modulus of all the nanocomposites, even at low loadings. As the clay concentration increases, the nanocomposites made from $(HE)_2M_1T_1$ produce the largest increase in Young's modulus, while the ones made from $M_2(HT)_2$ present the smallest. Fig. 7.10a shows that the one-tailed organoclay leads to higher stiffness values than the two-tailed organoclay, while there is not much difference in the Young's modulus for nanocomposites based on the saturated and unsaturated organoclays. There is a significantly higher increase in Young's modulus of samples made from the organoclay containing $(HE)_2M_1T_1$ (Fig. 7.10b), suggesting that the hydroxy ethyl functional groups and a longer alkyl tail lead to greater TPU matrix reinforcement.

Figure 7.10c shows that the stress at 300% elongation is highest in samples made from $(HE)_2M_1T_1$, while $M_2(HT)_2$ produces the lowest 300% stress overall. M_3T_1 and $(HE)_2M_1C^*_1$ produce a substantial increase in the 300% stress, even at high clay concentration, as opposed to the behavior observed for $M_2(HT)_2$, where it gradually decreases with MMT concentration. On the other hand, the 300% stress for the samples made from $M_3(HT)_1$ increases slightly at low loadings and then remains almost constant. It should be noted that the 300% stress for the nanocomposites containing $(HE)_2M_1T_1$ is presented only at low concentrations, since the elongation at break is less than 300% for composites with higher concentrations.

The effect of organoclay structure on elongation at break could not be fully evaluated in this study since most of the samples prepared did not break before the Instron machine limit of 400% elongation. The only sample that broke before the 400%

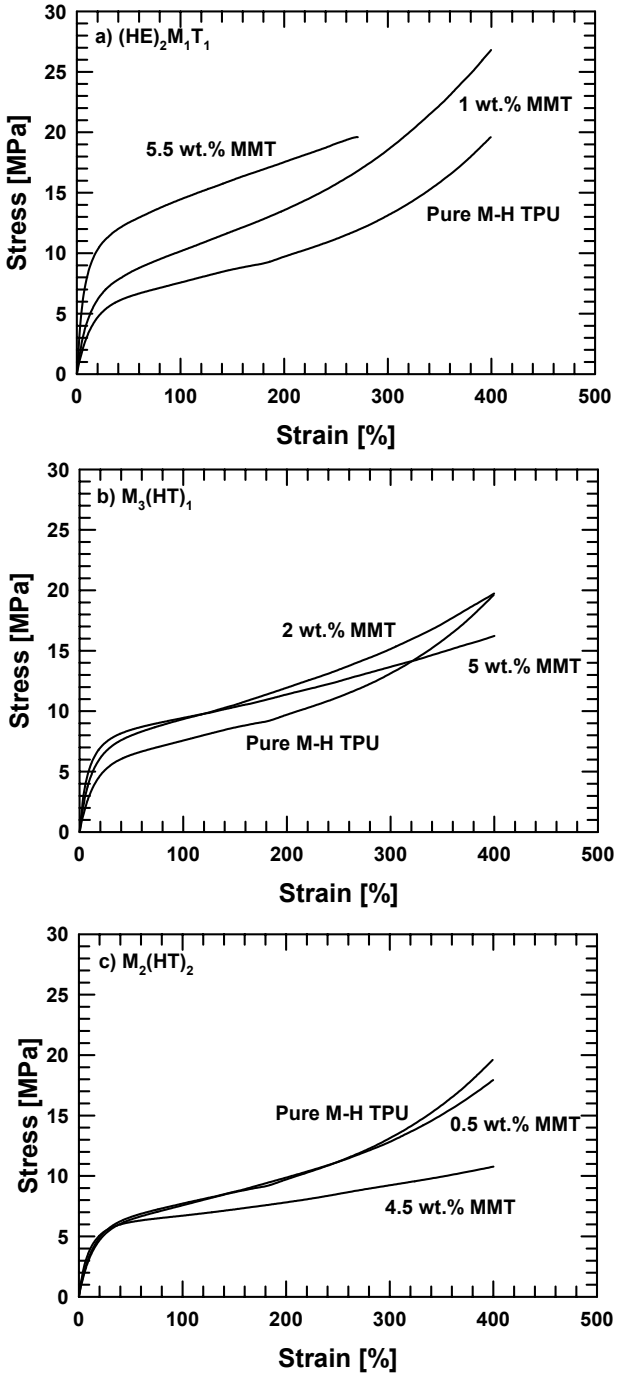

Figure 7.9 Stress-strain behavior of M-H TPU and its nanocomposites. a) $(HE)_2M_1T_1$, b) $M_3(HT)_1$, and c) $M_2(HT)_2$.

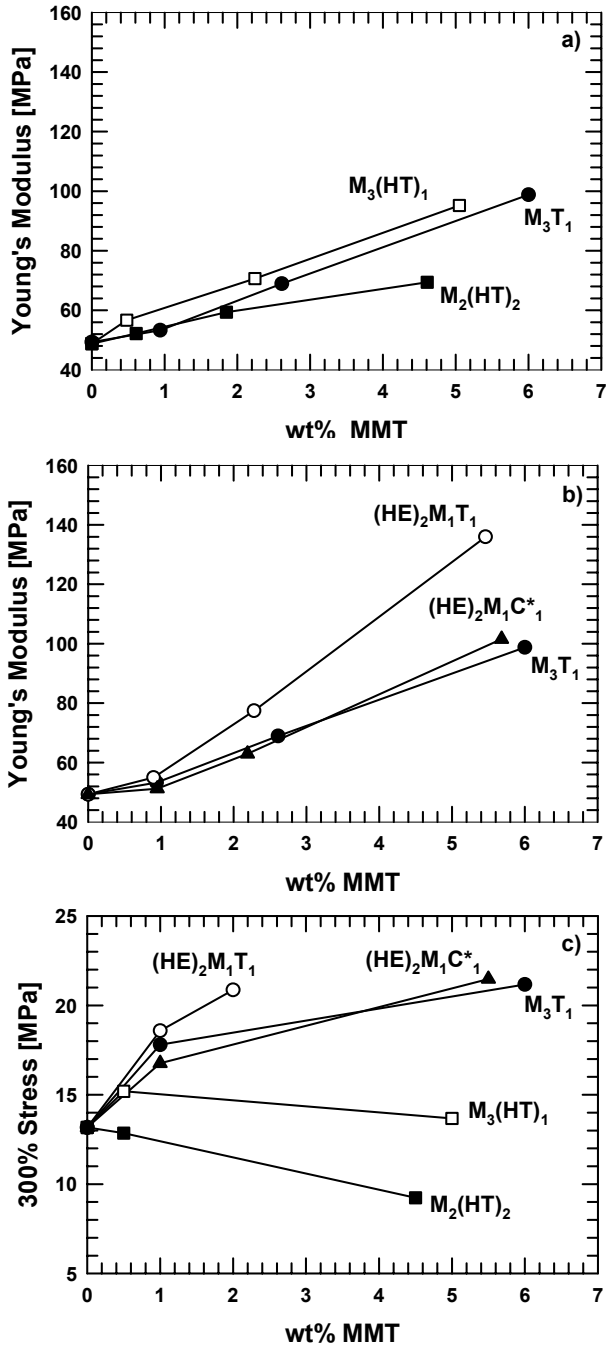

Figure 7.10 Young's modulus and 300% stress for M-H TPU nanocomposites. a) Young's modulus of nanocomposites made from $M_3(HT)_1$, $M_2(HT)_2$, and M_3T_1, and b) M_3T_1, $(HE)_2M_1T_1$, and $(HE)_2M_1C^*_1$, c) 300% stress.

limit was the highest concentration sample made from $(HE)_2M_1T_1$. Reports in the literature show somewhat mixed results regarding the elongation at break. Some reports show an increase in elongation at break with increasing clay concentration and dispersion [5], others show a decrease [12-14], while others show a maximum of ultimate tensile properties at a low clay concentration (some mention 1 wt% and others mention 3 wt% of clay) [6-9, 11, 13, 16, 17].

The evidence described above suggests that the organoclay containing one long alkyl tail leads to better dispersion of MMT platelets and greater matrix reinforcement than the organoclay that contains two long alkyl tails. It was also seen that the unsaturated organoclay produces a very similar structure to that obtained from the saturated organoclay, which suggests that hydrogenating the tallow tail has no significant effects on morphology and mechanical properties. This was also found for PA-6, where Fornes et al. proposed that polar polymers like polyamides, and apparently polyurethanes, have a relatively good affinity for the polar clay surface and that the single tail represents the best balance between reducing the platelet-platelet attraction and allowing the polymer to have access to the silicate surface; two alkyl tails limit the access of the polymer chains to the clay surface to a greater extent [1]. It was also suggested that the saturated and unsaturated organic treatments may give very similar morphologies and degrees of reinforcement because they provide almost the same access of the polymer matrix to the clay surface. Evidently, the TPU matrix interacts favorably with the silicate surface but not as well as PA-6, since the latter gives much higher platelet exfoliation. On the other hand, the results presented here also show that the organoclay with hydroxy ethyl functional groups leads to significantly higher clay dispersion and platelet exfoliation, producing a greater stiffness than the corresponding organoclay without these functional groups. This result deviates from what was seen for PA-6,

where organoclays having methyl functional groups produce a much higher reinforcement. Fornes et al. suggested that the hydroxy ethyl groups provide some degree of shielding of the clay surface, where the –OH moiety may be attracted to the polar clay surface [1]. Similar observations were reported for non-polar polymers, where organoclays that provide a higher shielding of the clay surface, i.e., $M_2(HT)_2$ and $(HE)_2M_1T_1$, gave better clay dispersion and matrix reinforcement [3]. Recently, Choi et al. showed that nanocomposites made from hydroxylated polyisoprene-*block*-polystyrene-*block*-polybutadiene (ISBOH) triblock copolymers had a higher degree of clay dispersion with $(HE)_2M_1T_1$ organoclay than those made from $M_2(HT)_2$-125. It was proposed that the presence of attractive interactions between the hydroxyl group of the ISBOH triblock copolymer and the hydroxyl group in the organoclay aided clay dispersion [22]. It seems like the hydroxy ethyl functional groups in the organoclay have the possibility to form hydrogen-bonds with either the surface of the clay or the polar groups in the polymer matrix. In the case of TPU nanocomposites, we propose that the high affinity of the polymer matrix to the hydroxy ethyl groups in the organoclay might make hydrogen bonding with the polymer matrix more favorable, aiding clay dispersion and exfoliation. Reports in the literature have shown in general, that organoclays containing hydroxy ethyl functional groups lead to higher silicate dispersion and delamination in polyurethanes [8, 10, 12, 13, 16, 17]. It was suggested that the hydroxy ethyl groups may match the polarity of the polyurethane matrix better than just having hydrocarbon chains, making dispersion more favorable [10].

Color formation

Fornes et al. and Yoon et al. [23, 24] have described color formation for PA-6 and polycarbonate (PC) nanocomposites made with different organoclays. They showed that

the level of color intensifies with clay content and that color formation depends on the nature of the organoclay used. Their study also indicates that organoclays with unsaturated surfactants lead to more color depth than organoclays with saturated structures, and that a deeper color was observed for the surfactant containing both hydroxy ethyl and unsaturated tallow. This is also true for these TPU nanocomposites. Figure 7.11 shows how the color of M-H TPU nanocomposites varies with organoclay structure. This figure shows that all the samples have high optical transparency, as observed by Chang et al [9], and that organoclays containing a hydrogenated tallow surfactant produce samples with a yellow tint, hydroxy ethyl functional groups produce a brown tone, while the unsaturated tallow surfactant generates a green hue. Fornes et al. and Yoon et al. mention that color formation is a product of clay-induced chemical reactions, such as matrix degradation and/or surfactant stability, and that a higher dispersion leads to a greater exposure of the clay surface and, hence, a greater opportunity for chemical reaction [23, 24]. PA-6 and PC nanocomposites only show shades of yellow and brown, while some TPU nanocomposites show shades of green as well. A clay purification experiment was done to determine if the greenish hue was produced by clay impurities. M_3T_1 organoclay was purified with methanol, and was later used to make TPU nanocomposites. The same green tint was observed in these samples, so we conclude that the green color formation is not due to clay impurities. Taking this into account, we suggest that the different colors may arise from specific chemical interactions between the specific organic treatment and the polymer material or additives therein.

Figure 7.11 Color formation of M-H TPU nanocomposites. (a) pure M-H TPU, (b) to (f) M-H TPU nanocomposites with ~5.5 wt% MMT: $M_3(HT)_1$, $M_2(HT)_2$, M_3T_1, $(HE)_2M_1T_1$, and $(HE)_2M_1C^*_1$ organoclays, respectively.

Structure and properties for the H-H TPU

Thermoplastic polyurethanes are composed of hard and soft segments, formed by aromatic isocyanates and long-chain diols. These segments segregate, like in semi-crystalline polymers, having a direct effect on the properties of the material. The long-chain diols are mainly polyether- or polyester-based, and the type of long-chain diol used also affects the properties of the final TPU. Reports in the literature suggest that the

structure of TPU materials, such as type of polyol and ratio of soft to hard segments, affects the mechanical properties and morphology of their nanocomposites [8, 12].

A series of nanocomposites were made from the high-hardness TPU described earlier and $(HE)_2M_1T_1$ and $M_3(HT)_1$ organoclays. The results are compared to the nanocomposites made from the medium-hardness TPU described in the previous section in an effort to explore the effect of different types of TPU materials on morphology and properties of nanocomposites. The high-hardness TPU is a polyether-based TPU with a Shore D Hardness of 73D, while the medium-hardness TPU is a polyester-based TPU with a Shore D hardness of 58D. The monomer precursors for the high-hardness TPU are MDI and polytetrahydrofuran, while the medium-hardness TPU is made from MDI, 1,4-butanediol, and ε-caprolactone. The differences in these TPU's were evidenced, in part, during the injection molding of these materials and its nanocomposites. The high-hardness materials required lower barrel temperatures, shorter injection times, longer cooling times, and a lower mold temperature for injection molding. For this TPU, no TEM images or mechanical testing are shown at high MMT concentrations since such samples could not be produced because the current injection molding machine could not achieve the low molding temperatures needed.

Morphology

WAXS patterns in Figure 7.12 show basal reflections for the H-H TPU nanocomposites, indicating the presence of tactoids. The d-spacing for the medium-hardness TPU, as mentioned before, increases from 1.77 to 3.05 nm and from 1.8 to 2.9 nm for hydroxy ethyl and one-tailed organoclays, respectively; while the H-H TPU nanocomposites show a low broad peak at 3.25 nm and an intense peak at 3.22 nm for $(HE)_2M_1T_1$ and $M_3(HT)_1$ organoclays, respectively.

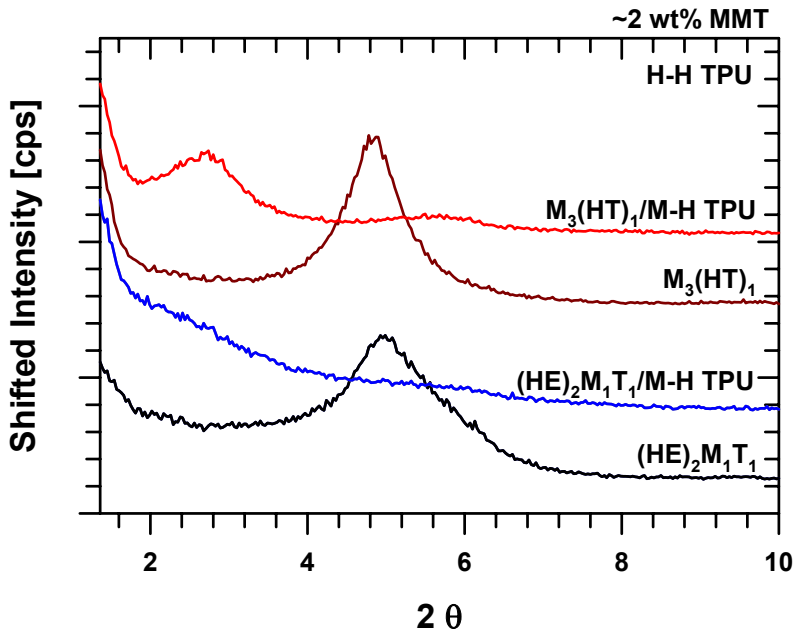

Figure 7.12 WAXS patterns of $M_3(HT)_1$ and $(HE)_2M_1T_1$ organoclays and its high-hardness TPU nanocomposites.

Figure 7.13 compares high magnification TEM images of these nanocomposites based on the two types of TPU. In both cases, the number of particles is higher for the samples made with hydroxy ethyl organoclay, where the particles are smaller in size and a larger number of single platelets exists. Even though the MMT concentration of the TEM micrograph for the M-H TPU/$M_3(HT)_1$ sample is lower than the MMT concentration of the other micrographs, particle analysis results shown previously show that the specific particle density of M-H TPU/$M_3(HT)_1$ nanocomposites at 1 wt% MMT is significantly lower than those made with $(HE)_2M_1T_1$, which is in accord with our observations.

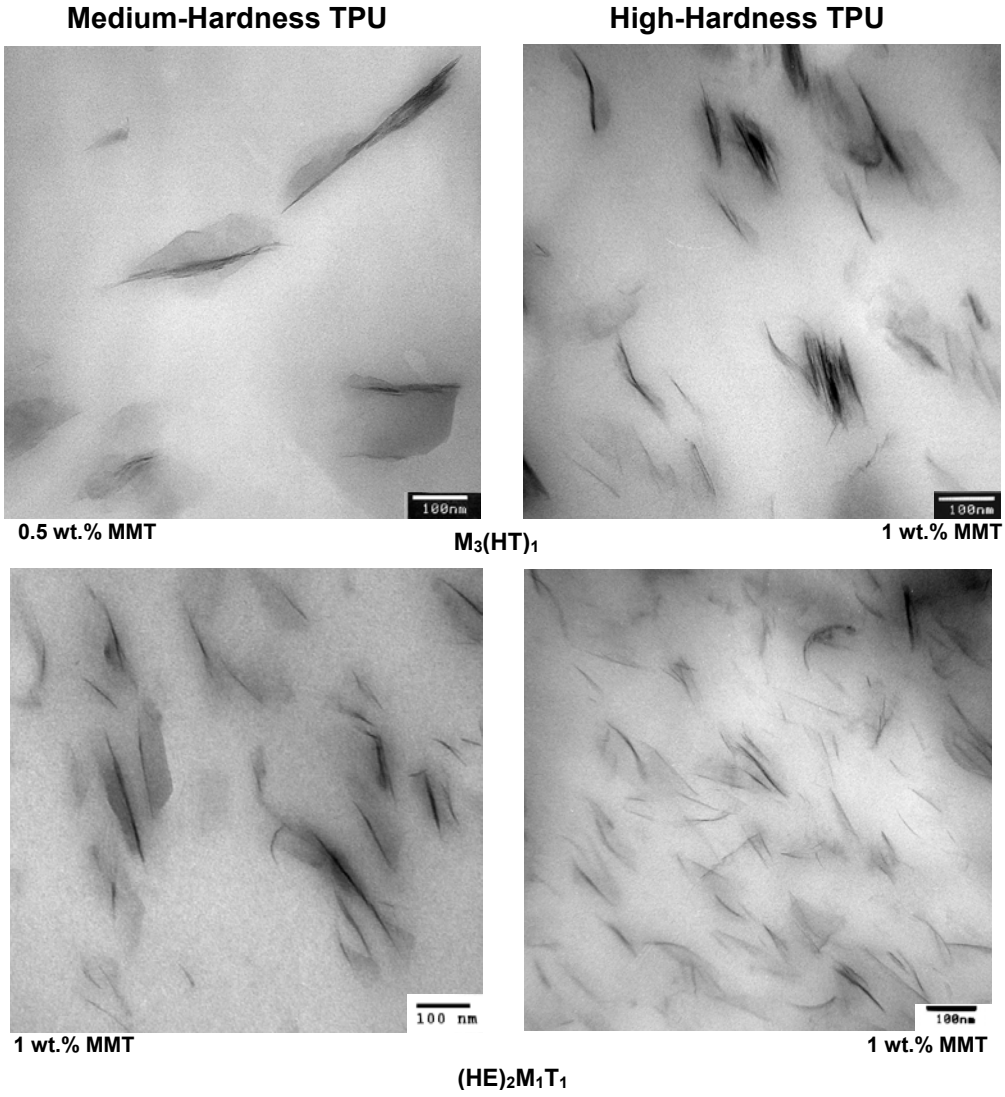

Figure 7.13 TEM micrographs of medium-hardness and high-hardness TPU nanocomposites containing $(HE)_2M_1T_1$ and $M_3(HT)_1$ organoclays.

Mechanical properties

The stress-strain behavior of the M-H and H-H TPU nanocomposites with $(HE)_2M_1T_1$ organoclay is compared in Fig. 7.14. The stress-strain diagrams of the pure

H-H TPU and its nanocomposites have a very different shape than those from M-H TPU; a yield point is observed for the H-H TPU materials, while no distinct yield point is observed for the M-H TPU nanocomposites. Regardless of clay concentration, the stress levels for the H-H TPU samples are much higher than that of the M-H TPU samples. H-H TPU samples, unlike the M-H TPU samples, show a yield point, after which a distinct drop in tensile stress is observed indicating the onset of necking. As the clay concentration increases the stress increases, similar to the behavior observed for the M-H TPU nanocomposites.

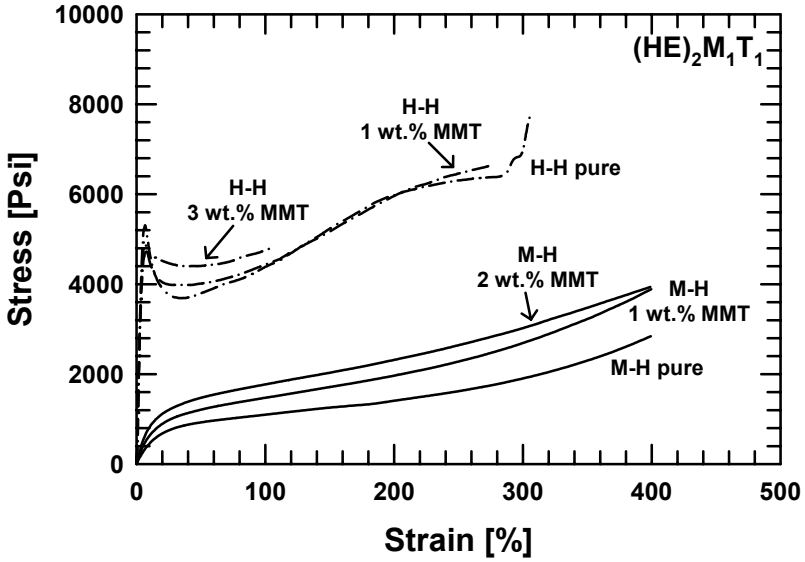

Figure 7.14 Stress-strain curves for medium-hardness and high-hardness TPU's and its nanocomposites containing $(HE)_2M_1T_1$ organoclay.

Figure 7.15 shows the Young's modulus of the nanocomposites made from H-H TPU at different MMT concentrations. The moduli of the H-H TPU matrix and its composites are much higher than the corresponding M-H TPU matrix and composites. Nevertheless, both TPU's have the same response to organoclay structure, i.e., better reinforcement is obtained with the hydroxy ethyl organoclay. The medium-hardness

TPU shows a large increase in modulus with increasing wt% MMT, while in the high hardness samples, $(HE)_2M_1T_1$ shows almost no enhancement until 1 wt% MMT and almost no enhancement at all for the one-tailed organoclay. This difference in modulus enhancement may be due in part to the considerably lower modulus of the M-H TPU matrix. As stated by Fornes et al. low-modulus matrices offer a higher potential for reinforcement than high-modulus matrices, for a given filler aspect ratio, as a result of the larger ratio of filler to matrix moduli. As this ratio increases, the nanocomposite modulus becomes more sensitive to the aspect ratio of the filler, so a larger increase in modulus may not suggest a higher degree of exfoliation or reinforcement [25]. This was also mentioned by Finnigan et al. for TPU nanocomposites [12].

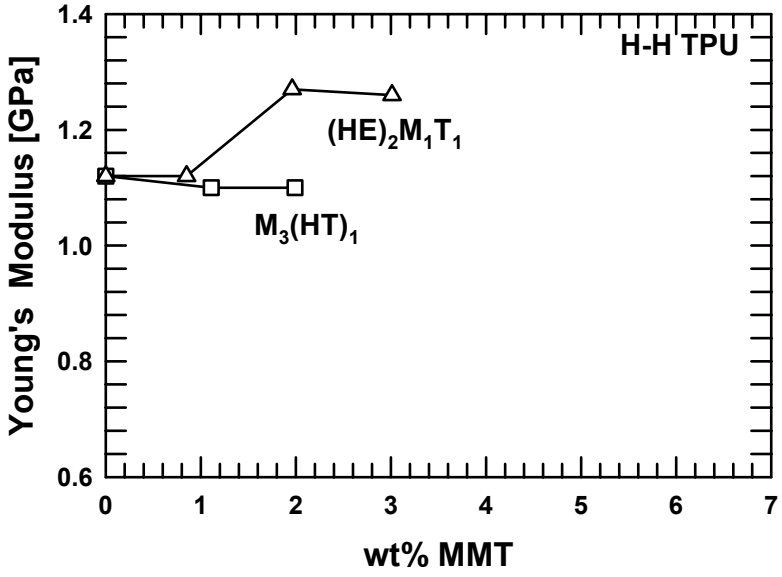

Figure 7.15 Young's modulus of high-hardness TPU nanocomposites containing $(HE)_2M_1T_1$ and $M_3(HT)_1$ organoclays.

The elongation at break also shows significant differences between the two types of TPU's. H-H TPU nanocomposite samples show noticeable necking, and the

elongation at break was lower than the 400% machine limit (Fig. 7.16). The elongation at break in the samples made with the H-H TPU matrix remains almost constant for the one-tailed organoclay while it decreases significantly with the hydroxy ethyl organoclay. This is consistent with the levels of reinforcement obtained with these two organoclays. Since the elongation at break of the M-H TPU could not be fully explored due to machine limitations, we cannot give any conclusions regarding the effect of the different types of TPU's on elongation at break. Tien et al. show an increase in Young's modulus and a decrease in elongation at break with increasing hard segment concentration [8]; the results here show an indication of similar behavior.

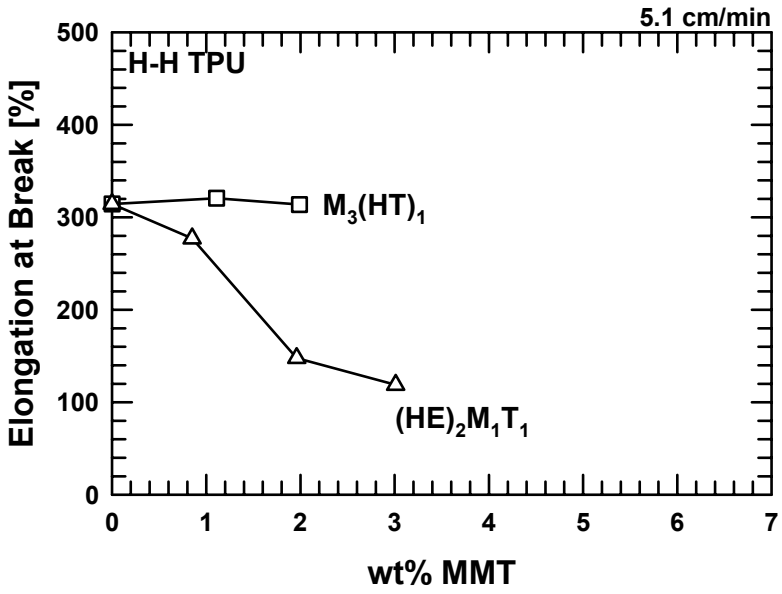

Figure 7.16 Elongation at break of high-hardness TPU nanocomposites containing $(HE)_2M_1T_1$ and $M_3(HT)_1$ organoclays.

Overall, both types of TPU's show the same trends with respect to organoclay structure, e.g., better clay dispersion and enhancement of mechanical properties is observed for the organoclay containing hydroxy ethyl functional groups as compared to

the organoclay with one-tailed hydrogenated tallow substituents. This supports the reasoning made in the previous section where it was proposed that the hydroxy ethyl functional groups lead to higher degrees of clay dispersion of TPU nanocomposites. Apparently, the soft to hard segment ratio and/or polyol structure have a noticeable effect in the morphology and mechanical properties of TPU nanocomposites. H-H TPU nanocomposites showed a slightly higher number of particles and clay dispersion, i.e., better exfoliation. However, adding clay to the M-H TPU causes a greater improvement in relative modulus, e.g., at a concentration of ~2 wt% MMT, the relative modulus for $(HE)_2M_1T_1$ nanocomposites made from the M-H TPU is 1.57, while it is 1.13 for the nanocomposites made from the H-H TPU. The primary reason for the greater relative modulus in the case of M-H TPU nanocomposites is due to the much lower absolute modulus of the M-H matrix, as predicted by composite theory [25].

Self consistent field theory calculations suggest that the polar hard segments are attracted to the silicate surface while the non-polar soft segments separate the individual platelets to regain entropy [26]. The structure of the TPU has an effect on the polarity of the polymer molecules, and different levels of polarity influence the affinity between the polymer and the organoclay. It is proposed here that these two materials interact differently with the organoclay, and the structure of the TPU may lead to differences in clay dispersion and relative mechanical property enhancement; however, at this point, it is not possible to be more definitive about the underlying causes for this difference.

CONCLUSION

Structure-property relationships for TPU nanocomposites prepared by melt processing from a series of alkyl ammonium/MMT organoclays and medium-hardness and high-hardness thermoplastic polyurethanes are presented here. The structure of the

organic modifier used to form the organoclay was systematically varied to determine the effect of specific functional groups on the degree of clay dispersion and matrix reinforcement for M-H TPU nanocomposites. Morphology analysis and mechanical property results show that overall, the $(HE)_2M_1T_1$ surfactant produces the best dispersion of organoclay particles and the highest matrix reinforcement, while the $M_2(HT)_2$ surfactant produces the lowest. More specifically, the results show that a) one long alkyl tail on the ammonium ion rather than two, b) hydroxy ethyl groups on the amine rather than methyl groups, and c) a longer alkyl tail as opposed to a shorter one lead to higher clay dispersion and stiffness enhancement for TPU nanocomposites. Most of these trends are similar to what was observed in PA-6 based nanocomposites, which suggests that polar polymers like polyamides, and apparently polyurethanes, have a relatively good affinity for the polar clay surface; and in the case of polyurethanes, the high affinity of the matrix for the hydroxy ethyl functional groups in the $(HE)_2M_1T_1$ organoclay aids clay dispersion and exfoliation. This suggests that an organic treatment that provides the best balance between reducing platelet-platelet attraction and increasing organoclay-polymer affinity will produce a higher degree of clay dispersion. A more limited study comparing a medium-hardness polyester-based TPU and a high-hardness polyether-based TPU shows that both types of TPU's exhibit similar trends with respect to organoclay structure, supporting the previous reasoning. Apparently the soft to hard segment ratio and/or polyol structure have a noticeable effect in the morphology and mechanical properties of TPU nanocomposites. H-H TPU nanocomposites showed a slightly higher number of particles and clay dispersion, i.e., better exfoliation. However, because of the much lower modulus of the M-H TPU, adding clay to this matrix causes a greater improvement in relative modulus. Finally, it should be noted that even though some organoclays lead to TPU nanocomposites with high degrees of clay dispersion and

platelet exfoliation, none exhibited degrees of exfoliation as high as those observed in PA-6 nanocomposites. Nevertheless, this study provides insights about the effect of the organoclay structure and polarity of the polymer matrix on morphology and mechanical properties of polymer-clay nanocomposites.

REFERENCES

[1] Fornes TD, Yoon PJ, Hunter DL, Keskkula H, Paul DR. Polymer 2002;43:5915-5933.

[2] Hotta S, Paul DR. Polymer 2004;45:7639-7654.

[3] Shah RK, Hunter DL, Paul DR. Polymer 2005;46:2646-2662.

[4] Lee HS, Fasulo PD, Rodgers WR, Paul DR. Polymer 2005;46:11673-11689.

[5] Wang Z, Pinnavaia TJ. Chem Mater 1998;10:3769-3771.

[6] Chen TK, Tien YI, Wei KH. Polymer 2000;41:1345-1353.

[7] Tien YI, Wei KH. Macromolecules 2001;34:9045-9052.

[8] Tien YI, Wei KH. Polymer 2001;42:3213-3221.

[9] Chang J-H, An YU. J Polym Sci, Part B: Polym Phys 2002;40:670-677.

[10] Osman MA, Mittal V, Morbidelli M, Suter UW. Macromolecules 2003;36:9851-9858.

[11] Choi WJ, Kim SH, Kim YJ, Kim SC. Polymer 2004;45:6045-6057.

[12] Finnigan B, Martin D, Halley P, Truss R, Campbell K. Polymer 2004;45:2249-2260.

[13] Finnigan B, Martin D, Halley P, Truss R, Campbell K. J Appl Polym Sci 2005;97:300-309.

[14] Xiong J, Liu Y, Yang X, Wang X. Polymer Degradation and Stability 2004;86:549-555.

[15] Pattanayak A, Jana SC. Polymer 2005;46:5183-5193.

[16] Pattanayak A, Jana SC. Polymer 2005;46:3394-3406.

[17] Pattanayak A, Jana SC. Polymer 2005;46:3275-3288.

[18] Song L, Hu Y, Li B, Wang S, Fan W, Chen Z. International Journal of Polymer Analysis and Characterization 2003;8:317-326.

[19] Cho JW, Paul DR. Polymer 2000;42:1083-1094.

[20] Fornes TD, Yoon PJ, Keskkula H, Paul DR. Polymer 2001;42:9929-9940.

[21] Vaia RA, Giannelis EP. Macromolecules 1997;30:7990-7999.

[22] Choi S, Lee KM, Han CD. Macromolecules 2004;37:7649-7662.

[23] Fornes TD, Yoon PJ, Paul DR. Polymer 2003;44:7545-7556.

[24] Yoon PJ, Hunter DL, Paul DR. Polymer 2003;44:5341-5354.

[25] Fornes TD, Paul DR. Polymer 2003;44:4993-5013.

[26] Balazs AC, Singh C, Zhulina E. Macromolecules 1998;31:8370-8381.

CHAPTER 8

CONCLUSIONS AND RECOMMENDATIONS

CONCLUSIONS

This dissertation addresses a number of fundamental issues involved in the formation of polymer-layered silicate nanocomposites by melt processing. More specifically, the effects of different polymer matrices, organoclay structures, and extruder processing conditions on the morphology and mechanical properties of polymer nanocomposites were explored with the purpose of obtaining a higher level of understanding of clay exfoliation during processing. Wide-angle X-ray scattering (WAXS) and transmission electron microscopy (TEM) were used to characterize the morphology of these nanocomposites, while tensile properties were used to assess the level of reinforcement achieved. A detailed particle analysis was performed in most cases to quantitatively characterize the morphology and correlate it with the mechanical property enhancements produced by the organoclay.

The comparison of two different polyamide matrices processed under comparable rheological conditions indicates a higher degree of exfoliation for the nanocomposites formed from nylon 6 (PA-6) than with nylon 66 (PA-66). The PA-6 nanocomposites showed superior mechanical properties compared to those made from PA-66; the latter showed a mixture of exfoliated and intercalated structures. It appears that the affinity of PA-6 for the organoclay is greater than that for PA-66, which must be related to some subtle aspect of the difference in the chemical structure. Even though PA-6 and PA-66 have the same ratio of methylene (CH_2) to amide (NCHO) units in their chains, the symmetry of their repeat units and the configuration of functional units at the chain ends

are different. PA-6 chains have no center of symmetry and their repeat unit is short, while PA-66 chains do have a center of symmetry and a longer repeat unit. In addition, PA-6 generally has one amine and one carboxylic acid group at the end of each chain; whereas, PA-66 contains a mixture of chains that have only amines, only acid groups, or combination of the two at their ends. These differences may vary the interactions between the polymer chains and the organoclay which may influence the affinity of the polymer for the organoclay.

The degree of exfoliation and clay dispersion in nanocomposites prepared by melt processing depends on both the affinity between the polymer and the organoclay and the details of the melt blending process. The amount of shear and the mixing conditions created by twin screw extruders have a significant effect on the morphology and properties of PA-6 nanocomposites: a) Melting the polymer before coming into contact with the organoclay followed by a low level of shear, and b) applying a medium level of shear throughout the extruder under a slightly longer residence time seem to produce the best platelet dispersion and matrix reinforcement for the cases studied here. In addition, applying high shear intensity on the solid polymer/organoclay mixture leads to extremely short particle lengths and lower matrix reinforcement; this is probably due to the attrition of clay platelets under high shear. Nanocomposites formed in a DSM micro-compounder under low shear and residence times of the order of 10 min had similar morphological and modulus trends as the ones obtained with conventional twin screw extruders. This shows that the DSM micro-compounder is a good alternative for nanocomposite research especially when only small amounts of material are available.

Under the best possible processing conditions, the affinity of the polymer with the polar clay surface and/or with the non-polar organic modifier is still very important for obtaining high clay platelet dispersion and mechanical property enhancement. The affinity between the polymer matrix and the organoclay is determined, to some extent, by the polarity of the polymer and the degree of silicate surface coverage given by the clay layer charge and the organoclay structure. Previous studies from our laboratories have shown that the best clay dispersion and mechanical property enhancement for PA-6 nanocomposites is obtained by a one-tailed organoclay that permits access of the polymer chains to the silicate surface, while the opposite is observed for nanocomposites made from polypropylene and various polyethylene copolymers, i.e., higher clay dispersion and mechanical property enhancement is observed using organic modifiers with more than one tail that provide large coverage of the polar clay surface [1-3]. An organoclay with reduced cation exchange capacity (CEC) may have a lower amount of organic modifier exchanged to its silicate surface and, hence, a lower degree of silicate surface coverage. Organoclays with different amounts of CEC reduction were prepared (in collaboration with CSIRO) to characterize the morphology and Young's modulus of PA-6 and polypropylene/polypropylene modified with maleic anhydride (PP/PP-g-MA) nanocomposites. The morphology and modulus results presented here show that reduced-CEC organoclays formed in this study lead to lower exfoliation and modulus enhancement for both PA-6 and PP/PP-g-MA nanocomposites, while no clear correlation could be found with respect to the amount of CEC reduction. This was attributed to differences in layer charge and charge distribution that could have been produced during the charge reduction process. On the other hand for organoclays with no CEC reduction,

a smaller amount of organic surfactant in the organoclay may increase its affinity with PA-6 while it may decrease its affinity with a non-polar matrix. More work is needed to truly explore this effect, since questions regarding the CEC reduction process and charge heterogeneity could not be fully addressed. In addition, the small amounts of charge-reduced clay produced from the current CEC-reduction process limited the extent of clay and nanocomposite characterization.

Structure-property relationships for thermoplastic polyurethane (TPU) nanocomposites prepared by melt processing from a series of alkyl ammonium/montmorillonite organoclays show that, overall, a surfactant containing one long alkyl tail and hydroxy ethyl substituents, i.e., $(HE)_2M_1T_1$, produces the best dispersion of organoclay particles and the highest matrix reinforcement while a surfactant with two long alkyl tails, i.e., $M_2(HT)_2$, produces the lowest. More specifically, the results show that a) one long alkyl tail on the ammonium ion rather than two, b) hydroxy ethyl groups on the amine rather than methyl groups, and c) a longer alkyl tail as opposed to a shorter one lead to higher clay dispersion and stiffness enhancement for TPU nanocomposites. Most of these trends are similar to what was observed in PA-6 based nanocomposites, which substantiates that polar polymers like polyamides, and apparently polyurethanes, have a relatively good affinity for the polar clay surface. In the case of polyurethanes, the high affinity of the matrix for the hydroxy ethyl functional groups in the $(HE)_2M_1T_1$ organoclay appears to aid clay dispersion and exfoliation. This suggests that an organic treatment that provides the best balance between reducing platelet-platelet attraction and increasing organoclay-polymer affinity will produce a higher degree of clay dispersion.

This work provides useful insights about the morphology and mechanical properties of various polymer nanocomposites, and on how a detailed particle analysis procedure helps quantify the morphology and relate it to the mechanical property enhancements. It shows that it is important to optimize the affinity between the polymer and the organoclay as well as the melt processing conditions to obtain high degrees of platelet delamination and dispersion and significant matrix reinforcement. Preliminary observations on the CEC reduction process have been described which give important insights for future work on this subject.

RECOMMENDATIONS FOR FUTURE WORK

Polyamide Type

The results shown in Chapter 4 where noticeable differences observed in the degree of platelet dispersion and mechanical property enhancement of nanocomposites made from PA-6 and PA-66 suggest that a difference in repeat unit structure and/or end group configuration may produce different degrees of exfoliation and mechanical property enhancements. Fornes et al. showed that changing the length of the aliphatic portion of the repeat structure also results in a change in the extent of exfoliation and matrix reinforcement; more specifically, increasing the number of methylene (CH_2) units from 6 to 12 carbon atoms results in less platelet delamination and lower reinforcement efficiency [4]. Proving whether the differences in end group configuration or in repeat unit structure have a more pronounced effect on the morphology and matrix reinforcement is an interesting project which may involve using polyamides that may only be available in small amounts, such as nylon 12,12 (PA-1212) for comparison with nylon 12 (PA-12), or more specific matrices such as polyamides having only amines or

only acid groups; the DSM micro-compounder may prove to be useful for these types of studies where only a small amount of material is available.

CEC reduction

As mentioned above and in Chapter 6, even though significant differences in morphology and modulus of PA-6 and PP/PP-g-MA nanocomposites was observed upon clay charge reduction, a clear relationship with the amount of CEC reduction could not observed. More work is needed to truly explore the effect of CEC reduction in polymer clay nanocomposites, so questions regarding the CEC reduction process can be fully addressed; more specifically, the ion exchange of Na^+ for Li^+ ions, the effects of temperature and duration of heating, and the heterogeneities in layer charge and charge distribution. Different methods described in the literature for CEC reduction through Li-fixation include mixing Li-MMT and Na-MMT in different proportions [5], completely exchanging Na-MMT with Li^+ [6], and exchanging specific proportions of Na^+ for Li^+ [7]; different temperatures and duration of heating are also reported [8, 9]. These methods of clay CEC reduction should be further explored to determine the most suitable method that produces higher and more specific charge reduction maintaining the swelling ability of the clay.

TEM imaging

Additional sample preparation techniques for TEM imaging may be interesting in order to expand our knowledge and characterization of polymer nanocomposites and of montmorillonite clay. Several sample preparation as well as TEM imaging techniques are available that provide three-dimensional structural information that can generate a

greater understanding of the complex microstructure of polymer-clay nanocomposites and its relationships with the properties of these materials. An example of the different techniques available is serial sectioning, which involves analyzing consecutive sections of a microtomed sample that provide a 3-dimensional representation of the object [10]. This process requires considerable experience and skill in the microtoming procedure as well as with TEM imaging. In addition, polymer nanocomposite samples are not always easily microtomed; however, this technique might be very useful in characterizing the spatial dimensions of clay particles and their actual position inside the polymer matrix [11]. Other techniques worth mentioning are ion milling and polishing techniques used primarily in metallographic materials, where TEM images of subsequent layers are obtained by milling microscopic layers of material one at a time. Another interesting technique that may be worth exploring is stereomicroscopy imaging; this technique also provides three-dimensional information on the structure of clay particles. It is based on the changes in elevation along the z-axis of the microtomed sections. A three-dimensional visualization is obtained from a stereo-pair of the same field of view, i.e., from two different TEM images of the same area, obtained by tilting the TEM sample-holder stage 4 to 10 degrees between each image [11, 12]. Electron holography also seems to be a promising imaging technique that enhances image resolution and contrast, providing three-dimensional imaging and analysis of specific nanometer-sized areas [13].

Dissolving the polymer from the sections arranged in a TEM grid by exposure to vapors of acid solvents and imaging the remaining clay particles may also provide new and attractive information on the characteristics of exfoliated and delaminated clay; techniques such as breaking the copper grid with the electron beam and imaging its lateral view may also offer details on the thickness of these particles [11].

Imaging of injection molded nanocomposite samples after being elongated or fractured during tensile tests may also provide morphological information on interfacial bonding and fracture properties.

Particle analysis

Finally, an accurate characterization of the morphology of polymer-clay nanocomposites through particle analysis is very important for obtaining proper quantitative results that can be employed in correlating morphology with mechanical property enhancements as well as in composite theory modeling. For this reason, the particle analysis procedure used for this dissertation should be optimized to become faster and more accurate and reliable. Some issues like operator and experimental error should be minimized and quantified by establishing general guidelines to follow while performing the analysis and by performing methodical experiments comparing the results obtained by different operators on the same TEM micrograph and/or by the same operator on different TEM micrographs. The time needed for such analyses should also be optimized in order to make this procedure more accessible; the minimum number of particles that need to be examined to obtain representative results that can be analyzed statistically should be determined at both high and low concentrations. Efforts should also be made to ensure representative sampling to attain meaningful results. As mentioned before, due to the nanometer-length scales of the clay particles, TEM imaging has to be performed at high magnifications, where the morphology observed may not be representative of the nanocomposite sample [14, 15].

Other techniques should also be explored and compared to the current particle analysis procedure, such as different stereological techniques and automated particle analysis programs. Stereology is the analysis of three-dimensional objects through the

interpretation two-dimensional images. It provides means for analyzing the microstructure quantitatively in a thorough and reliable way that minimizes error and generates results that can be analyzed statistically [16]. A small amount of research was done in this field, such as volume fraction determination by point and line-intercept counting techniques (ASTM E 562-02) with a number of TEM micrographs presented in this study. However, no noteworthy results were obtained due to uncertainties regarding image magnification, size of grids, etc. In spite of this, stereological methods should be investigated more thoroughly due to their great potential [14, 15, 17, 18]. Automated particle analysis has always been an appealing approach since it provides a fast, accurate, and reliable analysis of the morphology of materials; however the programs usually require a binary image, where the particles are seen in black over a white background. This is usually very difficult to obtain due to the low contrast of TEM images. However, new advances in TEM digital imaging and in particle analysis programs may be useful for constructing an automated procedure. Techniques such as the ones mentioned above should help address issues related to particle thickness estimations, as well as particle orientation and separation between clay particles [12, 18].

REFERENCES

[1] Fornes TD, Yoon PJ, Hunter DL, Keskkula H, Paul DR. Polymer 2002;43(22):5915-5933.

[2] Lee HS, Fasulo PD, Rodgers WR, Paul DR. Polymer 2005;46(25):11673-11689.

[3] Shah RK, Hunter DL, Paul DR. Polymer 2005;46(8):2646-2662.

[4] Fornes TD. Ph.D. Thesis, The University of Texas at Austin, 2003.

[5] Brindley GW, Ertem G. Clays and Clay Minerals 1971;19(399-404.

[6] Delozier DM, Orwoll RA, Cahoon JF, Ladislaw JS, J.G. SJ, Connell JW. Polymer 2003;44(8):2231-2241.

[7] Maes A, Stul MS, Cremers A. Clays and Clay Minerals 1979;27(5):387-392.

[8] Bujdak J, Slosiarikova H, Cicel B. Journal of Inclusion Phenomena and Molecular Recognition in Chemistry 1992;13:321-327.

[9] Hrobarikova J, Madejova J, Komadel P. Journal of Materials Chemistry 2001;11:1452-1457.

[10] Flegler SL, Heckman JW, Klomparens KL, *Scanning and Transmission Electron Microscopy: an Introduction*. Oxford University Press Inc., New York, 1993, pp. 220.

[11] Personal communication with Mendenhall J.

[12] Russ JC, *The Image Processing Handbook*. CRC Press LLC, Boca Raton, Fla., Third, 1999, pp. 771.

[13] Lichte H, Lehmann M, EUREM 12, Brno, Czech Republic, July 9-14, 2000.

[14] Brandon DD, Kaplan WD, Quantitative Analysis of Microstructure. in *Microstructural Characterization of Materials*. John Wiley and Sons, Inc., Chinchester, England, 1999 pp. 345-397.

[15] Kurzydlowski KJ, Ralph B, *The Quantitative Description of the Microstructure of Materials*. Ralph B, Ed., CRC Series in Materials Science and Technology. CRC Press, Inc., Boca Raton, Fla., 1995, pp. 418.

[16] Sundberg MD, Conference of the Association for Biology Laboratory Education (ABLE), Toronto, Ca., 1992.

[17] Quantitative Microscopy, 1968. McGraw-Hill Book Company.

[18] Russ JC, DeHoff RT, *Practical Stereology*. Plenum Publishers, New York, 2000, pp. 381.

Bibliography

ASTM E 562. Standard Test Method for Determining Volume Fraction by Systematic Manual Point Count.

Alexandre, M.; Dubois, P., Polymer-layered silicate nanocomposites: preparation, properties and uses of a new class of materials. *Materials Science & Engineering, R: Reports* **2000,** R28, 1-63.

Bailey, S. W., *Crystal Structures of Clay Minerals and their X-ray Identification*. ed.; Spottiswoode Ballantyne Ltd.: London, 1980; Monograph No. 5, p 945.

Balazs, A. C.; Singh, C.; Zhulina, E., Modeling the Interactions between Polymers and Clay Surfaces through Self-Consistent Field Theory. *Macromolecules* **1998,** 31, 8370-8381.

Brandon, D. D.; Kaplan, W. D., Quantitative Analysis of Microstructure. In *Microstructural Characterization of Materials*, First Edition ed.; John Wiley and Sons, Inc.: Chinchester, England, 1999; 345-397.

Brindley, G. W.; Ertem, G., Preparation and Solvation Properties of Some Variable Charge Montmorillonites. *Clays and Clay Minerals* **1971,** 19, 399-404.

Bujdak, J.; Slosiarikova, H.; Cicel, B., Interaction of long chain alkylammonium cations with reduced charge montmorillonite. *Journal of Inclusion Phenomena and Molecular Recognition in Chemistry* **1992,** 13, 321-327.

Calvet, R.; Prost, R., Cation Migration into Empty Octahedral Sites and Surface Properties of Clays. *Clays and Clay Minerals* **1971,** 19, 175-186.

Carrado, K. A., Polymer-Clay Nanocomposites. In *Advanced Polymeric Materials: Structure Property Relationships*, ed.; Shonaike, G. O.; Advani, S. G., CRC Press LLC: Boca Raton, FL, 2003; 349-396.

Chang, J.-H.; An, Y. U., Nanocomposites of polyurethane with various organoclays: thermomechanical properties, morphology, and gas permeability. *Journal of Polymer Science, Part B: Polymer Physics* **2002,** 40, 670-677.

Chavarria, F.; Paul, D. R., Comparison of nanocomposites based on nylon 6 and nylon 66. *Polymer* **2004,** 45, 8501-8515.

Chavarria, F.; Paul, D. R., Thermoplastic polyurethane nanocomposites: Effect of organoclay structure on morphology and properties. *Polymer* **2006,** Article in press.

Chavarria, F.; Shah, R. K.; Paul, D. R., Effect of processing on the exfoliation of nylon 6 nanocomposites. *Article in preparation*.

Chavarria, F.; Paul, D. R., Reduced-cation exchange capacity organoclays: Effect on morphology and properties of polymer-layered silicate nanocomposites. *Article in preparation*.

Chen, W.; Xu, Q.; Yuan, R. Z., Effect on ionic conductivity with modification of polymethyl methacrylate in poly(ethylene oxide)-layered silicate nanocomposites (PLSN). *Materials Science & Engineering, B: Solid-State Materials for Advanced Technology* **2000,** B77, 15-18.

Chen, T. K.; Tien, Y. I.; Wei, K. H., Synthesis and characterization of novel segmented polyurethane/clay nanocomposites. *Polymer* **2000,** 41, 1345-1353.

Chen, W.; Xu, Q.; Yuan, R. Z., The influence of polymer state on the electrical properties of polymer/layered-silicate nanocomposites. *Composites Science and Technology* **2001,** 61, 935-939.

Cho, J. W.; Paul, D. R., Nylon 6 nanocomposites by melt compounding. *Polymer* **2000,** 42, 1083-1094.

Choi, S.; Lee, K. M.; Han, C. D., Effects of Triblock Copolymer Architecture and the Degree of Functionalization on the Organoclay Dispersion and Rheology of Nanocomposites. *Macromolecules* **2004,** 37, 7649-7662.

Choi, W. J.; Kim, S. H.; Kim, Y. J.; Kim, S. C., Synthesis of chain-extended organifier and properties of polyurethane/clay nanocomposites. *Polymer* **2004,** 45, 6045-6057.

Clarke, S. M.; Rennie, A. R.; Convert, P., A diffraction technique to investigate the orientational alignment of anisotropic particles: studies of clay under flow. *Europhysics Letters* **1996,** 35, 233-238.

Clemenz, D. M.; Mortland, M. M., Properties of reduced charge montmorillonite: tetra-alkylammonium ion exchange forms. *Clays and Clay Minerals* **1974,** 22, 223-229.

Collister, J., Commercialization of Polymer Nanocomposites. In *Polymer Nanocomposites: Synthesis, Characterization, and Modeling*, ed.; Krishnamoorti, R.; Vaia, R. A., Oxford University Press: Washington, D.C., 2001; 804, 7-14.

Courtney, T. H., *Mechanical Behavior of Materials*. Second ed.; Mc Graw Hill: 2000; p 733.

Delozier, D. M.; Orwoll, R. A.; Cahoon, J. F.; Ladislaw, J. S.; J.G., S. J.; Connell, J. W., Polyimide nanocomposites prepared from high-temperature, reduced charge organoclays. *Polymer* **2003,** 44, 2231-2241.

Dennis, H. R.; Hunter, D. L.; Chang, D.; Kim, S.; White, J. L.; Cho, J. W.; Paul, D. R., Effect of melt processing conditions on the extent of exfoliation in organoclay-based nanocomposites. *Polymer* **2001,** 42, 9513-9522.

Finnigan, B.; Martin, D.; Halley, P.; Truss, R.; Campbell, K., Morphology and properties of thermoplastic polyurethane nanocomposites incorporating hydrophilic layered silicates. *Polymer* **2004,** 45, 2249-2260.

Finnigan, B.; Martin, D.; Halley, P.; Truss, R.; Campbell, K., Morphology and properties of thermoplastic polyurethane composites incorporating hydrophobic layered silicates. *Journal of Applied Polymer Science* **2005,** 97, 300-309.

Flegler, S. L.; Heckman, J. W.; Klomparens, K. L., *Scanning and Transmission Electron Microscopy: an Introduction*. ed.; Oxford University Press Inc.: New York, 1993; p 220.

Fornes, T. D.; Yoon, P. J.; Keskkula, H.; Paul, D. R., Nylon 6 nanocomposites: the effect of matrix molecular weight. *Polymer* **2001,** 42, 9929-9940.

Fornes, T. D.; Yoon, P. J.; Hunter, D. L.; Keskkula, H.; Paul, D. R., Effect of organoclay structure on nylon 6 nanocomposite morphology and properties. *Polymer* **2002,** 43, 5915-5933.

Fornes, T. D.; Paul, D. R., Crystallization behavior of nylon 6 nanocomposites. *Polymer* **2003,** 44, 3945-3961.

Fornes, T. D.; Paul, D. R., Formation and properties of nylon 6 nanocomposites. *Polymer* **2003,** 13, 212-217.

Fornes, T. D.; Paul, D. R., Modeling properties of nylon 6/clay nanocomposites using composite theories. *Polymer* **2003,** 44, 4993-5013.

Fornes, T. D. Ph.D. Thesis. The University of Texas at Austin, 2003.

Fornes, T. D.; Hunter, D. L.; Paul, D. R., Effect of sodium montmorillonite source on nylon 6/clay nanocomposites. *Polymer* **2004,** 45, 2321-2331.

Fornes, T. D.; Hunter, D. L.; Paul, D. R., Nylon-6 nanocomposites from alkylammonium-modified clay: the role of alkyl tails on exfoliation. *Macromolecules* **2004,** 37, 1793-1798.

Fornes, T. D.; Paul, D. R., Structure and properties of nanocomposites based on nylon-11 and -12 compared with those based on nylon-6. *Macromolecules* **2004,** 37, 7698-7709.

Garces, J. M.; Moll, D. J.; Bicerano, J.; Fibiger, R.; McLeod, D. G., Polymeric nanocomposites for automotive applications. *Advanced Materials (Weinheim, Germany)* **2000,** 12, 1835-1839.

Goettler, L., A.; Powell, C., E., Polymer Nanocomposite Composition. *US Patent No. WO 99/41299* **1999**.

Goettler, L., A.; Joardar, S., S.; Middleton, J., C., Methods for the preparation of polyamide nanocomposite compositions by in situ and solid state polymerizations. *US Patent No. WO 00/09571* **2000**.

Greene-Kelly, R., Identification of Montmorillonoids in Clays. *Journal of Soil Science* **1953,** 4, 233-237.

Han, B.; Ji, G.; Wu, S.; Shen, J., Preparation and characterization of nylon 66/montmorillonite nanocomposites with co-treated montmorillonites. *European Polymer Journal* **2003,** 39, 1641-1646.

Hine, P. J.; Rudolf Lusti, H.; Gusev, A. A., Numerical simulation of the effects of volume fraction, aspect ratio and fibre length distribution on the elastic and thermoelastic properties of short fibre composites. *Composites Science and Technology* **2002,** 62, 1445-1453.

Hoffman, U.; Klemen, R., Verlust der Austauschfahigkeit von Lithiumionen an Bentonit durch Erhitzung. *Zeitschrift fur anorganische und allegemeine Chemie* **1950,** 262, 95-99.

Hotta, S.; Paul, D. R., Nanocomposites formed from linear low density polyethylene and organoclays. *Polymer* **2004,** 45, 7639-7654.

Hrobarikova, J.; Madejova, J.; Komadel, P., Effect of heating temperature on Li-fixation, layer charge and properties of fine fractions of bentonites. *Journal of Materials Chemistry* **2001,** 11, 1452-1457.

Hu, Y.; Wang, S.; Ling, Z.; Zhuang, Y.; Chen, Z.; Fan, W., Preparation and Combustion Properties of Flame Retardant Nylon6/Montmorillonite Nanocomposite. *Macromolecular Materials and Engineering* **2003,** 288, 272-276.

Hylton, D. C., *Understanding Plastics Testing*. First Ed. ed.; Hanser Gardener Publications Inc.: Cincinnati, OH, 2004; p 93.

Inoue, M., Studies on the Crystallization of High Polymers by Differential Thermal Analysis. *Journal of Polymer Science, Part A: Polymer Chemistry* **1963,** 1, 2697-2709.

Kim, D. H.; Fasulo, P. D.; Rodgers, W. R.; Paul, D. R., Structure and properties of PP based nanocomposites. *Article in preparation*.

Kojima, Y.; Fukimori, K.; Usuki, A.; Okada, A.; Kurauchi, T., Gas permeabilities in rubber-clay hybrid. *Journal of Materials Science Letters* **1993,** 12, 889-890.

Kojima, Y.; Usuki, A.; Kawasumi, M.; Okada, A.; Fukushima, Y.; Kurauchi, T.; Kamigaito, O., Mechanical properties of nylon 6-clay hybrid. *Journal of Materials Research* **1993,** 8, 1185-9.

Kojima, Y.; Usuki, A.; Kawasumi, M.; Okada, A.; Kurauchi, T.; Kamigaito, O., Sorption of water in nylon 6-clay hybrid. *Journal of Applied Polymer Science* **1993,** 49, 1259-64.

Kojima, Y.; Usuki, A.; Kawasumi, M.; Okada, A.; Kurauchi, T.; Kamigaito, O., Synthesis of nylon 6-clay hybrid by montmorillonite intercalated with e-caprolactam. *Journal of Polymer Science, Part A: Polymer Chemistry* **1993,** 31, 983-6.

Komadel, P.; Hrobarikova, J.; Smrcok, L.; Koppelhuber-Bitschnau, B., Hydration of reduced-charge montmorillonite. *Clay Minerals* **2002,** 37, 543-550.

Komadel, P.; Madejova, J.; Bujdak, J., Preparation and Properties of Reduced-Charge Smectites: a Review. *Clays and Clay Minerals* **2005,** 53, 313-334.

Kurzydlowski, K. J.; Ralph, B., *The Quantitative Description of the Microstructure of Materials*. ed.; CRC Press, Inc.: Boca Raton, Fla., 1995; p 418.

Lagaly, G., The "Layer Charge" of Regular Interstratified 2:1Clay Minerals. *Clays and Clay Minerals* **1979,** 27, 1-10.

Lee, K. Y.; Paul, D. R., A model for composites containing three-dimensional ellipsoidal inclusions. *Polymer* **2005,** 46, 9064-9080.

Lee, H. S.; Fasulo, P. D.; Rodgers, W. R.; Paul, D. R., TPO based nanocomposites. Part 1. Morphology and mechanical properties. *Polymer* **2005,** 46, 11673-11689.

Lee, H. S.; Fasulo, P. D.; Rodgers, W. R.; Paul, D. R., TPO based nanocomposites. Part 2. Thermal expansion behavior. *Polymer* **2006,** 47, 3528-3539.

Lichte, H.; Lehmann, M. In *Off-axis Electron Holography - The Way to Use*, EUREM 12, Brno, Czech Republic, July 9-14, 2000; Brno, Czech Republic, 2000.

Liu, L.; Qi, Z.; Zhu, X., Studies on nylon 6/clay nanocomposites by melt-intercalation process. *Journal of Applied Polymer Science* **1999,** 71, 1133-1138.

Liu, X.; Wu, Q.; Zhang, Q.; Mo, Z., Phase transition in polyamide-66/montmorillonite nanocomposites on annealing. *Journal of Polymer Science, Part B: Polymer Physics* **2002,** 41, 63-67.

Liu, X.; Wu, Q., Polyamide 66/Clay Nanocomposites via Melt Intercalation. *Macromolecular Materials and Engineering* **2002,** 287, 180-186.

Liu, X., Polymorphism in polyamide 66/clay nanocomposites. *Polymer* **2002,** 43, 4967-4972.

Liu, X.; Wu, Q.; Berglund, L., Polymorphism in polyamide 66/clay nanocomposites. *Polymer* **2002,** 43, 4967-4972.

Lu, Y.; Zhang, G.; Feng, M.; Zhang, Y.; Yang, M.; Shen, D., Hydrogen bonding in polyamide 66/clay nanocomposite. *Journal of Polymer Science, Part B: Polymer Physics* **2003,** 41, 2313-2321.

Maes, A.; Stul, M. S.; Cremers, A., Layer charge-cation-exchange capacity relationship in montmorillonite. *Clays and Clay Minerals* **1979,** 27, 387-392.

Meier, L. P.; Nuesch, R., The Lower Cation Exchange Capacity Limit of Montmorillonite. *Journal of Colloid and Interface Science* **1999,** 217, 77-85.

Mendenhall, J., *Personal communication*.

Messersmith, P. B.; Giannelis, E. P., Synthesis and barrier properties of poly(e-caprolactone)-layered silicate nanocomposites. *Journal of Polymer Science, Part A: Polymer Chemistry* **1995,** 33, 1047-57.

Nair, S. V.; Goettler, L. A.; Lysek, B. A., Toughness of nanoscale and multiscale polyamide-6,6 composites. *Polymer Engineering and Science* **2002,** 42, 1872-1882.

Nielsen, L. E.; Landel, R. F., *Mechanical Properties of Polymers and Composites*. Second Ed. ed.; Marcel Dekker, Inc.: New York, NY, 1994; p 557.

Okada, A.; Usuki, A., The chemistry of polymer-clay hybrids. *Journal of Materials Research* **1995,** C3, 109-115.

Oshinski, A. J.; Keskkula, H.; Paul, D. R., Rubber toughening of polyamides with functionalized block copolymers: 1. Nylon 6. *Polymer* **1992,** 33, 268-83.

Oshinski, A. J.; Keskkula, H.; Paul, D. R., Rubber toughening of polyamides with functionalized block copolymers: 2. Nylon-6,6. *Polymer* **1992,** 33, 284-93.

Osman, M. A.; Mittal, V.; Morbidelli, M.; Suter, U. W., Polyurethane Adhesive Nanocomposites as Gas Permeation Barrier. *Macromolecules* **2003,** 36, 9851-9858.

Pattanayak, A.; Jana, S. C., Properties of bulk-polymerized thermoplastic polyurethane nanocomposites. *Polymer* **2005,** 46, 3394-3406.

Pattanayak, A.; Jana, S. C., Synthesis of thermoplastic polyurethane nanocomposites of reactive nanoclay by bulk polymerization methods. *Polymer* **2005,** 46, 3275-3288.

Pattanayak, A.; Jana, S. C., Thermoplastic polyurethane nanocomposites of reactive silicate clays: effects of soft segments on properties. *Polymer* **2005,** 46, 5183-5193.

Paul, D. R.; Zeng, Q. H.; Yu, A. B.; Lu, G. Q., The interlayer swelling and molecular packing in organoclays. *Journal of Colloid and Interface Science* **2005,** 292, 462-468.

Qin, H.; Su, Q.; Zhang, S.; Zhao, B.; Yang, M., Thermal stability and flammability of polyamide 66/montmorillonite nanocomposites. *Polymer* **2003,** 44, 7533-7538.

Russ, J. C., *The Image Processing Handbook*. Third ed.; CRC Press LLC: Boca Raton, Fla., 1999; p 771.

Russ, J. C.; DeHoff, R. T., *Practical Stereology*. ed.; Plenum Publishers: New York, 2000; p 381.

Russ, C.; Russ, J. C. *IPTK: Image processing Toolkit*, 5.0; Reindeer Graphics Inc.: 2003.

Schmidt, D.; Shah, D.; Giannelis, E. P., New advances in polymer/layered silicate nanocomposites. *Current Opinion in Solid State & Materials Science* **2002,** 6, 205-212.

Shah, R. K.; Paul, D. R., Nylon 6 nanocomposites prepared by a melt mixing masterbatch process. *Polymer* **2004,** 45, 2991-3000.

Shah, R. K.; Hunter, D. L.; Paul, D. R., Nanocomposites from poly(ethylene-co-methacrylic acid) ionomers: effect of surfactant structure on morphology and properties. *Polymer* **2005,** 46, 2646-2662.

Shah, R. K.; Krishnaswamy, R. K.; Takahashi, S.; Paul, D. R., Blown films of nanocomposites prepared from low density polyethylene and a sodium ionomer of poly(ethylene-co-methacrylic acid). *Polymer* **2006,** 47, 6187-6201.

Shah, R. K.; Paul, D. R., Organoclay degradation in melt processed polyethylene nanocomposites. *Polymer* **2006,** 47, 4075-4084.

Shon, K.; Chang, D.; White, J. L., A Comparative Study of Residence Time Distributions in a Kneader, Continuous Mixer, and Modular Intermeshing Co-Rotating and Counter-Rotating Twin Screw Extruders. *International Polymer Processing XIV* **1999,** 1, 44-50.

Song, L.; Hu, Y.; Li, B.; Wang, S.; Fan, W.; Chen, Z., A Study on the Synthesis and Properties of Polyurethane/Clay Nanocomposites. *International Journal of Polymer Analysis and Characterization* **2003,** 8, 317-326.

Stretz, H. A. Ph.D. Thesis. The University of Texas at Austin, 2005.

Stul, M. S.; Mortier, W. J., The Heterogeneity of the Charge Density in Montmorillonites. *Clays and Clay Minerals* **1974,** 22, 391-396.

Sundberg, M. D. In *An introduction to stereological analysis: morphometric techniques for beginning biologists*, Conference of the Association for Biology Laboratory Education (ABLE), Toronto, Ca., 1992; Goldman, C. A.; Andrews, S. E.; Hauta, P. L.; Ketchum, R., Toronto, Ca., 1992; 51-72.

Takeda, Y.; Keskkula, H.; Paul, D. R., Effect of polyamide functionality on the morphology and toughness of blends with a functionalized block copolymer. *Polymer* **1992,** 33, 3173-81.

Tanaka, G.; Goettler, L. A., Predicting the binding energy for nylon 6,6/clay nanocomposites by molecular modeling. *Polymer* **2001,** 43, 541-553.

Tien, Y. I.; Wei, K. H., High-Tensile-Property Layered Silicates/Polyurethane Nanocomposites by Using Reactive Silicates as Pseudo Chain Extenders. *Macromolecules* **2001,** 34, 9045-9052.

Tien, Y. I.; Wei, K. H., Hydrogen bonding and mechanical properties in segmented montmorillonite/polyurethane nanocomposites of different hard segment ratios. *Polymer* **2001,** 42, 3213-3221.

Usuki, A.; Kojima, Y.; Kawasumi, M.; Okada, A.; Fukushima, Y.; Kurauchi, T.; Kamigaito, O., Synthesis of nylon 6-clay hybrid. *Journal of Materials Research* **1993,** 8, 1179-84.

Usuki, A.; Koiwai, A.; Kojima, Y.; Kawasumi, M.; Okada, A.; Kurauchi, T.; Kamigaito, O., Interaction of nylon 6-clay surface and mechanical properties of nylon 6-clay hybrid. *Journal of Applied Polymer Science* **1995,** 55, 119-23.

Vaia, R. A.; Giannelis, E. P., Lattice Model of Polymer Melt Intercalation in Organically-Modified Layered Silicates. *Macromolecules* **1997,** 30, 7990-7999.

Vaia, R. A.; Giannelis, E. P., Polymer Melt Intercalation in Organically-Modified Layered Silicates: Model Predictions and Experiment. *Macromolecules* **1997,** 30, 8000-8009.

Vaia, R. A.; Krishnamoorti, R., *Polymer Nanocomposites: Synthesis, Characterization, and Modeling*. ed.; Oxford University Press: Washington, D.C., 2001; 804, p.

Van Olphen, H., Clay Mineralogy. In *An introduction to clay colloid chemistry: for clay technologists, geologists, and soil scientists*, 2nd ed. ed.; Wiley: New York, 1977; Chapter 5.

Wang, Z.; Pinnavaia, T. J., Nanolayer Reinforcement of Elastomeric Polyurethane. *Chemistry of Materials* **1998,** 10, 3769-3771.

Wu, T.-M.; Wu, J.-Y., Structural analysis of polyamide/clay nanocomposites. *Journal of Macromolecular Science, Physics* **2002,** B41, 17-31.

Xie, W.; Gao, Z.; Pan, W.-P.; Hunter, D. L.; Singh, A.; Vaia, R. A., Thermal Degradation Chemistry of Alkyl Quaternary Ammonium Montmorillonite. *Chemistry of Materials* **2001,** 13, 2979-2990.

Xiong, J.; Liu, Y.; Yang, X.; Wang, X., Thermal and mechanical properties of polyurethane/montmorillonite nanocomposites based on a novel reactive modifier. *Polymer Degradation and Stability* **2004,** 86, 549-555.

Yalcin, B.; Valladares, D.; Cakmak, M., Amplification effect of platelet type nanoparticles on the orientation behavior of injection molded nylon 6 composites. *Polymer* **2003,** 44, 6913-6925.

Yalcin, B.; Cakmak, M., Superstructural hierarchy developed in coupled high shear/high thermal gradient conditions of injection molding in nylon 6 nanocomposites. *Polymer* **2004,** 45, 2691-2710.

Yamamoto, S.; Matsuoka, T., Dynamic simulation of a platelike particle dispersed system. *J. Chem. Phys.* **1997,** 107, 3300-3308.

Yano, K.; Usuki, A.; Okada, A.; Kurauchi, T.; Kamigaito, O., Synthesis and properties of polyimide-clay hybrid. *Journal of Polymer Science, Part A: Polymer Chemistry* **1993,** 31, 2493-8.

Yoon, P. J.; Fornes, T. D.; Paul, D. R., Thermal expansion behavior of nylon 6 nanocomposites. *Polymer* **2002,** 43, 6727-6741.

Yoon, P. J.; Hunter, D. L.; Paul, D. R., Polycarbonate nanocomposites. Part 1. Effect of organoclay structure on morphology and properties. *Polymer* **2003,** 44, 5323-5339.

Yoon, P. J.; Hunter, D. L.; Paul, D. R., Polycarbonate nanocomposites: Part 2. Degradation and color formation. *Polymer* **2003,** 44, 5341-5354.

Yu, Z.-Z.; Yang, M.; Zhang, Q.; Zhao, C.; Mai, Y.-W., Dispersion and Distribution of Organically Modified Montmorillonite in Nylon-66 Matrix. *Journal of Polymer Science, Part B: Polymer Physics* **2003,** 41, 1234-1243.

Zhang, Q.-x.; Yu, Z.-z.; Yang, M.; Ma, J.; Mai, Y.-w., Multiple melting and crystallization of nylon-66/montmorillonite nanocomposites. *Journal of Polymer Science, Part B: Polymer Physics* **2003,** 41, 2861-2869.

Vita

Florencia Chavarria Sierra was born in Mexico City, Mexico on August 22, 1978 to Claudia Sierra Campuzano and Jaime Chavarria Silva, and sister to Deborah Chavarria Sierra. After graduating from high school, she attended the Universidad Nacional Autónoma de México (UNAM) where she received her Bachelor of Science Degree in Chemical Engineering in 2001. In August of 2001, she entered graduate school at the University of Texas at Austin under the supervision of Dr. Don Paul. She married Ian D. Wilson in May 2004.

Permanent address: Tetela 14, Tlaltenango
Cuernavaca, Morelos
Mexico

This dissertation was typed by the author.